Scaling the mountain

The search for bimetallic CO2 reduction electrocatalysts

van den Berg, D.

DOI
10.4233/uuid:df1c4cd1-f917-48ea-87ae-3380c27b7ec6

Publication date
2024

Document Version
Final published version

Citation (APA)
van den Berg, D. (2024). *Scaling the mountain: The search for bimetallic CO2 reduction electrocatalysts*. [Dissertation (TU Delft), Delft University of Technology]. https://doi.org/10.4233/uuid:df1c4cd1-f917-48ea-87ae-3380c27b7ec6

SCALING THE MOUNTAIN

THE SEARCH FOR BIMETALLIC CO_2 REDUCTION ELECTROCATALYSTS

SCALING THE MOUNTAIN

THE SEARCH FOR BIMETALLIC CO_2 REDUCTION ELECTROCATALYSTS

Dissertation

for the purpose of obtaining the degree of doctor
at Delft University of Technology
by the authority of the Rector Magnificus prof. dr. ir. T.H.J.J. van der Hagen,
chair of the Board for Doctorates
to be defended publicly on Thursday, 19 september, 2024, at 15:00 o'clock

by

Daniël VAN DEN BERG

Master of Science in Chemical Engineering, Delft University of Technology,
the Netherlands

born in Leiden, The Netherlands

This dissertation has been approved by the promotors.

Composition of the doctoral committee:

Rector Magnificus,	voorzitter
Prof. dr. ir. W. de Jong,	Delft University of Technology, promotor
Dr. R. Kortlever,	Delft University of Technology, copromotor

Independent members:

Dr. A. B. Bansode,	Technische Universiteit Delft
Prof. dr. M. Escudero Escribano	Institut Catalá de Nanociéncia i Nanotecnologia, Spain
Prof. dr. M. K. M. Koper	Leiden University
Prof. dr. ir. J. R. van Ommen	Delft University of Technology
Prof. dr. M. Tromp	University of Groningen
Prof. dr. ir. J. T. Padding	Delft University of Technology, reserve member

Keywords: CO_2 electroreduction, Bimetallic Alloys, Electrocatalysis, Analytical chemistry

Printed by: Ridderprint

Front & Back: Richard Guenne - Persoonlijk Proefschrift

ISBN 978-94-6384-611-0

An electronic version of this dissertation is available at
http://repository.tudelft.nl/.

”Ich musste mich vergleichen einem Bergsteiger, der, ohne den Weg zu kennen, langsam und mühselig hinaufklimmt, oft umkehren muss, weil er nicht weiter kann, der bald durch Überlegung, bald durch Zufall neue Wegspuren entdeckt, die ihn wieder ein Stück vorwärts leiten, und endlich, wenn er sein Ziel erreicht, zu seiner Beschämung einen königlichen Weg findet, auf dem er hätte herauffahren können, wenn er gescheit genug gewesen wäre, den richtigen Anfang zu finden.“

”I should compare myself to a mountain climber who, not knowing the path, climbs up slowly and laboriously, and is often compelled to turn around because his progress is blocked; who, sometimes by reasoning and sometimes by accident, discovers new tracks that take him a little further, and who, when he finally reaches his goal, discovers to his shame a magnificent road that he could have taken, if he had been clever enough to find the right place to start from.“

Hermann von Helmholtz, 1891

To *my parents*, who have helped me start the climb …

… To *Meera*, with whom I will happily keep climbing.

CONTENTS

Summary xiii

Samenvatting xv

1 Introduction 1
- 1.1 Threading the needle . . . 2
- 1.2 Challenges ahead . . . 2
- 1.3 Finding the right catalyst . . . 3
- 1.4 Electrochemical CO_2 reduction . . . 5
- 1.5 Thesis outline . . . 7

2 Can we go beyond copper in CO_2 electrolysis? 13
- 2.1 Introduction . . . 15
- 2.2 Product quantification is generally slow . . . 15
- 2.3 Cell geometries and hydrodynamics are not standardised and poorly defined. 16
- 2.4 The reported structure may not be the in-situ catalyst structure . . . 18
- 2.5 Future Outlook . . . 20

3 The Effect of Surface Conditions on the Electrochemical CO_2 Reduction Performance of Bimetallic AuPd Electrocatalysts 29
- 3.1 Introduction . . . 31
- 3.2 Experimental . . . 32
  - 3.2.1 Materials . . . 32
  - 3.2.2 Electrochemical Measurements . . . 32
  - 3.2.3 Electrode preparation . . . 33
  - 3.2.4 Material analysis . . . 34
- 3.3 Results & Discussion . . . 34
- 3.4 Conclusion . . . 40

4 Direct Quantification of Electrochemical CO_2 Reduction Products with an Improved DEMS Setup 45
- 4.1 Introduction . . . 47
- 4.2 Experimental . . . 48
  - 4.2.1 Materials . . . 48
  - 4.2.2 Electrochemical Measurements . . . 48
  - 4.2.3 Electrode preparation . . . 48
  - 4.2.4 Ferro/ferricyanide experiments . . . 49
  - 4.2.5 Formate quantification . . . 49
  - 4.2.6 Mass spectrometer settings . . . 50
  - 4.2.7 Product calibration . . . 50

4.3 Results & Discussion . . . 50
4.3.1 Cell Design . . . 50
4.3.2 Cell mass transfer . . . 50
4.3.3 Reproducible collection efficiency . . . 52
4.3.4 Product detection and quantification . . . 56
4.3.5 Mass peak deconvolution and product quantification . . . 57
4.3.6 Rapid electrocatalyst screening . . . 59
4.4 Conclusion . . . 61

5 Experimental screening of intermetallic alloys for electrochemical CO_2 reduction 67
5.1 Introduction . . . 69
5.2 Experimental . . . 70
5.2.1 Materials . . . 70
5.2.2 Electrochemical Measurements . . . 71
5.2.3 Intermetallic alloy synthesis . . . 71
5.2.4 XRD measurements . . . 72
5.2.5 Electrode preparation . . . 72
5.2.6 Product analysis . . . 72
5.3 Results & Discussion . . . 73
5.3.1 Synthesis and characterisation of intermetallic alloys . . . 73
5.3.2 Electrochemical measurements . . . 74
5.4 Conclusion . . . 78

6 Conclusions & Recommendations 83
6.1 Conclusion . . . 84
6.2 Recommendations . . . 85

Acknowledgements 87

A Appendix Chapter 3 91
A.1 SEM-EDX results . . . 91
A.2 XPS results . . . 92
A.3 Ferro/ferricyanide experiments . . . 93

B Appendix Chapter 4 97
B.1 Film Theory . . . 97
B.2 Calculating limiting currents . . . 98
B.3 Gas and liquid inlet designs . . . 99
B.4 Mass spectrometer settings . . . 100
B.5 Coefficient matrix . . . 100
B.6 Partial current densities . . . 101
B.7 Nyquist plot . . . 101
B.8 Chronoamperometry measurements . . . 102

C Appendix Chapter 5 105
C.1 Faradaic Efficiencies . . . 105

Curriculum Vitæ **107**

List of Publications **109**

SUMMARY

Over the coming decades, human society has to transition from being dependent on fossil fuels to renewable energy sources. However, renewable energy sources bring with them several inherent problems that need to be solved to integrate them into our society. The power supply of renewable energy sources is intermittent and does not match the global energy demand, necessitating the need for energy storage to bridge the gap. Additionally, the chemical industry relies heavily upon the usage of fossil fuels as chemical feedstocks that cannot be directly replaced by (electrical) renewable energy. Electrochemical CO_2 reduction to these synthetic fuels and chemicals provides a promising approach to both these problems. However, finding a suitable catalyst for this electrochemical reaction has proven difficult. So far, among the monometallic transition metals, only copper has been shown to actively reduce CO_2 into the desired synthetic fuels and chemicals. Unfortunately, these reactions take place at high overpotentials and unselectively. Alloying different metals together provides an elegant way to find new promising catalyst materials for the electrochemical reduction of CO_2 to synthetic fuels and chemicals. This thesis investigates different aspects of bimetallic electrochemical CO_2 reduction to synthetic fuels and chemicals.

Chapter 1 starts by outlining the issue of climate change and the inherent problems of renewable energy sources. Then, it touches upon fundamental concepts and challenges of catalysis and in particular (bi-)metallic electrochemical CO_2 reduction. Finally, it sketches a chapter-wise outline of this thesis.

Chapter 2 discusses the question of why no significant improvements have been made compared to the performance of monometallic copper even after thirty years of research on bimetallic electrochemical CO_2 reduction. The chapter subsequently proposes three ways to overcome shortcomings that are currently hindering rapid progress in the field. First, the high limit of detection of the most common product quantification techniques in the field forces researchers to extend the time of their experiments. As a result, only a handful of catalyst materials can be tested under a single reaction condition. Second, the use of non-standardised cell designs with poorly defined hydrodynamics could lead to discrepancies between research groups or results that are influenced by mass transfer limitations. Finally, the (in-situ) catalyst structure is often poorly defined, obscuring the link between the catalyst structure and its activity. For each of these shortcomings, the chapter provides different solutions and finally recommends several ways how to further speed up research.

Chapter 3 investigates an observed discrepancy in hydrocarbon selectivity among four studies that investigated the same metal combination of gold-palladium. To explore the influence of different buffer choices and the influence of each metal (combination), the electrocatalytic CO_2 reduction activities of three catalysts (gold, palladium, gold-palladium) are tested in two buffers (0.1 M $KHCO_3$ and 0.1 M KH_2PO_4 + 0.1 M K_2HPO_4). The results show that while all catalysts produce hydrocarbons in the phosphate buffer, these products are much less prevalent or even absent in the bicarbonate buffer. Further testing reveals that hydrocarbon activity increases with increasingly higher concentrations of bicarbonate.

Therefore, the choice of buffer indirectly influences the catalyst activity through its effect on the local surface pH. From these observations, the conclusion is drawn that on non-copper (bimetallic) catalysts, C_{2+} production mainly follows a Fisher-Tropsch mechanism instead of via pH-independent CO-dimerisation, the main reaction pathway to C_{2+} products on copper.

Chapter 4 outlines the development of an improved differential electrochemical mass spectrometry (DEMS) setup for the rapid quantification of the major CO_2RR products. The chapter covers several aspects of the improved design. First, the new cell design for the improved bubble removal is presented, leading to a more stabilised current. Second, the hydrodynamics of this cell are investigated and an improved mass transfer of CO_2 is demonstrated compared to conventional cell designs. Additionally, the hydrodynamics are well-defined and can be expressed by a Koutecky-Levich expression. Next, several modifications between the cell and the DEMS inlet are presented and their contribution to mass signal stability is discussed. To correctly convert the measured mass signals and quantify the catalyst activities, a method to deconvolute the different signals and correctly calibrate for the main products is derived. Finally, as a proof of concept, the catalytic activities of monometallic copper and silver are determined with the improved setup. These results match well with the literature and show that the new DEMS setup can determine the catalyst selectivity over a certain potential range four times as fast as conventional quantification techniques.

Chapter 5 experimentally screens a promising class of intermetallic alloys for the electrochemical reduction of CO_2 toward hydrocarbon products. In literature, combinations of strong CO-binding transition metals and weak CO-binding p-block metals are predicted to be selective towards further reduced products. Following this hypothesis, a series of six intermetallic alloys (AlFe, AlNi, CoSn, $FeGa_3$, $FeZn_4$, and NiGa) are synthesised using a two-step process: here, the desired catalyst material is first obtained through thermal diffusion and subsequently pressed into a solid shape using spark plasma sintering so that it can be tested in the newly developed DEMS setup. Most catalysts produce (higher) hydrocarbons but are mostly selective towards hydrogen. Reasons for this mismatch between predicted selectivity from the computational studies and experimental results are discussed. Moreover, a more holistic approach to DFT-screening studies is proposed to better predict the experimental selectivities of bimetallic catalysts in the future.

Chapter 6 states the overall conclusions of this thesis and discusses several recommendations for future research.

SAMENVATTING

In de komende decennia moeten we als maatschappij overstappen van fossiele brandstoffen naar duurzame energiebronnen. Hernieuwbare energiebronnen brengen echter een aantal problemen met zich mee die opgelost dienen te worden voordat ze in onze samenleving kunnen worden geïntegreerd: Allereerst is de beschikbaarheid van hernieuwbare energie onregelmatig en komt vaak niet overeen met wanneer wij energie nodig hebben. Om deze kloof te overbruggen, is grootschalige energieopslag nodig. Bovendien is de chemische industrie op dit moment sterk afhankelijk van fossiele brandstoffen als grondstoffen. Deze fysieke grondstoffen kunnen niet direct worden vervangen door (elektrische) hernieuwbare energie. Door met behulp van hernieuwbare energie CO_2 elektrochemisch te reduceren tot brandstoffen en chemicaliën kunnen beide problemen worden opgelost. Het is echter lastig een geschikte katalysator voor deze elektrochemische reacties te vinden. Van de overgangsmetalen is tot nu toe alleen koper in staat CO_2 actief te reduceren tot de gewenste producten. Helaas vinden deze reacties dan plaats bij hoge overpotentialen en zijn ze niet selectief. Dit maakt de reactie een stuk minder efficiënt. Het samenvoegen van verschillende metalen (legeren) biedt een elegante manier om nieuwe verbeterde katalysatoren te vinden voor de elektrochemische reductie van CO_2 tot synthetische brandstoffen en chemicaliën. Dit proefschrift onderzoekt verschillende aspecten van legeringen voor de elektrochemische reductie van CO_2 tot synthetische brandstoffen en chemicaliën.

Hoofdstuk 1 legt eerst klimaatverandering en de problemen van hernieuwbare energiebronnen uit. Vervolgens worden in het kort de fundamentele concepten en uitdagingen van katalyse en in het bijzonder van (bi-)metallische-elektrochemische CO_2-reductie behandeld. Ten slotte wordt er hoofdstuksgewijs een overzicht van dit proefschrift geschetst.

Hoofdstuk 2 behandelt de vraag waarom, na dertig jaar onderzoek naar elektrochemische CO_2 reductie op legeringen, er geen significante verbeteringen zijn gevonden vergeleken met de prestaties van monometallisch koper. Het hoofdstuk noemt vervolgens drie manieren om de huidige tekortkomingen in de literatuur te verhelpen die momenteel verdere vooruitgang op dit gebied belemmeren. Ten eerste door de hoge detectielimiet van de meest voorkomende productkwantificeringstechnieken in dit onderzoeksgebied zijn onderzoekers ertoe gedwongen om de duur van hun experimenten te verlengen. Als gevolg hiervan kunnen per onderzoek slechts een handvol katalysatoren onder enkele omstandigheden worden getest. Ten tweede zou het gebruik van niet-gestandaardiseerde celontwerpen met een slecht gedefiniëerde hydrodynamica kunnen leiden tot onbedoelde verschillen tussen onderzoeksgroepen of tot resultaten die worden beïnvloed door limitaties in de massatransport. Ten slotte is de (in-situ) structuur van de katalysator vaak slecht gedefiniëerd, waardoor het verband tussen de structuur en de activiteit van de katalysator onduidelijk blijft. Voor elk van deze tekortkomingen biedt het hoofdstuk verschillende oplossingen en tot slot doet het verschillende aanbevelingen om toekomstig onderzoek verder te versnellen.

Hoofdstuk 3 onderzoekt de reden waarom vier onderzoeken verschillende selectiviteiten voor koolwaterstoffen rapporteerden met dezelfde metaalcombinatie (goud-palladium).

Om de invloed van de verschillende buffers en de invloed van elk(e) metaal(combinatie) te onderzoeken, worden de activiteit voor CO_2-reductie van drie katalysatoren (goud, palladium, goud-palladium) in twee buffers (0,1 molair $KHCO_3$ en 0,1 M KH_2PO_4 + 0,1 M K_2HPO_4) getest. De resultaten laten zien dat alhoewel alle katalysatoren koolwaterstoffen produceren in de fosfaatbuffer, de katalysatoren deze koolwaterstoffen veel minder of zelfs helemaal niet in de bicarbonaatbuffer produceren. Uit verder onderzoek blijkt dat de koolwaterstofactiviteit toeneemt met de concentratie bicarbonaat. Deze observaties laten zien dat de keuze van de buffer indirect de katalysatoractiviteit via de lokale oppervlakte-pH aan het elektrode oppervlak beïnvloedt. Hieruit wordt de conclusie getrokken dat op (bimetaal) katalysatoren zonder koper de productie van C_{2+} voornamelijk een Fisher-Tropsch-mechanisme volgt in plaats van via de pH-onafhankelijke CO-dimerisatie route, wat de belangrijkste reactieroute naar C_{2+} producten op koper is.

Hoofdstuk 4 ontwikkelt een verbeterd ontwerp van een differentiële elektrochemische massaspectrometrie (DEMS) opstelling om de belangrijkste CO_2RR-producten sneller te kunnen kwantificeren. In dit hoofdstuk worden verschillende aspecten van het verbeterde ontwerp besproken. Eerst wordt het nieuwe ontwerp gepresenteerd waarin bellen makkelijker kunnen worden verwijderd van de elektrode, wat leidt tot een stabiliere stroom. Daarna wordt de hydrodynamica van deze cel onderzocht en wordt aangetoond dat deze cell een verbeterde massaoverdracht van CO_2 heeft vergeleken met standaard celontwerpen. Bovendien is de hydrodynamica goed gedefiniëerd en kan deze worden uitgedrukt door een Koutecky Levich-uitdrukking. Vervolgens worden verschillende toevoegingen tussen de cel en de ingang naar de DEMS besproken voor het verbeteren van de stabiliteit van het massasignaal. Om de productactiviteit van een katalysator correct te berekenen met behulp van de gemeten massasignalen, wordt een methode afgeleid om de verschillende signalen uit elkaar te halen en deze correct te kalibreren voor de belangrijkste CO_2RR-producten. Ten slotte worden, als proof-of-concept, de katalytische activiteit van koper en zilver bepaald met de verbeterde opstelling. Deze resultaten komen goed overeen met de literatuur en laten zien dat de nieuwe DEMS-opstelling de katalysatorselectiviteit van een katalysator vier keer zo snel over een reeks potentialen kan bepalen dan met behulp van conventionele kwantificeringstechnieken.

Hoofdstuk 5 test een aantal veelbelovende intermetallische legeringen voor de elektrochemische reductie van CO_2 naar koolwaterstofproducten. In de literatuur wordt voorspeld dat combinaties van sterk-CO-bindende overgangsmetalen en zwak-CO-bindende p-blokmetalen selectief zijn voor verder gereduceerde producten. Zes van deze intermetallische legeringen (AlFe, AlNi, CoSn, $FeGa_3$, $FeZn_4$ en NiGa) worden gesynthetiseerd via een tweestapsproces: eerst wordt het gewenste katalysatormateriaal gemaakt met behulp van thermal diffusion en vervolgens met behulp van Spark Plasma Sintering in een vaste vorm geperst, zodat het in de nieuw ontwikkelde DEMS-opstelling kan worden getest. De meeste van de geteste katalysatoren produceren inderdaad (hogere) koolwaterstoffen, maar zijn voornamelijk selectief voor waterstof. Om dit veschil tussen de voorspelde selectiviteit uit de computationele studies en experimentele resultaten te verklaren, worden er verschillende redenen besproken. Tot slot wordt een meer holistische aanpak van DFT-screeningstudies voorgelegd zodat in de toekomst deexperimentele selectiviteiten van bimetaalkatalysatoren beter te voorspellen zijn.

Hoofdstuk 6 vat de algemene conclusies van dit proefschrift samen en bespreekt verschillende aanbevelingen voor toekomstig onderzoek.

1

INTRODUCTION

1

1.1. THREADING THE NEEDLE

Without the atmosphere to absorb and retain the energy from the sun, the Earth would be much cooler (by about 33 degrees celcius) and life would not be able to exist. Carbon dioxide plays a decisive role in this greenhouse effect by trapping a large part of the emitted radiation [1]. For thousands of years, the Earth's CO_2 level has stayed relatively stable as can be seen in Figure 1.1. However, since the start of the industrial revolution, the amount of CO_2 in the atmosphere has increased exponentially in a short period due to the combustion of fossil fuels. Since CO_2 is such an excellent heat retainer, the global temperature has rapidly risen. This increase in temperature and CO_2 concentration have irreversibly affected life on Earth as higher temperatures cause storms, forest fires, droughts, flooding, and declining biodiversity [2]. Clearly, even though the concentration of CO_2 is relatively low (currently about 400 parts per million), small perturbations from this concentration can dramatically alter the conditions on Earth. Therefore, it is essential to restore the balance to pre-industrial levels. For this to happen, the atmospheric CO_2 concentration needs to be reduced and the consumption of fossil fuels needs to be halted.

1.2. CHALLENGES AHEAD

To reduce the atmospheric CO_2 concentration and stop fossil fuel usage, several challenges need to be solved. Firstly, without the use of fossil fuels, there will be a massive gap in our energy supply. To fill this gap, alternative sources of energy need to be found to keep up with

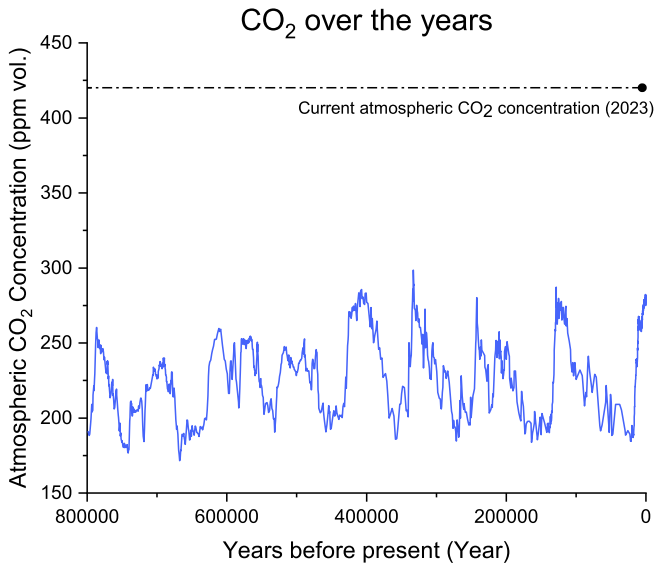

Figure 1.1: Atmospheric CO_2 concentration over the last eight hundred thousand years. Data was taken from Lüthi, et al. [3].

the Earth's increasing population and standard of living. The most promising alternative sources are solar and wind power. Over the coming years, these renewable sources of energy are expected to expand quickly and supply the majority of the global electricity demand [4]. However, harnessing solar and wind power on a large scale raises other challenges. The supply of these renewable resources is intermittent and therefore not always available everywhere when needed. These periods of shortage can currently be filled by fossil fuels or nuclear energy but this cannot be a long-term solution. In the future, excess generated energy needs to be stored and used later in times of shortage.

Secondly, the chemical industry currently heavily depends upon the use of fossil fuels and feedstocks for the production of many bulk chemicals, such as ammonia and methanol [5]. However, most renewable energy sources only provide electrical power, while the chemical industry needs a tangible, renewable chemical feedstock. Therefore, alternative, renewable routes to produce bulk chemicals need to be developed.

Finally, atmospheric excess CO_2 needs to be captured and subsequently stored or utilised. This process is commonly referred to as carbon capture, utilisation, and sequestration (CCUS). Examples of carbon sequestration include (re-)forestation, geological storage e.g. in depleted oil and gas fields, and mineral storage where CO_2 is stored as metal carbonates by reacting exothermically with metal oxides [6]. Carbon sequestration does not, however, offer a long-term sustainable solution to reduce CO_2 emissions and does not make use of the inherent value of carbon dioxide as a chemical reactant.

Instead, if CO_2 is utilised to produce fuels using a renewable source of energy, all challenges above are solved at once: these synthetically produced fuels and chemicals can act as an energy buffer when the intermittent supply of renewable energy sources is low and they can be used to substitute fossil fuels in the chemical industry. To convert CO_2 into these synthetic fuels and chemicals, it needs to selectively undergo a chemical reaction for which a selective and stable catalyst is required. Such catalysts already exist for the indirect catalytic conversion of CO_2 and hydrogen to synthetic fuels and chemicals such as methanol or methane. Here, the hydrogen can be electrochemically produced using renewable energy. However, such a catalyst has yet to be found for the direct electrochemical conversion of CO_2, where these synthetic fuels and chemicals are produced from water and CO_2. Direct electrochemical reduction of CO_2 would be more advantageous as it can be operated at mild conditions rather than the elevated temperatures and pressures that are needed for the indirect route. Also, the direct route could provide a more efficient, one-step alternative process. Therefore, this thesis will focus on the direct electrochemical CO_2 reduction reaction (CO_2RR) and its goal is to find the right electrocatalyst for this process.

1.3. FINDING THE RIGHT CATALYST

During a chemical reaction, a compound (reactant) reacts to form a new compound (product). Most chemical reactions, however, consist of multiple reaction steps that need to occur in succession to complete the reaction. These reaction steps are referred to as elementary reactions, while the intermediate forms of each reaction step are called reaction intermediates. All the steps together make up the reaction mechanism. To successfully undergo an elementary reaction, the molecules involved must first have enough energy to overcome a certain amount of energy, called the activation energy (E_a). If the intermediates involved do not have enough energy, the reaction will not occur. Catalysts are materials that partake in a

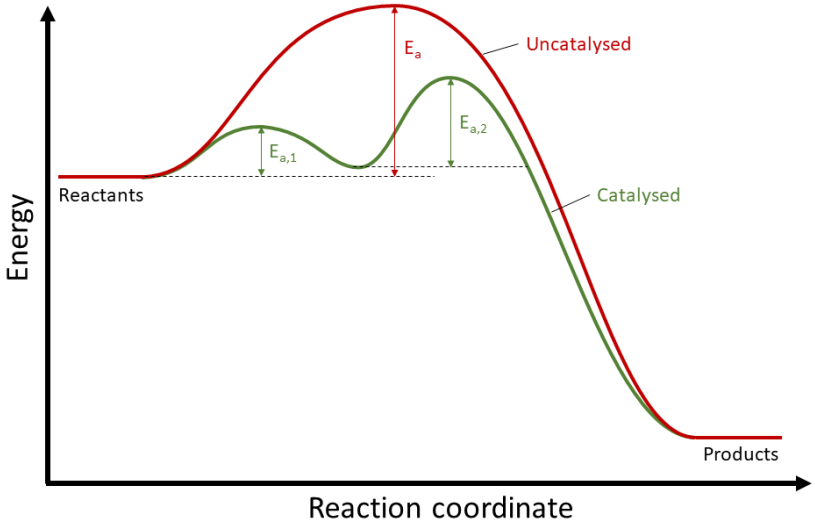

Figure 1.2: The energy profile as a function of the reaction coordinate for a reaction both catalysed and uncatalysed. Note that the activation energy of a catalysed reaction is lower.

chemical reaction but do not get consumed themselves. By participating in the reaction, catalysts can provide an alternative reaction mechanism that has a lower activation energy than the original uncatalysed reaction, see figure 1.2. As a result, more molecules have enough energy to successfully react and as a result, the reaction speeds up as a whole.

A successful catalyst binds the reaction intermediate(s) in such a way that they are not bound too strongly or too weakly. If the bond between the catalyst and intermediate is too strong, it would not be energetically favourable to react to the next reaction intermediate. On the other hand, if the bond is too weak, the intermediate will not stay bound to the catalyst or fail to react. This concept is known as the Sabatier principle and can be made visual by plotting the activity of different catalysts towards the reaction of interest against their computed binding energy based on DFT calculations. This plot is known as a volcano plot. In figure 1.3, two examples from the field of electrochemical CO_2 reduction are shown. However, if a reaction mechanism consists of multiple reaction intermediates, a catalyst needs to optimally bind each of them. This makes the catalyst design more complex because when a catalyst binds optimally with one intermediate, it does not necessarily bind optimally with the other one(s). Therefore, a catalyst often needs to fulfil multiple roles at once. This multifunctionality can be achieved in different ways.

This thesis will focus on the mixing of metals (alloying) to achieve synergy between the two metals in a catalyst. By mixing two metals, several different active sites can be placed close to one another. Each of these active sites could be tailored to optimally bind the reaction intermediates involved. Successful examples of this concept have been shown in literature e.g. for ammonia production [7] and oxygen reduction [8].

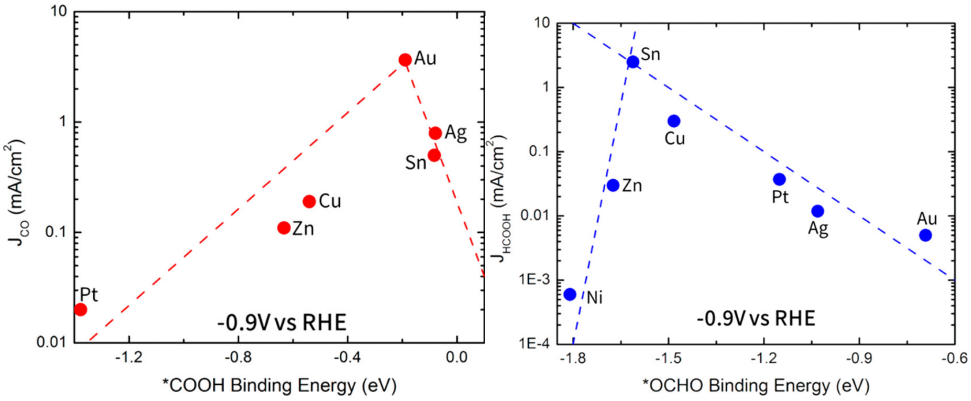

Figure 1.3: By plotting different descriptors versus the partial current densities of carbon monoxide and formate on various monometallic compounds it suggests that the products have different key intermediates. The figures above were taken with permission from Feaster et al. [9] and plot the binding energy of *COOH and *OCHO versus the partial current density towards carbon monoxide and formic acid at -0.9 V vs. RHE. respectively.

1.4. ELECTROCHEMICAL CO_2 REDUCTION

To find the right catalyst, one should first analyse the reaction mechanism of the electrochemical reduction of CO_2 to the formed products. This reaction mechanism is a good example of a reaction mechanism with multiple reaction intermediates that each must be optimally bound to the catalyst surface. In figure 1.4 a general simplified overview of different CO_2 reduction pathways on a metal surface is given. To reduce CO_2, the CO_2 molecule has to first adsorb onto the metal electrode surface. There, the adsorbed CO_2 has to be protonated or undergo an electrophilic attack.

If this does not happen or is not favoured on the metal surface, CO_2 will not be reduced, and the main product is hydrogen that is produced from water splitting when the reaction occurs in an aqueous electrolyte. Metals from groups 4-7 of the periodic system are an example of this. They reduce little CO_2 and mainly produce hydrogen when an aqueous electrolyte is used. Even under higher pressures, when more CO_2 is available at the electrode surface compared to ambient systems, mostly hydrogen is produced together with low amounts of formate and CO [10]. However, molybdenum has been shown to produce methanol, be it in small quantities [11].

If CO_2 is bound strongly enough to be reduced, the orientation and structure of the intermediate determine whether CO or formate production is favoured [12]. Hori and coworkers state that CO is formed from a strongly bound CO_2 radical, while formate is formed when this radical is weakly bounded [13]. However, DFT-based models suggest that formate and CO have a different intermediate. This was illustrated by an article by Feaster et al., which plotted the DFT binding energies for both intermediates, *COOH and *OCHO, against the partial current density for both CO and formate. Here, the *OCHO binding energy showed a volcano-like trend for the formate production while the *COOH did not [9]. Tin was located at the top of this volcano plot. Other publications also show a high selectivity of tin(oxide) towards the production of HCOOH [14], [15]. Other p-block metals, such as lead, mercury, and indium, also favour the production of formate over other CO_2 reduction products under

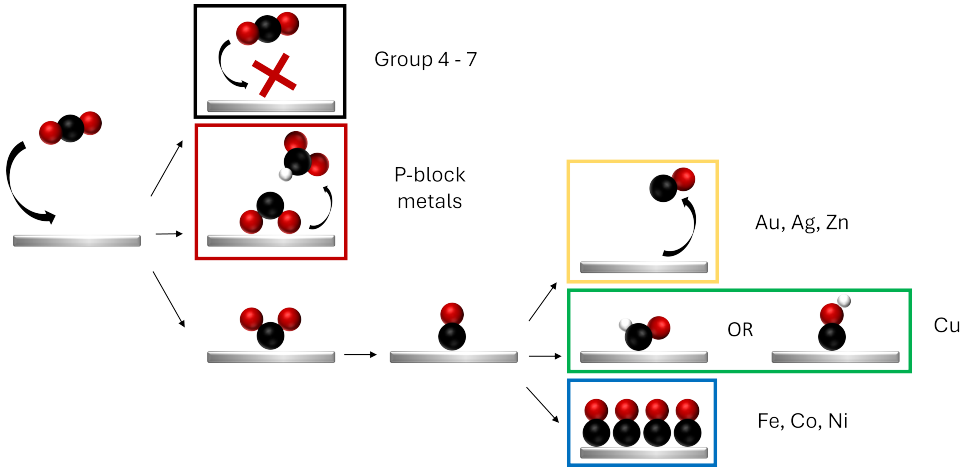

Figure 1.4: Generalisation of the CO_2 reduction mechanism on a metal surface.

both laboratory [16] and industrial conditions [17]. However, high overpotentials (-1.75 V vs. NHE [17]) are needed to be able to form HCOOH on these metals. Once the CO_2 has been reduced to CO*, the binding strength of this key intermediate determines the main reduction product. If it is not adsorbed strongly enough, it readily desorbs and CO gas is observed as the main product [18]. This is the case for silver [16], [19], gold [13], [20], and zinc [21]. There is some disagreement within research groups on whether or not zinc mainly produces CO or formate [10]. This could be explained by contamination of p-block metals in the zinc which have a detrimental effect on the CO selectivity of the zinc surface [13]. With an increased binding strength, desorption from the surface becomes less favourable which gives a chance for the CO to reduce further. However, when CO binding to the surface becomes too strong, the CO becomes inaccessible for further reduction. On these metal surfaces, CO_2 reduction becomes limited and the main product selectivity shifts to hydrogen. Examples of this are iron, nickel, and cobalt [10], [16].

Among the monometallic transition metals, only copper stands out. Copper has an optimal binding strength of key intermediates such as H* and CO* and is therefore able to produce hydrocarbons, alcohols and aldehydes [22]. Moreover, its favourable binding strength of C* [23] and ideal atomic spacing [24] enable it to form C-C bonds and produce C_{2+} products making the metal an interesting catalyst towards valuable products such as ethylene. Unfortunately, copper is not selective in its reduction products. A wide range of 16 different products are produced over a range of potentials [25]. This is undesirable as it necessitates the introduction of many expensive and energy-costly separation steps.

1.5. THESIS OUTLINE

The research goal of this thesis is to identify bimetallic catalysts that selectively reduce CO_2 towards further reduced products involving more than two electrons. After the discovery of Hori and co-workers that among the monometallic transition metals only copper is able to reduce CO_2 into hydrocarbons such as methane and ethylene, research into CO_2RR catalyst materials has heavily focused on this metal [21]. Many multimetallic electrocatalysts tested so far are combinations of copper with other metals [26], [27]. However, these materials have shown to be not significantly more selective or active than monometallic copper, according to Nitopi and coworkers [12]. In **Chapter 2**, we attempt to find an explanation for this absence. We will discuss several shortcomings that are prevalent in the available literature on bimetallic CO_2 reduction electrocatalysts. The lessons learned can be used to prevent several pitfalls while selecting new bimetallic catalysts. In the chapters following, we address several of these lessons learned.

First, we take a look at the other side of the reaction interface: while most research into electrochemical CO_2 conversion focuses on improving electrode materials, the role of the electrolyte (buffer) is often not taken into account, thereby creating a one-sided view of the process. In **Chapter 3**, we show the influence of two buffers, $KHCO_3$ and KH_2PO_4/K_2HPO_4, on the selectivity of a bimetallic gold-palladium electrode in an effort to elucidate observed inconsistencies between different studies into this metal combination. The results show that the electrolyte choice plays a crucial role in determining the reaction conditions at the electrode surface and hereby the selectivity of the electrode.

Next, we observed that current quantification techniques that are commonly used in the field of electrochemical CO_2 reduction are slow and have high limits of detection. Because of this, the researcher is forced to extend the duration of experiments and accumulate sufficient concentrations of products to surpass the detection limit slowing down research considerably. Therefore, considerable research has been done to develop a technique that is able to quantify the production rates of major CO_2RR products directly and in real-time. Differential electrochemical mass spectrometry (DEMS) is a membrane inlet mass spectroscopy (MIMS) based analytical technique that uses a pervaporation membrane to separate (dissolved) gasses and volatile organic compounds from the electrolyte. However, despite considerable efforts made, none of the currently available setups is able to quantify all major gaseous and liquid-phase products. In **Chapter 4**, we develop a setup capable of direct quantification of major CO_2RR products from both phases. In the new cell design, special attention is also given to the hydrodynamics of the cell to avoid mass transfer limitations and bubble buildup in the cell. Furthermore, by applying soft ionisation mass spectrometry and multivariate calibration, product fragment overlap is limited allowing for quantification of all major CO_2RR products without pre-existing knowledge about the catalyst selectivity.

Finally, in **Chapter 5**, we manufacture and test a selection of copper-free intermetallic electrocatalysts, made by combining different p-block metals (Sn, Al, Ga, Zn) and transition metals (Fe, Co, Ni) to optimise the binding strength of key intermediates in the CO_2 reduction mechanism. Several DFT-based catalyst screenings found that combinations of these metals could provide selective CO_2RR catalysts [28], [29]. Even though these materials are difficult to manufacture, several catalyst materials were successfully synthesised, using a two-step process of thermal diffusion and subsequent spark plasma sintering.

BIBLIOGRAPHY

[1] S. Drury, *Stepping Stones: The making of our home world*. Oxford University Press, 1999.

[2] V. Masson-Delmotte, P. Zhai, A. Pirani, *et al.*, "IPCC, 2021: Climate change 2021: The physical science basis. the working group i contribution to the sixth assessment report", *Cambridge University Press: Cambridge, UK*, 2021.

[3] D. Lüthi, M. Le Floch, B. Bereiter, *et al.*, "High-resolution carbon dioxide concentration record 650,000–800,000 years before present", *Nature*, vol. 453, no. 7193, pp. 379–382, 2008, ISSN: 0028-0836. DOI: https://doi.org/10.1038/nature06949.

[4] IEA, *World energy outlook 2022*, 2022.

[5] IEA, *Chemicals*, https://www.iea.org/reports/chemicals, License: CC BY 4.0, 2022.

[6] A. Kulmatiski, K. H. Beard, J. R. Stevens, and S. M. Cobbold, "Plant–soil feedbacks: A meta-analytical review", *Ecology letters*, vol. 11, no. 9, pp. 980–992, 2008.

[7] C. J. Jacobsen, S. Dahl, B. S. Clausen, S. Bahn, A. Logadottir, and J. K. Nørskov, "Catalyst design by interpolation in the periodic table: Bimetallic ammonia synthesis catalysts", *Journal of the American Chemical Society*, vol. 123, no. 34, pp. 8404–8405, 2001.

[8] J. Greeley, I. Stephens, A. Bondarenko, *et al.*, "Alloys of platinum and early transition metals as oxygen reduction electrocatalysts", *Nature chemistry*, vol. 1, no. 7, pp. 552–556, 2009.

[9] J. T. Feaster, C. Shi, E. R. Cave, *et al.*, "Understanding selectivity for the electrochemical reduction of carbon dioxide to formic acid and carbon monoxide on metal electrodes", *ACS Catalysis*, vol. 7, no. 7, pp. 4822–4827, 2017, ISSN: 2155-5435. DOI: https://doi.org/10.1021/acscatal.7b00687.

[10] M. Azuma, K. Hashimoto, M. Hiramoto, M. Watanabe, and T. Sakata, "Electrochemical reduction of carbon dioxide on various metal electrodes in low-temperature aqueous $KHCO_3$ media", *Journal of the Electrochemical Society*, vol. 137, no. 6, pp. 1772–1778, 1990, ISSN: 0013-4651. DOI: https://doi.org/10.1149/1.2086796.

[11] D. P. Summers, S. Leach, and K. W. Frese Jr, "The electrochemical reduction of aqueous carbon dioxide to methanol at molybdenum electrodes with low overpotentials", *Journal of electroanalytical chemistry and interfacial electrochemistry*, vol. 205, no. 1-2, pp. 219–232, 1986, ISSN: 0022-0728.

[12] S. Nitopi, E. Bertheussen, S. B. Scott, *et al.*, "Progress and perspectives of electrochemical CO_2 reduction on copper in aqueous electrolyte", *Chemical Reviews*, vol. 119, no. 12, pp. 7610–7672, 2019, ISSN: 0009-2665. DOI: https://doi.org/10.1021/acs.chemrev.8b00705.

[13] Y. Hori, H. Wakebe, T. Tsukamoto, and O. Koga, "Electrocatalytic process of CO selectivity in electrochemical reduction of CO_2 at metal electrodes in aqueous media", *Electrochimica Acta*, vol. 39, no. 11-12, pp. 1833–1839, 1994, ISSN: 0013-4686. DOI: https://doi.org/10.1016/0013-4686(94)85172-7.

[14] G. Frankel, A. Agarwal, and N. Sridhar, "Degradation and deactivation of Sn catalyst used for CO_2 reduction as function of overpotential", *Electrochimica Acta*, vol. 133, pp. 188–196, 2014, ISSN: 0013-4686. DOI: https://doi.org/10.1016/j.electacta.2014.04.057.

[15] Y. Chen and M. W. Kanan, "Tin oxide dependence of the reduction efficiency on tin electrodes and enhanced activity for tin/tin oxide thin-film catalysts", *Journal of the American Chemical Society*, vol. 134, no. 4, pp. 1986–1989, 2012, ISSN: 0002-7863. DOI: https://doi.org/10.1021/ja2108799.

[16] H. Noda, S. Ikeda, Y. Oda, K. Imai, M. Maeda, and K. Ito, "Electrochemical reduction of carbon dioxide at various metal electrodes in aqueous potassium hydrogen carbonate solution", *Bulletin of the Chemical Society of Japan*, vol. 63, no. 9, pp. 2459–2462, 1990, ISSN: 1348-0634.

[17] M. Todoroki, K. Hara, A. Kudo, and T. Sakata, "Electrochemical reduction of high pressure CO_2 at Pb, Hg and In electrodes in an aqueous $KHCO_3$ solution", *Journal of Electroanalytical Chemistry*, vol. 394, no. 1-2, pp. 199–203, 1995, ISSN: 1572-6657.

[18] R. Chaplin and A. Wragg, "Effects of process conditions and electrode material on reaction pathways for carbon dioxide electroreduction with particular reference to formate formation", *Journal of Applied Electrochemistry*, vol. 33, no. 12, pp. 1107–1123, 2003, ISSN: 0021-891X. DOI: https://doi.org/10.1023/B%3AJACH.0000004018.57792.B8.

[19] T. Hatsukade, K. P. Kuhl, E. R. Cave, D. N. Abram, and T. F. Jaramillo, "Insights into the electrocatalytic reduction of CO_2 on metallic silver surfaces", *Physical Chemistry Chemical Physics*, vol. 16, no. 27, pp. 13 814–13 819, 2014. DOI: https://doi.org/10.1039/C4CP00692E.

[20] E. R. Cave, J. H. Montoya, K. P. Kuhl, *et al.*, "Electrochemical reduction on au surfaces: Mechanistic aspects regarding the formation of major and minor products", *Physical Chemistry Chemical Physics*, vol. 19, no. 24, pp. 15 856–15 863, 2017. DOI: https://doi.org/10.1039/C7CP02855E.

[21] Y. Hori, K. Kikuchi, and S. Suzuki, "Production of CO and CH_4 in electrochemical reduction of CO_2 at metal electrodes in aqueous hydrogencarbonate solution", *Chemistry Letters*, vol. 14, no. 11, pp. 1695–1698, 1985, ISSN: 1348-0715. DOI: https://doi.org/10.1246/cl.1985.1695.

[22] A. Bagger, W. Ju, A. S. Varela, P. Strasser, and J. Rossmeisl, "Electrochemical reduction: A classification problem", *ChemPhysChem*, vol. 18, no. 22, pp. 3266–3273, 2017, ISSN: 1439-4235. DOI: https://doi.org/10.1002/cphc.201700736.

[23] Y. Peng, M. Cui, Z. Zhang, *et al.*, "Bimetallic composition-promoted electrocatalytic hydrodechlorination reaction on silver–palladium alloy nanoparticles", *ACS Catalysis*, vol. 9, no. 12, pp. 10 803–10 811, 2019, ISSN: 2155-5435. DOI: https://doi.org/10.1021/acscatal.9b02282.

[24] F. Calle-Vallejo, J. Martínez, J. M. García-Lastra, J. Rossmeisl, and M. Koper, "Physical and chemical nature of the scaling relations between adsorption energies of atoms on metal surfaces", *Physical review letters*, vol. 108, no. 11, p. 116 103, 2012. DOI: https://doi.org/10.1103/PhysRevLett.108.116103.

[25] K. P. Kuhl, E. R. Cave, D. N. Abram, and T. F. Jaramillo, "New insights into the electrochemical reduction of carbon dioxide on metallic copper surfaces", *Energy & Environmental Science*, vol. 5, no. 5, pp. 7050–7059, 2012, ISSN: 1754-5692. DOI: https://doi.org/10.1039/C2EE21234J.

[26] J. He, N. J. J. Johnson, A. Huang, and C. P. Berlinguette, "Electrocatalytic alloys for CO_2 reduction", *ChemSusChem*, vol. 11, no. 1, pp. 48–57, 2018, ISSN: 1864-5631. DOI: https://doi.org/10.1002/cssc.201701825.

[27] Z. Chen, G. Zhang, H. Chen, J. Prakash, Y. Zheng, and S. Sun, "Multi-metallic catalysts for the electroreduction of carbon dioxide: Recent advances and perspectives", *Renewable and Sustainable Energy Reviews*, vol. 155, p. 111 922, 2022, ISSN: 1364-0321. DOI: https://doi.org/10.1016/j.rser.2021.111922.

[28] J. Li, J. H. Stenlid, M. T. Tang, H.-J. Peng, and F. Abild-Pedersen, "Screening binary alloys for electrochemical CO_2 reduction towards multi-carbon products", *Journal of Materials Chemistry A*, vol. 10, no. 30, pp. 16 171–16 181, 2022. DOI: https://doi.org/10.1039/D2TA02749F.

[29] K. Tran and Z. W. Ulissi, "Active learning across intermetallics to guide discovery of electrocatalysts for CO_2 reduction and H_2 evolution", *Nature Catalysis*, vol. 1, no. 9, pp. 696–703, 2018, ISSN: 2520-1158. DOI: https://doi.org/10.1038/s41929-018-0142-1.

2

CAN WE GO BEYOND COPPER IN CO_2 ELECTROLYSIS?

Despite the hundreds of articles that are published every year on CO_2 electrolysis, monometallic copper is still the all-round best catalyst to reduce CO_2 to hydrocarbons, even though it suffers from several drawbacks like high overpotential, low selectivity, and instability. To help speed up the process and make improvements on the monometallic copper catalyst, coordination between research groups should be promoted and their approach to research should be more structured. Most research papers into CO_2RR catalyst development look into one or just a handful of catalysts, do their catalytic testing in custom-built electrochemical cells under one reaction condition, and often analyse only the pristine catalyst materials. These practices make it hard to compare results between research groups and identify interesting materials or discard unselective ones. In this perspective, we will identify several underlying problems that hinder researchers and suggest several solutions to them.

2.1. INTRODUCTION

In 1985, Hori and co-workers discovered that among the monometallic transition metals, only copper is able to reduce CO_2 into hydrocarbons such as methane and ethylene with high faradaic efficiencies [1]. This property of copper makes it unique among the transition metals and therefore research into CO_2RR has heavily focused on this metal. Copper is able to produce these hydrocarbons due to its optimal binding strength of key intermediates such as H* and CO* [2]. By binding CO* not too strong nor too weak and not having underpotential deposited hydrogen (H_{upd}), copper is able to reduce CO_2 beyond CO. Moreover, by having a favourable binding strength of C* [3] and ideal atomic spacing for CO dimerisation [4], copper is also able to produce C_{2+} products making the metal an interesting catalyst towards valuable products such as ethylene. However, copper has several downsides: copper is in general not very selective towards a single product. The methane/ethylene production ratio varies strongly depending on crystallographic structure [5] and applied process conditions such as surface pH [6] and choice of cation [7]. Additionally, copper suffers from high overpotential and material stability issues [8], [9].

Therefore, multiple studies have set out to make copper more selective towards a single CO_2RR product and to suppress the hydrogen evolution reaction (HER) using different approaches. One of these approaches is to combine copper with other metals or by combining two different metals. This process is referred to as alloying. Through alloying, the binding strength of surfaces to the key intermediates can be fine-tuned. Moreover, several distinct active sites for multiple key intermediates can be created near one another by varying the composition or orientation. Furthermore, alloying of different metals has been proven successful for several other electrocatalytic reactions such as the HER [10], the ORR [11], and in heterogeneous catalysis for ammonia production [12]. The number of metals in theory is not limited, but in this chapter, we will mostly limit ourselves to bimetallic systems. When a multimetallic catalyst contains five or more metals, they are referred to as high entropy alloys (HEAs) [13]. Recently, Biswas and coworkers have developed and experimentally tested HEAs for the reduction of CO_2 to hydrocarbons. However, since these alloys are relatively new and their performances complex, we will not refer to them further in detail [14].

Not surprisingly, most research into multimetallic electrocatalysts so far involved copper [15], [16]. However, Nitopi et al. showed that these multimetallic materials are not significantly more selective or active than monometallic copper [17]. This observation leads to the question: After almost four decades of research into multimetallic CO_2RR catalysts, why is there still no improvement in selective activity towards > 2 e^- products for any of the studied catalysts compared to monometallic copper? Surely, after this much time and CO_2 reduction being such a hot research topic nowadays, some improvement on copper should have been made. In this chapter, we highlight the main shortcomings in the literature that are hindering the progress in the field of multimetallic CO_2RR catalyst and recommend several strategies to guide this and future work.

2.2. PRODUCT QUANTIFICATION IS GENERALLY SLOW

While high throughput catalyst screenings for the hydrogen evolution reaction (HER), oxygen evolution reaction (OER), and methanol oxidation reaction (MOR) are already common

in literature [18]–[20], CO_2RR screenings are not. Other than is the case for HER or OER, multiple reactions can take place during CO_2RR producing a variety of different products, which complicates high throughput screening. Also, because CO_2RR competes with the hydrogen evolution reaction, solely determining the catalyst activity by mapping the current density responses at different potentials is not sufficient. Thus, unlike high throughput catalyst screenings for HER, OER, and MOR, the CO_2RR selectivity must be measured.

To assess whether a catalyst is selectively active for the CO_2RR, quantification of all produced products is necessary. Typically for CO_2RR catalysts, gaseous products are quantified using (inline) gas chromatography (GC), while liquid products are quantified using high-performance liquid chromatography (HPLC) or nuclear magnetic resonance spectroscopy (^{1}H NMR). However, these techniques are generally slow and have relatively high limits of detection. To surpass the detection limits, experiments need to be prolonged to accumulate sufficient concentrations of products. As a result, research is delayed, and per study often only one or a couple of catalysts are tested in a single electrolyte. This limited scope makes comparison between different materials more difficult.

Also, since the catalyst is often only studied in one electrolyte (mostly aqueous bicarbonate solutions), the electrolyte influence remains unknown despite the major influence that the electrode-electrolyte interactions have on the product selectivity for CO_2RR: both the choice of buffer and its concentration influence the local pH thereby influencing the local reaction conditions and selectivity of CO_2RR and HER [6]. Moreover, the choice for a specific cation can also significantly shift the selectivity [7]. Furthermore, the lack of comparison between different electrolytes can lead to discrepancies between results on similar materials from different authors. For example, different studies either observed or did not observe hydrocarbon production on Au-Pd electrodes [21]–[24]. By studying this material in both 0.1 M $KHCO_3$ and 0.1 M KH_2PO_4 + 0.1 M K_2HPO_4 buffer, the electrolyte was shown to have a significant impact upon the product selectivity of Au-Pd, see chapter 3.

More research should therefore be focused on developing setups and quantification techniques to rapidly screen different catalytic materials. Several high-throughput systems have been developed, but so far, they are limited to qualitative detection of the main reduction products [25], [26]. So, rapid quantification setups need to be further developed. For example, Differential Electrochemical Mass Spectrometry (DEMS) uses a pervaporation membrane to separate (dissolved) gases and volatile organic compounds from the electrolyte [27], [28]. Mass spectrometry has a low limit of detection, is fast and enables direct measurement of both liquid and gaseous products within the same experimental setup. Thereby, research into new CO_2 reduction catalysts can be accelerated significantly. So far, several successful setups have already been published that employ DEMS [29], [30]. In chapter 4, a setup is developed that can quantify all major CO_2RR products using a modified DEMS setup.

2.3. CELL GEOMETRIES AND HYDRODYNAMICS ARE NOT STANDARDISED AND POORLY DEFINED

With the sheer size of possible catalysts to be tested, not only high throughput screening is important but also that the results from these screenings show the intrinsic performance of the catalyst unaffected by transport phenomena or reactor design. To achieve this goal, the surface conditions need to be similar under all experimental conditions and as close to the

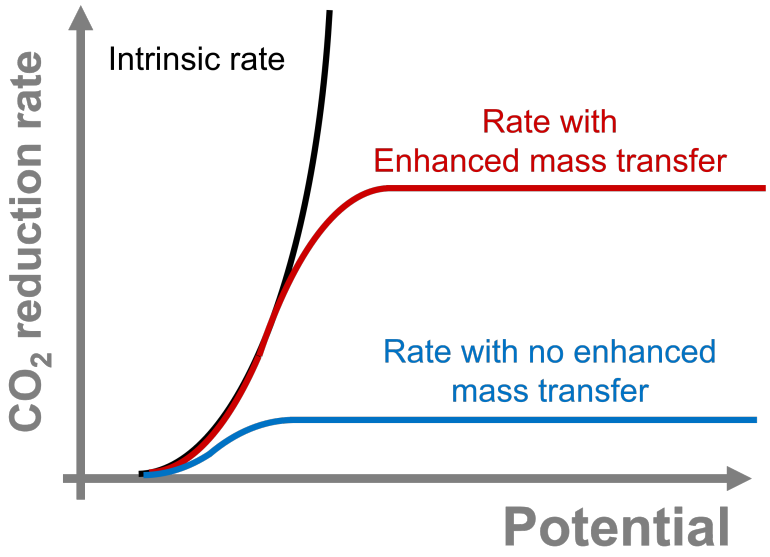

Figure 2.1: Graph showing the difference between the intrinsic rate of a catalyst (in black) and the measured rate with enhanced and without enhanced mass transfer to the catalyst surface in red and blue respectively. Without enhanced mass transfer the measured CO_2RR rate will quickly deviate from the real catalytic rate of the catalyst.

bulk concentrations as possible. Two transport rates need to be considered: the transport of reactants from the bulk to the edge of the diffusion layer (external mass transport) and the transport from the diffusion layer to the catalyst surface (internal mass transport). In the case of planar electrodes, both rates are determined by the hydrodynamics of the cell. However, many research groups use their own custom-built cell designs that have different governing hydrodynamics. Often the governing hydrodynamics are not analysed prior to the experiments. Unfortunately, hydrodynamics could have a great influence on the CO_2RR behaviour. For example, Watkins and co-workers showed that the hydrodynamics of the electrochemical cell directly affect the ethylene and methane Tafel slopes [31]. So, comparing the published results of different research groups quantitatively in this respect is difficult. Also, if the hydrodynamics of the cell are not a-priori analysed, researchers do not know when the results are affected by mass transfer limitations. As a result, many published results might be influenced by mass transfer limitations of CO_2 to the surface [32]–[35]. Mass transfer limited results give a skewered representation of reality. However, since the cell designs are often not published or the hydrodynamics of the cell are not defined, it is hard to see what data points are affected

An ideal solution to this problem is to design and employ one standard cell design for all research groups with an enhanced rate of CO_2 mass transfer to the surface. An enhanced mass transfer rate to the surface will allow the researcher to measure the intrinsic rate of conversion over a broader range than without any enhanced mass transfer, as can be seen in Figure 2.1. To this end, Lobacarro and co-workers bubble CO_2 through a PEEK frit into

the cell. Thereby, they enhanced the mass transfer rate of CO_2 through a larger bubble-electrolyte interface, maintained the electrolyte CO_2 concentration during higher current densities, and doubled the methane/hydrogen ratio [36]. Another example of an electrochemical cell with well-defined hydrodynamics is the inverted RDE setup coupled with an online GC setup designed by Garcia et al. [37]. Other examples of RDE setups with online product quantification can be found in literature [38], [39]. An RDE has well-defined hydrodynamics which can be adjusted based on the spin rate. However, it could be difficult to implement a single design for all measurements, as different experiments require different cell configurations or measurements that have specific requirements such as in-situ spectroscopy or high-density measurements. Alternatively, the hydrodynamics of each cell design should be quantified before using it for studies towards catalytic research. Publishing these results will help keep surface conditions consistent between different cell designs and indicate when results may suffer from mass transfer limitations. To determine the hydrodynamics of a cell, one could use the limiting current of ferri-/ferrocyanide redox system on a glassy carbon electrocatalyst or using hexachloroiridate(IV)/hexachloroiridate(III) redox system [40]. From the limiting current, one can derive the mass transfer rate of reactants to the surface and get a corresponding Sherwood number. Using this number, one can estimate the limiting mass transfer rate of CO_2 to the surface during CO_2RR with other catalysts. This technique was applied in chapters 3 and 4 of this thesis. Alternatively, one could use numerical models to estimate the rate of CO_2 transfer [31], [41], [42].

2.4. THE REPORTED STRUCTURE MAY NOT BE THE IN-SITU CATALYST STRUCTURE

Over the last decades, a lot of work has been done to test many different catalyst compositions and structures through a wide variety of production methods. Crucially, CO_2 reduction takes place at the surface of these catalysts. Therefore, it is essential that the local surface composition of the material is accurately described. Unfortunately, this is not always the case. For example, the reported catalyst name is often based on the overall composition of the catalyst, such as the stoichiometric atomic ratio between the two metals that was used during their production [43] or measured using bulk material characterization e.g. inductively coupled plasma atomic emission spectroscopy (ICP-AES) [44]. However, the overall composition is rarely the same as the surface composition. Moreover, even using the surface ratio obtained from XPS [45], [46] or STEM-EDS [35], [47] to name the catalyst, could lead to confusion since the local structure of the catalyst also strongly influences the selectivity of the catalyst [48]. These quantitative overall compositions are irrelevant to catalyst performance and could give a distorted view when comparing the different catalysts.

Moreover, catalyst materials are often only analysed in pristine, ex-situ conditions that often are not maintained under reaction conditions. Firstly, two metals could be fully mixed after the material has been freshly prepared but separated into two distinct phases during the experiment [33], [34], [49], [50]. Phase segregation often happens quickly at the beginning of the experiment and severely alters the performance of the catalyst [34]. A reorganisation of the catalyst structure can also occur depending on the applied potential thereby causing a shift in selectivity [51]. Also, other (Faradaic) processes can influence the surface composition such as surface oxide reduction [33], [34], [52], hydride formation [53], [54], or metal

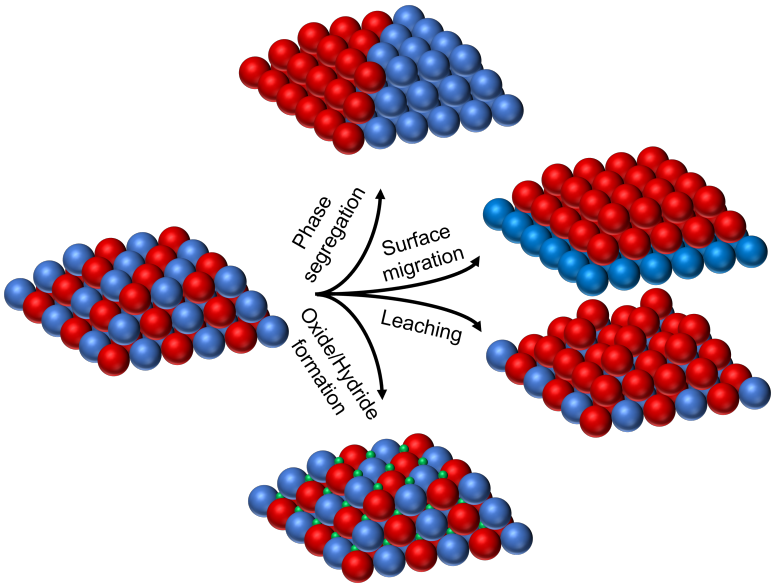

Figure 2.2: Different processes that can occur in-situ during CO_2RR when a potential is applied or when a catalyst comes into contact with an electrolyte.

leaching [55], see figure 2.2.

To prevent these inconsistencies, researchers should not only analyse the catalyst material in pristine, ex-situ conditions but instead probe the surface before, during, and after CO_2 reduction. Ideally, the material should be analysed using in situ material analysis techniques, such as XAFS, ATR-SEIRAS, or Raman spectroscopy [56]. Preferably, multiple techniques should be measured together to get a better picture of the catalyst and what happens during the reaction[57]. However, it is not always possible to know how a material behaves in operando: not all spectroscopy techniques can be used in-situ due to the need for an ultra-high vacuum and in-situ setups are not available everywhere. In that case, it is important that the researcher refrains from drawing definite conclusions regarding the in-operando structure of the catalyst. Additionally, some simple experiments can instead be performed to get some idea of how the catalyst might behave in operando: by performing a postmortem material analysis of the catalyst, one can determine whether phase segregation or leaching has occurred during CO_2 reduction. Furthermore, by performing simple electrochemical techniques such as cyclic voltammetry under both CO_2R and inert conditions, other faradaic processes such as surface reduction or hydride formation can be analysed. Also, researchers can already have an a priori indication of whether a bimetallic catalyst may phase separate using phase diagrams [58] or be reduced in situ using Pourbaix diagrams [59]. Be aware that these diagrams only give the thermodynamically stable phase given certain conditions and provide indication of the rate of phase separation or surface reduction. Also, since the surface pH during CO_2RR varies from the bulk concentration, the catalyst structure could be different than what is obtained from the Pourbaix diagram alone [60].

Given the difficulty in determining the in-situ catalyst structure, it is important that researchers refrain from giving the catalysts in question quantitative names and drawing misleading inferences between the composition and catalytic performance. Rather the catalysts in question should be given arbitrary names or clearly state the bulk composition explicitly to avoid confusion [61]. Also, dynamic in-situ catalyst conditions are not ideal for investigating catalytic processes such as spillover. Instead, only well-defined surfaces should be used to properly investigate these processes [62], [63].

2.5. FUTURE OUTLOOK

Finally, we have several general suggestions that could greatly benefit the field of catalytic CO_2RR. Firstly, further development of high-pressure CO_2 laboratory setups will have several benefits over standard atmospheric CO_2 reduction cells; they have higher mass transport rates to the surface, due to the higher concentration of CO_2 in the bulk. Also, these setups suffer less from bubble formation at the surface due to the enhanced solubility of gaseous products at higher pressures creating a more stable system and finally, the process conditions are much closer to industrial levels, making eventual scale-up much easier.

Furthermore, with the help of a high-pressure setup with controlled hydrodynamics, kinetic testing of catalysts becomes possible. Deriving kinetic rate equations for CO_2RR catalysts under well-defined hydrodynamics is still not widespread in current literature, while it is a great tool to identify rate-determining steps in the complex CO_2 reduction mechanism. Identifying these rate-determining steps can greatly help further catalytic development.

Finally, given the slow rate of catalytic testing and the large number of possible catalysts that are still to be tested, a centralised overview of all tested catalysts should be created between researchers, including the unsuccessful ones. By combining efforts and cooperating, interesting new catalysts can be found faster and more efficiently.

In conclusion, with global attention on sustainable energy solutions, many resources are being directed towards electrochemical CO_2 reduction. However, there is much room for advancement to make better use of the opportunities that are presented. By adopting a more structured approach and standardising certain methods, the discovery of promising new bimetallic catalysts can be further accelerated.

BIBLIOGRAPHY

[1] Y. Hori, K. Kikuchi, and S. Suzuki, "Production of CO and CH_4 in electrochemical reduction of CO_2 at metal electrodes in aqueous hydrogencarbonate solution", *Chemistry Letters*, vol. 14, no. 11, pp. 1695–1698, 1985, ISSN: 1348-0715. DOI: https://doi.org/10.1246/cl.1985.1695.

[2] A. Bagger, W. Ju, A. S. Varela, P. Strasser, and J. Rossmeisl, "Electrochemical reduction: A classification problem", *ChemPhysChem*, vol. 18, no. 22, pp. 3266–3273, 2017, ISSN: 1439-4235. DOI: https://doi.org/10.1002/cphc.201700736.

[3] Y. Peng, M. Cui, Z. Zhang, *et al.*, "Bimetallic composition-promoted electrocatalytic hydrodechlorination reaction on silver–palladium alloy nanoparticles", *ACS Catalysis*, vol. 9, no. 12, pp. 10 803–10 811, 2019, ISSN: 2155-5435. DOI: https://doi.org/10.1021/acscatal.9b02282.

[4] F. Calle-Vallejo, J. Martínez, J. M. García-Lastra, J. Rossmeisl, and M. Koper, "Physical and chemical nature of the scaling relations between adsorption energies of atoms on metal surfaces", *Physical review letters*, vol. 108, no. 11, p. 116 103, 2012. DOI: https://doi.org/10.1103/PhysRevLett.108.116103.

[5] Y. Hori, I. Takahashi, O. Koga, and N. Hoshi, "Electrochemical reduction of carbon dioxide at various series of copper single crystal electrodes", *Journal of Molecular Catalysis A: Chemical*, vol. 199, no. 1-2, pp. 39–47, 2003, ISSN: 1381-1169. DOI: https://doi.org/10.1016/S1381-1169(03)00016-5.

[6] K. J. P. Schouten, E. P. Gallent, and M. T. Koper, "The influence of pH on the reduction of CO and CO_2 to hydrocarbons on copper electrodes", *Journal of Electroanalytical Chemistry*, vol. 716, pp. 53–57, 2014, ISSN: 1572-6657. DOI: https://doi.org/10.1016/j.jelechem.2013.08.033.

[7] A. Murata and Y. Hori, "Product selectivity affected by cationic species in electrochemical reduction of CO_2 and CO at a Cu electrode", *Bulletin of the Chemical Society of Japan*, vol. 64, no. 1, pp. 123–127, 1991, ISSN: 1348-0634. DOI: https://doi.org/10.1246/bcsj.64.123.

[8] S. Popović, M. Smiljanić, P. Jovanovič, J. Vavra, R. Buonsanti, and N. Hodnik, "Stability and degradation mechanisms of copper-based catalysts for electrochemical CO_2 reduction", *Angewandte Chemie*, vol. 132, no. 35, pp. 14 844–14 854, 2020, ISSN: 0044-8249. DOI: https://doi.org/10.1002/anie.202000617.

[9] J. Vavra, G. P. Ramona, F. Dattila, *et al.*, "Solution-based Cu^+ transient species mediate the reconstruction of copper electrocatalysts for CO_2 reduction", *Nature Catalysis*, pp. 1–9, 2024, ISSN: 2520-1158. DOI: https://doi.org/10.1038/s41929-023-01070-8.

[10] J. Greeley, T. F. Jaramillo, J. Bonde, I. Chorkendorff, and J. K. Nørskov, "Computational high-throughput screening of electrocatalytic materials for hydrogen evolution", *Nature materials*, vol. 5, no. 11, pp. 909–913, 2006, ISSN: 1476-1122. DOI: https://doi.org/10.1038/nmat1752.

[11] N. K. Chaudhari, J. Joo, B. Kim, B. Ruqia, S.-I. Choi, and K. Lee, "Recent advances in electrocatalysts toward the oxygen reduction reaction: The case of PtNi octahedra", *Nanoscale*, vol. 10, no. 43, pp. 20 073–20 088, 2018. DOI: https://doi.org/10.1039/C8NR06554C.

[12] C. J. Jacobsen, S. Dahl, B. S. Clausen, S. Bahn, A. Logadottir, and J. K. Nørskov, "Catalyst design by interpolation in the periodic table: Bimetallic ammonia synthesis catalysts", *Journal of the American Chemical Society*, vol. 123, no. 34, pp. 8404–8405, 2001, ISSN: 0002-7863. DOI: https://doi.org/10.1021/ja010963d.

[13] S. Nellaiappan, N. K. Katiyar, R. Kumar, *et al.*, "High-entropy alloys as catalysts for the CO_2 and CO reduction reactions: Experimental realization", *ACS Catalysis*, vol. 10, no. 6, pp. 3658–3663, 2020, ISSN: 2155-5435. DOI: https://doi.org/10.1021/acscatal.9b04302.

[14] N. K. Katiyar, K. Biswas, J.-W. Yeh, S. Sharma, and C. S. Tiwary, "A perspective on the catalysis using the high entropy alloys", *Nano Energy*, vol. 88, p. 106 261, 2021, ISSN: 2211-2855. DOI: https://doi.org/10.1016/j.nanoen.2021.106261.

[15] J. He, N. J. J. Johnson, A. Huang, and C. P. Berlinguette, "Electrocatalytic alloys for CO_2 reduction", *ChemSusChem*, vol. 11, no. 1, pp. 48–57, 2018, ISSN: 1864-5631. DOI: https://doi.org/10.1002/cssc.201701825.

[16] Z. Chen, G. Zhang, H. Chen, J. Prakash, Y. Zheng, and S. Sun, "Multi-metallic catalysts for the electroreduction of carbon dioxide: Recent advances and perspectives", *Renewable and Sustainable Energy Reviews*, vol. 155, p. 111 922, 2022, ISSN: 1364-0321. DOI: https://doi.org/10.1016/j.rser.2021.111922.

[17] S. Nitopi, E. Bertheussen, S. B. Scott, *et al.*, "Progress and perspectives of electrochemical CO_2 reduction on copper in aqueous electrolyte", *Chemical Reviews*, vol. 119, no. 12, pp. 7610–7672, 2019, ISSN: 0009-2665. DOI: https://doi.org/10.1021/acs.chemrev.8b00705.

[18] A. Shinde, R. J. Jones, D. Guevarra, *et al.*, "High-throughput screening for acid-stable oxygen evolution electrocatalysts in the (Mn–Co–Ta–Sb)O_x composition space", *Electrocatalysis*, vol. 6, pp. 229–236, 2015, ISSN: 1868-2529. DOI: https://doi.org/10.1007/s12678-014-0237-7.

[19] F. G. Welsch, K. Stowe, and W. F. Maier, "Fluorescence-based high throughput screening for noble metal-free and platinum-poor anode catalysts for the direct methanol fuel cell", *ACS Combinatorial Science*, vol. 13, no. 5, pp. 518–529, 2011, ISSN: 2156-8952. DOI: https://doi.org/10.1021/000967.

[20] C. Xiang, S. K. Suram, J. A. Haber, *et al.*, "High-throughput bubble screening method for combinatorial discovery of electrocatalysts for water splitting", *ACS combinatorial science*, vol. 16, no. 2, pp. 47–52, 2014, ISSN: 2156-8952. DOI: https://doi.org/10.1021/co400151h.

[21] R. Kortlever, I. Peters, C. Balemans, *et al.*, "Palladium–gold catalyst for the electrochemical reduction of CO_2 to C_1 hydrocarbons", *Chemical Communications*, vol. 52, no. 67, pp. 10 229–10 232, 2016, ISSN: 1359-7345. DOI: https://doi.org/10.1039/C6CC03717H.

[22] J. J. L. Humphrey, D. Plana, V. Celorrio, *et al.*, "Electrochemical reduction of carbon dioxide at gold-palladium core–shell nanoparticles: Product distribution versus shell thickness", *ChemCatChem*, vol. 8, no. 5, pp. 952–960, 2016, ISSN: 1867-3880. DOI: https://doi.org/10.1002/cctc.201501260.

[23] Y. Wang, L. Cao, N. J. Libretto, *et al.*, "Ensemble effect in bimetallic electrocatalysts for CO_2 reduction", *Journal of the American Chemical Society*, 2019, ISSN: 0002-7863. DOI: https://doi.org/10.1021/jacs.9b05766.

[24] C. Hahn, D. N. Abram, H. A. Hansen, *et al.*, "Synthesis of thin film AuPd alloys and their investigation for electrocatalytic CO_2 reduction", *Journal of Materials Chemistry A*, vol. 3, no. 40, pp. 20 185–20 194, 2015, ISSN: 2050-7488. DOI: https://doi.org/10.1039/C5TA04863J.

[25] J.-P. Grote, A. R. Zeradjanin, S. Cherevko, *et al.*, "Screening of material libraries for electrochemical CO_2 reduction catalysts–improving selectivity of Cu by mixing with Co", *Journal of catalysis*, vol. 343, pp. 248–256, 2016, ISSN: 0021-9517. DOI: https://doi.org/10.1016/j.jcat.2016.02.026.

[26] Y. Lai, R. J. Jones, Y. Wang, L. Zhou, M. H. Richter, and J. Gregoire, "The sensitivity of Cu for electrochemical carbon dioxide reduction to hydrocarbons as revealed by high throughput experiments", *Journal of Materials Chemistry A*, vol. 7, no. 47, pp. 26 785–26 790, 2019. DOI: https://doi.org/10.1039/C9TA10111J.

[27] H. Baltruschat, "Differential electrochemical mass spectrometry", *Journal of the American Society for Mass Spectrometry*, vol. 15, no. 12, pp. 1693–1706, 2004, ISSN: 1044-0305. DOI: https://doi.org/10.1016/j.jasms.2004.09.011.

[28] A. H. Wonders, T. H. Housmans, V. Rosca, and M. T. Koper, "On-line mass spectrometry system for measurements at single-crystal electrodes in hanging meniscus configuration", *Journal of applied electrochemistry*, vol. 36, no. 11, pp. 1215–1221, 2006, ISSN: 0021-891X. DOI: http://dx.doi.org/10.1007/s10800-006-9173-4.

[29] E. L. Clark, M. R. Singh, Y. Kwon, and A. T. Bell, "Differential electrochemical mass spectrometer cell design for online quantification of products produced during electrochemical reduction of CO_2", *Analytical chemistry*, vol. 87, no. 15, pp. 8013–8020, 2015, ISSN: 0003-2700. DOI: https://doi.org/10.1021/acs.analchem.5b02080.

[30] E. L. Clark and A. T. Bell, "Direct observation of the local reaction environment during the electrochemical reduction of CO_2", *Journal of the American Chemical Society*, vol. 140, no. 22, pp. 7012–7020, 2018, ISSN: 0002-7863. DOI: https://doi.org/10.1021/jacs.8b04058.

[31] N. B. Watkins, Z. J. Schiffer, Y. Lai, *et al.*, "Hydrodynamics change tafel slopes in electrochemical CO_2 reduction on copper", *ACS Energy Letters*, vol. 8, pp. 2185–2192, 2023, ISSN: 2380-8195. DOI: https://doi.org/10.1021/acsenergylett.3c00442.

[32] D. Ren, B. S.-H. Ang, and B. S. Yeo, "Tuning the selectivity of carbon dioxide electroreduction toward ethanol on oxide-derived Cu_xZn catalysts", *ACS Catalysis*, vol. 6, no. 12, pp. 8239–8247, 2016, ISSN: 2155-5435. DOI: https://doi.org/10.1021/acscatal.6b02162.

[33] S. Kunze, P. Grosse, M. Bernal Lopez, *et al.*, "Operando NRIXS and XAFS investigation of segregation phenomena in Fe and Fe nanoparticle catalysts during CO_2 electroreduction", *Angewandte Chemie*, vol. 132, no. 50, pp. 22 856–22 863, 2020, ISSN: 0044-8249. DOI: https://doi.org/10.1002/anie.202010535.

[34] N. Martić, C. Reller, C. Macauley, *et al.*, "$Ag_2Cu_2O_3$ – a catalyst template material for selective electroreduction of CO to C_{2+} products", *Energy & Environmental Science*, vol. 13, no. 9, pp. 2993–3006, 2020. DOI: https://doi.org/10.1039/d0ee01100b.

[35] C.-J. Chang, S.-C. Lin, H.-C. Chen, *et al.*, "Dynamic reoxidation/reduction-driven atomic interdiffusion for highly selective reduction toward methane", *Journal of the American Chemical Society*, vol. 142, no. 28, pp. 12 119–12 132, 2020, ISSN: 0002-7863. DOI: https://doi.org/10.1021/jacs.0c01859.

[36] P. Lobaccaro, M. R. Singh, E. L. Clark, Y. Kwon, A. T. Bell, and J. W. Ager, "Effects of temperature and gas–liquid mass transfer on the operation of small electrochemical cells for the quantitative evaluation of CO_2 reduction electrocatalysts", *Physical Chemistry Chemical Physics*, vol. 18, no. 38, pp. 26 777–26 785, 2016. DOI: https://doi.org/10.1039/C6CP05287H.

[37] P. Moreno-García, N. Kovács, V. Grozovski, M. d. J. Gálvez-Vázquez, S. Vesztergom, and P. Broekmann, "Toward CO_2 electroreduction under controlled mass flow conditions: A combined inverted RDE and gas chromatography approach", *Analytical chemistry*, vol. 92, no. 6, pp. 4301–4308, 2020, ISSN: 0003-2700. DOI: https://doi.org/10.1021/acs.analchem.9b04999.

[38] S. Jung, R. Kortlever, R. J. Jones, *et al.*, "Gastight hydrodynamic electrochemistry: Design for a hermetically sealed rotating disk electrode cell", *Analytical chemistry*, vol. 89, no. 1, pp. 581–585, 2017, ISSN: 0003-2700. DOI: https://doi.org/10.1021/acs.analchem.6b04228.

[39] J. Jang, M. Rüscher, M. Winzely, and C. G. Morales-Guio, "Gastight rotating cylinder electrode: Toward decoupling mass transport and intrinsic kinetics in electrocatalysis", *AIChE Journal*, vol. 68, no. 5, e17605, 2022, ISSN: 0001-1541. DOI: https://doi.org/10.1002/aic.17605.

[40] S. Petrovic, "Cyclic voltammetry of hexachloroiridate (iv): An alternative to the electrochemical study of the ferricyanide ion", *The Chemical Educator*, vol. 5, pp. 231–235, 2000. DOI: https://doi.org/10.1007/s00897000416a.

[41] N. Gupta, M. Gattrell, and B. MacDougall, "Calculation for the cathode surface concentrations in the electrochemical reduction of CO_2 in $KHCO_3$ solutions", *Journal of applied electrochemistry*, vol. 36, no. 2, pp. 161–172, 2006, ISSN: 0021-891X. DOI: http://doi.org/10.1007/s10800-005-9058-y.

[42] A. R. Morrison, V. van Beusekom, M. Ramdin, L. J. van den Broeke, T. J. Vlugt, and W. de Jong, "Modeling the electrochemical conversion of carbon dioxide to formic acid or formate at elevated pressures", *Journal of The Electrochemical Society*, vol. 166, no. 4, E77, 2019, ISSN: 1945-7111. DOI: https://doi.org/10.1149/2.0121904jes.

[43] A. M. Ismail, G. F. Samu, H. C. Nguyën, E. Csapó, N. López, and C. Janáky, "Au/Pb interface allows the methane formation pathway in carbon dioxide electroreduction", *ACS catalysis*, vol. 10, no. 10, pp. 5681–5690, 2020, ISSN: 2155-5435. DOI: https://doi.org/10.1021/acscatal.0c00749.

[44] D. Chen, Y. Wang, D. Liu, *et al.*, "Surface composition dominates the electrocatalytic reduction of on ultrafine CuPd nanoalloys", *Carbon Energy*, vol. 2, no. 3, pp. 443–451, 2020, ISSN: 2637-9368. DOI: https://doi.org/10.1002/cey2.38.

[45] S. Chandrashekar, N. T. Nesbitt, and W. A. Smith, "Electrochemical reduction over bimetallic Au thin films: Comparing activity and selectivity against morphological, compositional, and electronic differences", *The Journal of Physical Chemistry C*, vol. 124, no. 27, pp. 14 573–14 580, 2020, ISSN: 1932-7447. DOI: https://doi.org/10.1021/acs.jpcc.0c01894.

[46] W. Luc, C. Collins, S. Wang, *et al.*, "Ag bimetallic catalyst with a core–shell structure for CO_2 reduction", *Journal of the American chemical society*, vol. 139, no. 5, pp. 1885–1893, 2017, ISSN: 0002-7863. DOI: https://doi.org/10.1021/jacs.6b10435.

[47] Y. Takatsuji, I. Nakata, M. Morimoto, T. Sakakura, R. Yamasaki, and T. Haruyama, "Highly selective methane production through electrochemical CO_2 reduction by electrolytically plated Cu – Co electrode", *Electrocatalysis*, vol. 10, pp. 29–34, 2019, ISSN: 1868-2529. DOI: https://doi.org/10.1007/s12678-018-0492-0.

[48] S. Ma, M. Sadakiyo, M. Heima, *et al.*, "Electroreduction of carbon dioxide to hydrocarbons using bimetallic Cu catalysts with different mixing patterns", *Journal of the American Chemical Society*, vol. 139, no. 1, pp. 47–50, 2017, ISSN: 0002-7863. DOI: https://doi.org/10.1021/jacs.6b10740.

[49] E. L. Clark, C. Hahn, T. F. Jaramillo, and A. T. Bell, "Electrochemical reduction over compressively strained CuAg surface alloys with enhanced multi-carbon oxygenate selectivity", *Journal of the American Chemical Society*, vol. 139, no. 44, pp. 15 848–15 857, 2017, ISSN: 0002-7863. DOI: https://doi.org/10.1021/jacs.7b08607.

[50] M. Bernal, A. Bagger, F. Scholten, *et al.*, "CO_2 electroreduction on copper-cobalt nanoparticles: Size and composition effect", *Nano Energy*, vol. 53, pp. 27–36, 2018, ISSN: 2211-2855. DOI: https://doi.org/10.1016/j.nanoen.2018.08.027.

[51] J. S. Jirkovský, I. Panas, S. Romani, E. Ahlberg, and D. J. Schiffrin, "Potential-dependent structural memory effects in Au nanoalloys", *The Journal of Physical Chemistry Letters*, vol. 3, no. 3, pp. 315–321, 2012, ISSN: 1948-7185. DOI: https://doi.org/10.1021/jz201660t.

[52] Y. Hori, A. Murata, S.-y. Ito, Y. Yoshinami, and O. Koga, "Nickel and iron modified copper electrode for electroreduction of CO_2 by in-situ electrodeposition", *Chemistry Letters*, vol. 18, no. 9, pp. 1567–1570, 1989, ISSN: 1348-0715. DOI: https://doi.org/10.1246/cl.1989.1567.

[53] J. H. Lee, S. Kattel, Z. Jiang, *et al.*, "Tuning the activity and selectivity of electroreduction of CO_2 to synthesis gas using bimetallic catalysts", *Nature Communications*, vol. 10, no. 1, p. 3724, 2019, ISSN: 2041-1723. DOI: https://doi.org/10.1038/s41467-019-11352-0.

[54] K. Ohkawa, K. Hashimoto, A. Fujishima, Y. Noguchi, and S. Nakayama, "Electrochemical reduction of carbon dioxide on hydrogenstoring materials: Part 1. the effect of hydrogen absorption on the electrochemical behavior on palladium electrodes", *Journal of Electroanalytical Chemistry*, vol. 345, no. 1-2, pp. 445–456, 1993, ISSN: 1572-6657. DOI: https://doi.org/10.1016/0022-0728(93)80495-4.

[55] K. Sun, T. Cheng, L. Wu, *et al.*, "Ultrahigh mass activity for carbon dioxide reduction enabled by gold–iron core–shell nanoparticles", *Journal of the American Chemical Society*, vol. 139, no. 44, pp. 15 608–15 611, 2017, ISSN: 0002-7863. DOI: https://doi.org/10.1021/jacs.7b09251.

[56] J. De Ruiter, H. An, L. Wu, *et al.*, "Probing the dynamics of low-overpotential CO_2-to-CO activation on copper electrodes with time-resolved raman spectroscopy", *Journal of the American Chemical Society*, vol. 144, no. 33, pp. 15 047–15 058, 2022, ISSN: 0002-7863. DOI: https://doi.org/10.1021/jacs.2c03172.

[57] W. van der Stam, "The necessity for multiscale in situ characterization of tailored electrocatalyst nanoparticle stability", *Chemistry of Materials*, vol. 35, no. 2, pp. 386–394, 2023, ISSN: 0897-4756. DOI: https://doi.org/10.1021/acs.chemmater.2c03286.

[58] H. Okamoto, *Desk handbook: phase diagrams for binary alloys*, 1st ed. Materials Park: ASM International, 2000, ISBN: 0871706822 9780871706829.

[59] M. Pourbaix, *Atlas of Electrochemical Equilibria in Aqueous Solutions*, 2nd ed. National Association of Corrosion Engineers, 1974, p. 644, ISBN: 9780915567980. [Online]. Available: https://books.google.nl/books?id=QjxRAAAAMAAJ.

[60] A. Dutta, A. Kuzume, M. Rahaman, S. Vesztergom, and P. Broekmann, "Monitoring the chemical state of catalysts for electroreduction: An in operando study", *ACS Catalysis*, vol. 5, no. 12, pp. 7498–7502, 2015, ISSN: 2155-5435. DOI: https://doi.org/10.1021/acscatal.5b02322.

[61] X. Zhang, C. Liu, Y. Zhao, *et al.*, "Atomic nickel cluster decorated defect-rich copper for enhanced C_2 product selectivity in electrocatalytic CO_2 reduction", *Applied Catalysis B: Environmental*, vol. 291, p. 120 030, 2021, ISSN: 0926-3373. DOI: https://doi.org/10.1016/j.apcatb.2021.120030.

[62] G. O. Larrazábal, T. Shinagawa, A. J. Martín, and J. Pérez-Ramírez, "Microfabricated electrodes unravel the role of interfaces in multicomponent copper-based CO_2 reduction catalysts", *Nature Communications*, vol. 9, no. 1, p. 1477, 2018, ISSN: 2041-1723. DOI: https://doi.org/10.1038/s41467-018-03980-9.

[63] Y. Lum and J. W. Ager, "Sequential catalysis controls selectivity in electrochemical CO_2 reduction on Cu", *Energy & Environmental Science*, vol. 11, no. 10, pp. 2935–2944, 2018. DOI: https://doi.org/10.1039/C8EE01501E.

3

The Effect of Surface Conditions on the Electrochemical CO_2 Reduction Performance of Bimetallic AuPd Electrocatalysts

Renewable energy-based production of chemicals through electrochemical CO_2 conversion has gained a lot of interest and has a vital role in the energy transition. Most research into electrochemical CO_2 conversion focuses on improving electrode materials. However, the role of the electrolyte (buffer) is often not taken into account, thereby creating a one-sided view of the process. Here we show the influence of two buffers, $KHCO_3$ and KH_2PO_4/K_2HPO_4, on the selectivity of a bimetallic gold-palladium electrode in an effort to elucidate observed inconsistencies between different studies into this metal combination. The results show that while hydrocarbons are produced in the phosphate buffer, they remain absent in the bicarbonate buffer. Further investigation reveals that the difference in buffer strength between both electrolytes causes the difference in activity. These results show that the electrolyte choice plays a crucial role in determining the selectivity of the electrode and therefore must be considered during catalyst development for CO_2 electrochemical reduction.

This chapter has been published in https://doi.org/10.1039/D3CY01411H

3.1. INTRODUCTION

In order to shift away from fossil resources as main source for fuels and bulk chemicals, new and sustainable production processes based on renewable energy inputs need to be developed. Interest in the electrochemical reduction of CO_2 to base chemicals such as CO, methane and ethylene has therefore significantly increased in the last decades. Copper-based electrode materials have been the main focus of research, ever since the discovery by Hori and co-workers that copper is able to reduce CO_2 to hydrocarbons and alcohols [1]. However, copper produces a wide range of C_1-C_3 products, with limited selectivity towards one product [2], [3]. The selectivity of a monometallic copper electrode can be tuned by controlling the local conditions at the surface and by coating the electrode with organic layers [4]–[6]. Alternatively, the design of multimetallic catalysts provides a means to tailor the electronic and structural properties, thereby modifying its catalytic properties. Many recent studies have been devoted to investigating the electrocatalytic properties of copper-based alloys [4], [7]–[10]. In most cases, these copper-based alloys were not able to outperform the intrinsic activity of copper towards the production of multi-carbon hydrocarbons. However, some alloys display higher selectivities towards CO or suppress the hydrogen evolution reaction (HER), such as CuAg or CuIn alloys [4], [7], [11].

So far, only two classes of copper-free alloys have been found that are able to produce hydrocarbon products. The first are combinations of nickel and group 13 metals (aluminium, gallium) that produce C_1-C_3 products [12]–[14], and the second are gold palladium combinations that have yielded C_1-C_5 products [15], [16]. The Ni-Ga combination was chosen following DFT-calculations of oxygen-adsorption energies for several alloys. Here, the oxygen-adsorption energy of a material was found to be determining for its catalytic activity of the thermochemical CO_2 reduction towards methanol [17]. For AuPd, the combination of metals was chosen to optimally bind CO_{ads} to the electrode surface. The CO_{ads} intermediate is important for CO_2 reduction towards further reduced products; if the intermediate is bound too weakly, it will desorb before it can be reduced further, which is the case for a gold electrode, while if CO_{ads} is bound too strongly, which is the case for a palladium electrode, it is not energetically favourable to reduce it further and little to no CO_2 reduction products will be observed [18]. By bringing both metals together on the same surface, the binding energies of the metals to CO_{ads} will be "averaged" leading to further reduction of CO_{ads} to hydrocarbons [19].

Interestingly, studies into electrochemical reduction of CO_2 on AuPd obtained different findings; Kortlever et al. studied palladium electrodeposited on a polycrystalline gold foil in a 0.1 M KH_2PO_4 + 0.1 M K_2HPO_4 buffer (pH = 6.7) and observed a mixture of C_1-C_5 products from an onset potential of -0.8 V vs. RHE [15]. Humphrey et al. investigated the same metal combination as core-shell nanoparticles in a 0.1 M Na_2SO_4 electrolyte at pH 4 with different shell thicknesses of palladium. In their study, hydrocarbons (C_1-C_2) and formate were observed with nanoparticles with a Pd shell thickness of 5 nm or higher, while thinner Pd shells only produced CO and H_2 [16]. Contrary to previous studies, Wang et al. did not observe any hydrocarbon formation when studying AuPd nanoparticles with varying Pd surface compositions in 0.1 M $KHCO_3$ [20]. Neither did Hahn et al. when investigating different compositions of thin film AuPd alloys in a 0.1 M $KHCO_3$ buffer [21]. To elucidate the origin of the differences in observed product selectivity between the aforementioned studies, electrodeposited palladium on a gold surface was studied in aqueous 0.1 M $KHCO_3$

and 0.1 M KH_2PO_4 + 0.1 M K_2HPO_4 electrolytes. As a comparison, electrodeposited palladium on a glassy carbon electrode and a polycrystalline gold electrode were studied in both buffers to investigate the effect on the separate counterparts.

3.2. Experimental

3.2.1. Materials

All solutions were prepared using ultrapure water (Millipore Milli-Q IQ 7000 system, 18 MΩcm) and reagents of trace metal purity. Electrolytes were prepared from KH_2PO_4 (99.995 %, Supelco), K_2HPO_4 (99.99%, Supelco) and $KHCO_3$ (≥ 99.95%, Sigma-Aldrich). Polycrystalline gold foils (25x25x1 mm, 99.995%) were obtained from MaTecK GmbH, while glassy carbon electrodes (25x25x1 mm) were purchased from HTW (Sigradur®, polished). As counter electrode either a platinum foil (MaTeck Gmbh, 25x25x0.1 mm, 99.995%) or glassy carbon electrode (HTW, Sigradur®, polished) was used.

3.2.2. Electrochemical Measurements

Prior to all measurements, the resistance of the system was determined using potentiostatic electrochemical impedance spectroscopy (PEIS) at open circuit potential on a Biologic 200 SP potentiostat. The potentiostat corrected for 85% of the ohmic drop during the measurement, while the remaining 15% was manually compensated. All potentials were converted to the RHE scale, unless mentioned otherwise, using $V_{RHE} = V_{(Ag/AgCl)} + 0.197 + 0.059 \cdot pH_{bulk}$.

Chronoamperometry measurements were performed for 1 hour to determine the electrocatalytic performance. The measurements were carried out in a custom-made electrochemical cell made of PEEK consisting of a cathodic and anodic compartment separated by a Selemion membrane (ForBlue Selemion AMVN, AGC Engineering, Japan), following the design from Lobacarro et al. [22]. The cell compartments were stored in 20 vol.% HNO_3 (Sigma, ACS reagent, 70%) overnight and washed with ultrapure water prior to each experiment. The electrode of interest was used as working electrode, while platinum foil (25x25x0.1 mm, 99.995 %, MaTeck GmbH) was used as a counter electrode. The electrodes were held in place by copper tape (AT528, Advance Tapes), which also provided electrical connection to the potentiostat. A leak-free Ag/AgCl electrode (LF-1.6-48, Innovative Instruments) was used as a reference electrode. The leak-free electrode was stored in 3.0 M KCl saturated with silver chloride (Supelco).

Prior to the experiment, each cell compartment was filled with 1.8 mL of the electrolyte. Humidified CO_2 gas (4.5 N, Linde Benelux B.V., The Netherlands) was flown through the cathodic compartment with a flow rate of 8 mL_n/min for at least 15 minutes to remove any other (dissolved) gasses and to saturate the electrolyte. The CO_2 gas flow was maintained over the duration of the chronoamperometry measurement to supply fresh CO_2 and remove any formed gaseous products from the cathode compartment headspace. The outgoing gas stream was sampled every 2 minutes by an inline gas chromatograph (Compact GC 4.0, GAS). The GC was calibrated with a series of calibration gasses containing product gasses with concentrations in the range of 50 ppm – 8000 ppm, balanced with CO_2 (Linde Benelux B.V., The Netherlands). The faradaic efficiencies and partial currents for gaseous products during chronoamperometry measurements were determined by averaging the measured

values between 34 min and 55 min after the start of the chronoamperometry measurement. After the experiment, the electrolyte in the cathodic chamber was collected and 100 µL was injected into a high-performance liquid chromatograph (HPLC, Agilent Technologies 1260 Infinity, USA) to quantify the formed liquid products. The HPLC was calibrated with a dilution series in the range of 0.01 mM to 5 mM of formic acid (95%, Sigma–Aldrich). The flowrate of the eluent (1 mM H_2SO_4 (aq)) was set to 0.6 mL min^{-1} and the measurement ran for one hour. The HPLC used two Aminex HPX-87H columns (Biorad) in series heated to 60 °C. A refractive index detector (RID) was used for the detection of products.

3.2.3. ELECTRODE PREPARATION

Three electrodes were examined as working electrode: polycrystalline gold (Au), palladium electrodeposited on polycrystalline gold foil (AuPd) and palladium electrodeposited on glassy carbon (Pd/C).

Prior to every measurement, the platinum counter electrode was washed with ultrapure water and flame annealed until the surface glowed red-hot. Polycrystalline gold foil was first wetted and manually sanded using ultrafine sandpaper (2000, Struers, USA) for one to two minutes to make sure any contaminants were removed from the surface. After sanding, the electrode was washed using ultrapure water, subsequently dried using compressed air, and flame annealed to the point that the electrode glowed red hot to remove any organics left on the surface. Glassy carbon electrodes were first cleaned using acetone to remove any left-over glue on the surface from the copper tape used in the previous experiments. Next, the electrode was ultrasonicated using ultrapure water for at least 15 minutes and manually polished for one to two minutes using undiluted alumina paste and a microfiber cloth (DP-floc, Struers, USA). After another washing step with ultrapure water, the electrode was ultrasonicated in water for 15 minutes to remove any residual alumina particles from the surface. Subsequently, the electrodes were ultrasonicated for 15 min in 20 vol.% HNO_3 (aq) (Sigma-Aldrich, ACS reagent grade, 70%) solution to make sure all leftover alumina dissolved from the electrode surface. Then, the electrode was washed and ultrasonicated for at least 15 minutes using ultrapure water to ensure all acid was removed from the electrode. Finally, the electrodes were dried using compressed air.

The AuPd and Pd/C electrodes were prepared using the cleaned gold foil or glassy carbon electrode respectively, following the procedure of Kortlever et al. [15]. In short, the freshly cleaned electrode was placed in a single compartment cell with one side of the electrode exposed to electrolyte. A glassy carbon counter electrode was placed perpendicular to the working electrode. A leakless Ag/AgCl electrode (LF-1.6-100, Innovative Instruments) was used as reference electrode and the electrolyte chamber was filled with a 0.1 M H_2SO_4 (Sigma-Aldrich, ACS reagent grade, 95.0-98.0%) + 1 mM $PdCl_2$ (Alfa Aesar, Premion, 99.999%) solution. After performing potentiostatic electrochemical impedance spectroscopy (PEIS) at open circuit potential to determine the resistance of the setup, chronoamperometry was performed at 0.315 V vs. Ag/AgCl for 60 seconds. During the process, palladium ions from the solution were reduced and deposited on the surface of the electrode.

3.2.4. Material analysis

X-ray photoemission spectroscopy (XPS) spectra were obtained using a Thermo Scientifc Kα spectrometer utilizing a monochromatic Al Kα excitation source. The base pressure inside the analysis chamber was about $2 \cdot 10^{-9}$ mbar. High resolution XPS spectra were recorded using 400 mm spot size, 0.1 eV step size and 50 eV pass energy (200 eV for the survey). All spectra were charge-corrected to the C 1s adventitious carbon (284.8 eV). The obtained XPS spectra were deconvoluted with CasaXPS v2.3 software. Scanning electron microscopy (SEM) images were obtained using JEOL 6500F microscope at an acceleration voltage of 15 kV, coupled with an energy dispersed X-ray analysis detector (Ultradry, Thermo Scientific).

3.3. Results & Discussion

In Figure 3.1, SEM images of the gold-palladium electrode can be found. The images show a fairly uniform surface except for some bright and dark spots, which is further supported by the XPS data of the electrode (appendix A section A.2). In Figure 3.2A-C, the EDX mapping image shows that these dark spots on the SEM image are not identified as either gold, palladium, or any other element. Therefore, these dark spots are assumed to be small cavities in the electrode. Lighter streaks on the SEM image can be excess islands of gold as they are also observed on the pure gold electrode (see Figure 3.1C and 3.1D), taking into account that no other element was detected by the EDX mapping (see Figure A.1). In contrast, palladium forms small particles when electrodeposited on the glassy carbon rather than forming a uniform monolayer. The difference is clearly visible from the SEM images of the Pd/C (Figure 3.1E and 3.1F). The particles were confirmed as palladium using EDX mapping of the surface (Figure 3.2D-3.2F).

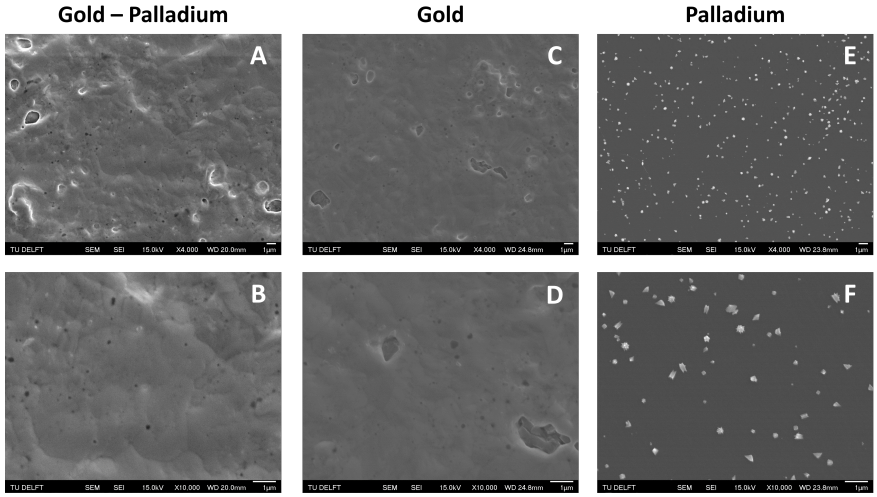

Figure 3.1: Scanning electron microscopy (SEM) images of electrodeposited palladium on a gold electrode (A & B), pure gold electrode (C & D), and electrodeposited palladium on a glassy carbon electrode (E & F) at different magnifications.

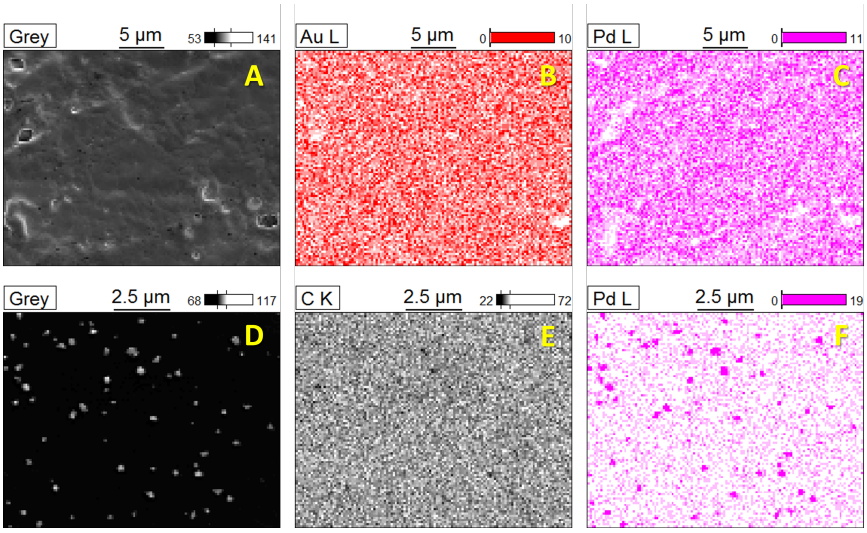

Figure 3.2: Elemental mapping of the gold-palladium electrode surface (A-C) and electrodeposited palladium on a glassy carbon electrode (D-F) using energy-dispersive X-ray spectroscopy (EDX)

Both palladium and gold are identified on the AuPd surface by XPS (see Figure A.2 in appendix A). The Pd 3d spectra have two predominant metallic Pd peaks at 335 eV and 341.3 eV, which matches the peaks of the palladium foil (Figure A.3 in Appendix A). On the gold-palladium and palladium foil, the inevitable formation of Pd-oxide species was observed at 336.1 eV and 337.5 eV. The sharp peaks in the Au $4f_{7/2}$ spectra at 83.9 eV do not show a negative shift of 0.6-0.8 eV with respect to the metallic Au state (Figure A.4 in Appendix A). The absence of this shift suggests that a layer of metallic Pd covers the Au foil rather than that the gold and palladium have formed an alloyed phase [23], [24].

The faradaic efficiencies toward the major products on all three electrodes in the phosphate buffer are shown in Figure 3.3A, 3.3C and 3.3E for gold-palladium, gold, and palladium, respectively. The partial current densities towards the major products on the same electrodes are shown in Figure 3.4A, 3.4C, and 3.4E. Using the phosphate buffer, small amounts of hydrocarbons with partial current densities between a few and tens of microamperes are observed on all electrodes. These results agree fairly well with literature results, as Kortlever et al. observed hydrocarbons within the C_1-C_5 range with a higher selectivity in the same phosphate buffer [15]. The difference in selectivity can be explained by a difference in cell hydrodynamics between both studies since both studies used different cell setups. Also, while only hydrocarbons in the C_1-C_2 range could be quantified in this study, propane/propene was observed qualitatively. However, since the gas chromatograph was not calibrated for propane or propene, these products are not included in the figures. Higher hydrocarbons (C_4-C_5) are not observed, meaning that if they were produced their concentrations remained under the limit of detection. On gold small amounts of hydrocarbons were observed in the phosphate buffer with a faradaic efficiency of around 0.2 % at 0.8 V vs. RHE, which agrees with the findings of Noda and co-workers [25]. Using a phosphate electrolyte of pH 6.8, they observed small amounts of hydrocarbons with a selectivity

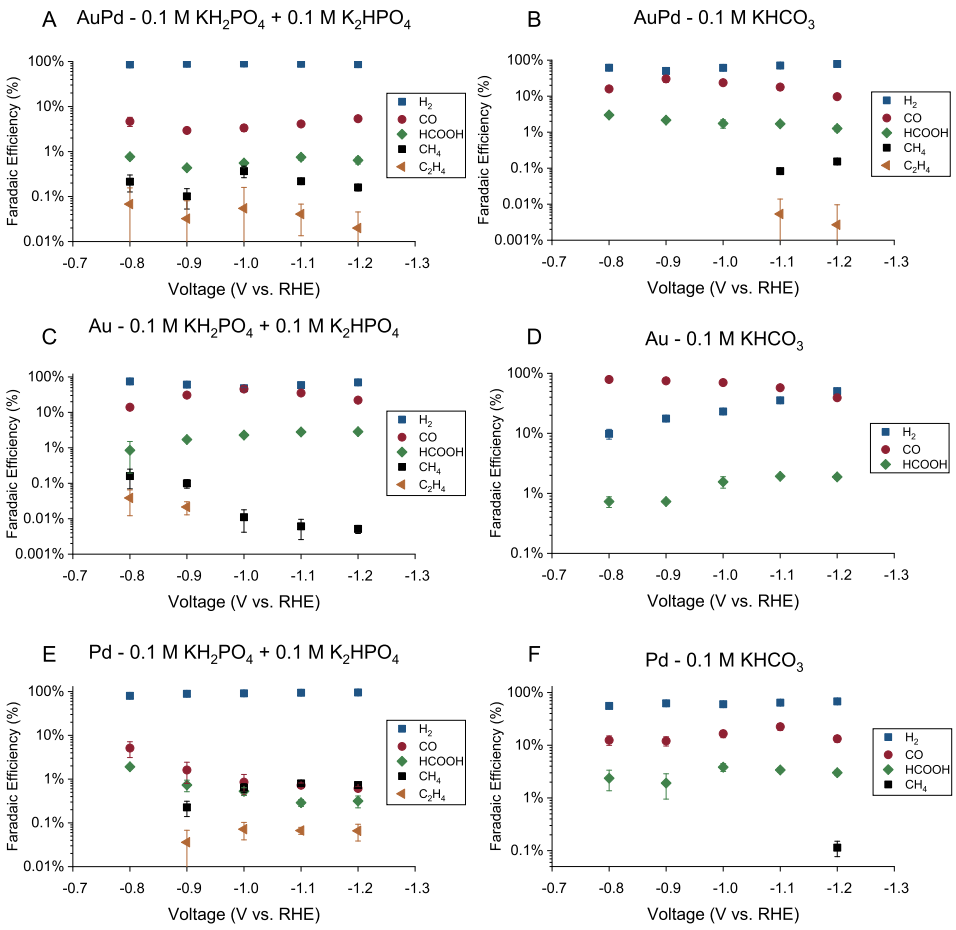

Figure 3.3: Faradaic efficiencies for CO_2 reduction for gold-palladium, gold, and palladium electrode in both phosphate (0.1 M KH_2PO_4/ 0.1 M K_2HPO_4) and bicarbonate (0.1 M $KHCO_3$) electrolyte. The major products observed on the electrodes are hydrogen (■), carbon monoxide (●), formate (◆), methane (■), and ethene (◀). The error bars show the standard deviation over the triplicate results.

of 0.6 % at -0.8 V vs. RHE on a polycrystalline gold electrode. The difference in selectivity could again be attributed to differences in cell hydrodynamics.

The faradaic efficiencies toward the major products on all three electrodes in the bicarbonate buffer are shown in Figure 3.3B, 3.3D and 3.3F for gold-palladium, gold, and palladium respectively. The partial current densities towards the major products on the same electrodes are shown in Figure 3.4B, 3.4D, and 3.4F. Interestingly, these results show that while hydrocarbons are produced in the phosphate electrolyte, they remain mostly absent in the bicarbonate electrolyte or are produced at much smaller rates. For AuPd, hydrocarbons were observed at more negative potentials in the bicarbonate electrolyte in comparison to

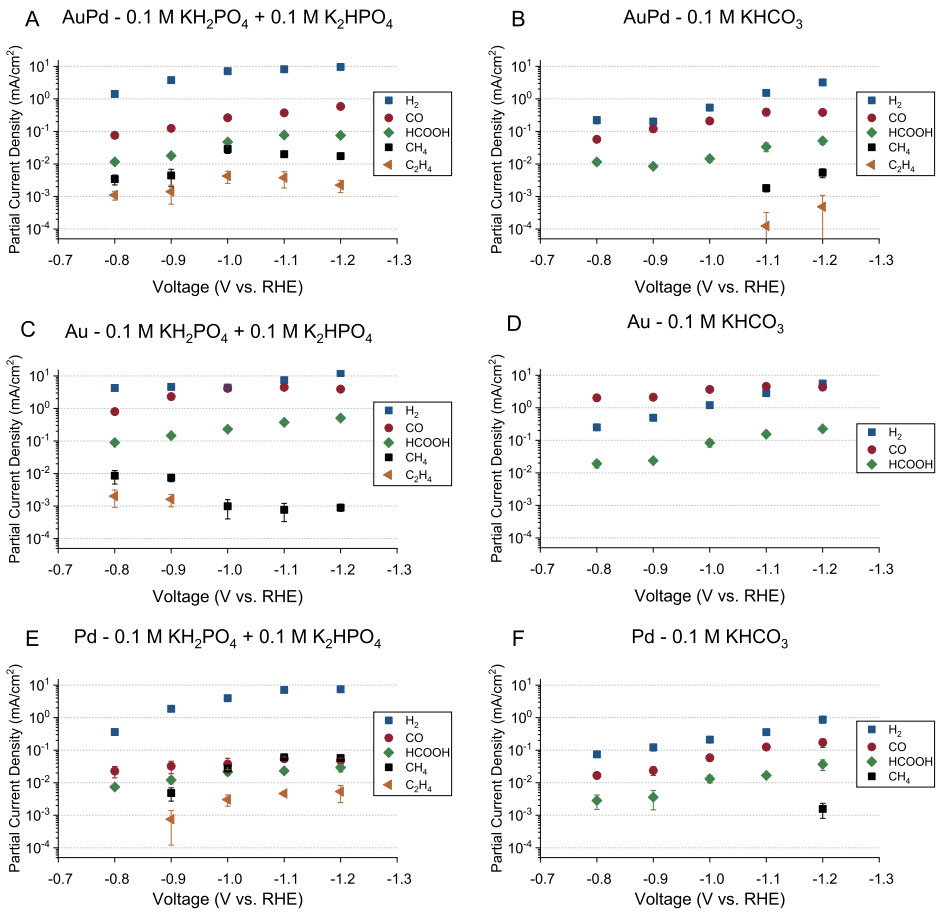

Figure 3.4: Partial current densities for CO_2 reduction for gold-palladium, gold, and palladium electrode in both phosphate (0.1 M KH_2PO_4/0.1 M K_2HPO_4) and bicarbonate (0.1 M $KHCO_3$) electrolyte. The major products observed on the electrodes are hydrogen (■), carbon monoxide (●), formate (◆), methane (■), and ethene (◀). The error bars show the standard deviation over the triplicate results.

the phosphate electrolyte, with methane and ethylene production at -1.1 V and -1.2 V vs. RHE. In the literature, AuPd in a bicarbonate electrolyte was only tested up to a potential of -1.0 V vs. RHE in the case of Hahn et al. [21], while Wang and co-workers only tested up to a potential of -0.8 V. Hori et al. report that a small amount of methane (2.9 % selectivity) is produced on palladium in 0.1 M $KHCO_3$, with a total faradaic efficiency balance of 60% [18]. This discrepancy in the total faradaic efficiency was explained by the absorption of hydrogen into the electrode. Additionally, Azuma and co-workers observed small amounts of hydrocarbons ($C_1 - C_6$) on a palladium electrode in a 0.05 M $KHCO_3$ electrolyte at -2.16 V vs. RHE [26]. Their obtained selectivities of the hydrocarbons decrease with increasing hydrocarbon size from 0.3 % for methane to about 0.001 % for the highest hydrocarbons.

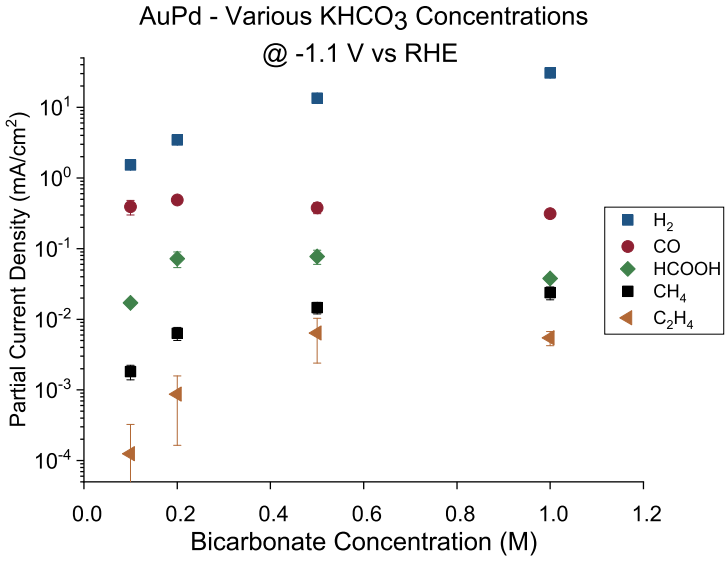

Figure 3.5: Partial current densities for CO_2 reduction for gold-palladium, gold, and palladium electrode in increasingly more concentrated bicarbonate (0.1 M $KHCO_3$) electrolyte. The major products observed on the electrodes are hydrogen (■), carbon monoxide (●), formate (◆), methane (■), and ethene (◀). The error bars show the standard deviation over the triplicate results.

Other major reduction products also follow a similar trend in the two electrolytes for all electrodes. The HER activity and formate production rate are higher in the phosphate electrolyte compared to the bicarbonate electrolyte. On the other hand, the activity towards CO production remains mostly unaffected by the electrolyte choice. However, we note that on the gold electrode, CO production tapers off around 4.5 mA cm^{-2} in both buffers. A stagnation in production rate could indicate either a kinetic limitation of the catalyst or a limitation of CO_2 transfer to the electrode. To assess this hypothesis, the hydrodynamics of the cell setup were measured using the ferro-/ferricyanide redox couple. The experimental approach and results can be found in the appendix (section A.3). From the calculations, it is estimated that when the CO_2 consumption rate exceeded 27 nmol s^{-1}, the concentration of CO_2 at the surface reaches zero and its transport rate becomes mass transfer limited. The consumption rate of CO_2 on gold in both buffers approached 25 nmol s^{-1} (see Table A.2). Hence, the CO_2 reduction on the gold electrode was mass transfer limited for both buffers over the whole potential range.

In summary, the dependency of the product selectivity upon the choice of electrolyte shows that apart from the catalyst material, the local conditions at the electrode play a key role. The cause of this dependency could be due to the different anions that enhance or impede the formation of products on the electrode. Alternatively, since the buffer strength of the phosphate buffer is higher than the bicarbonate buffer, the buffer strength of the electrolyte could influence the formation of hydrocarbons by causing different surface conditions (for instance, differences in local pH and CO_2 availability). To determine the cause for the

observed differences, the AuPd catalyst activity was measured in a series of electrolytes with increasing bicarbonate concentration at a fixed potential. The purpose of these experiments is two-fold: if the cause for the observed difference is due to buffer strength, increasing the buffer strength will mimic the conditions of the phosphate buffer and an enhancement in the formation of hydrocarbons is expected. However, if the observed differences are due to the different anions, an increased presence of HCO_3^- or CO_3^{2-} would not yield any significant differences. The potential chosen for these experiments was -1.1 V vs. RHE, since this is the lowest potential at which hydrocarbons were observed initially in the 0.1 M bicarbonate electrolyte. In Figure 3.5, the partial current densities are shown for AuPd at -1.1 V vs. RHE in bicarbonate buffers with increasing $KHCO_3$ concentration. Hydrogen, formate, and hydrocarbon production rates all increase linearly with $KHCO_3$ concentration. Meanwhile, the CO activity remains mostly unaffected by the changing buffer strength. If the presence of HCO_3^- or CO_3^{2-} would impede the reactions towards certain products, the production rates towards hydrogen, formate, and hydrocarbons should not have increased with increasing buffer concentration. Therefore, based on these results, we conclude that it is the difference in buffer strength between the phosphate and bicarbonate electrolyte that leads to the earlier observed differences in product activities.

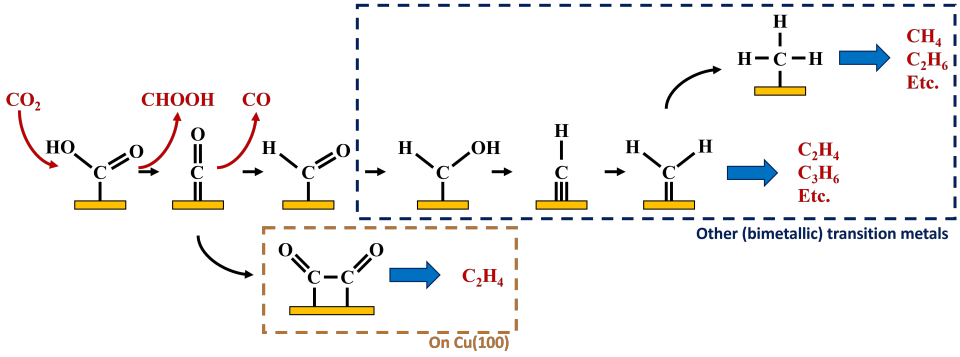

Figure 3.6: Possible pathways towards multi-carbon hydrocarbons on Cu (100) and other (bimetallic) transition metals based on literature and data in this article [4], [27]

Since stronger buffers will result in a lower surface pH during reaction, the rate-determining step towards hydrocarbon products on these three catalysts can be assumed to be pH-dependent. On copper, ethylene is formed via two different reaction mechanisms: CO-dimerisation, which is pH-independent, and a pH-dependent route that shares a common intermediate with methane formation CHO* [28]. On other transition metals, higher hydrocarbon formation has been observed as well, often following a Schulz-Flory distribution. This mechanism was first suggested by Cook et al. based on the correlated production of hydrocarbons on various transition metals [29] and subsequently by Kudo and co-workers on iron, cobalt, and nickel [30]. The same conclusion was also drawn by Kortlever et al. for the gold-palladium electrode that was discussed earlier in this chapter [15]. Which exact intermediate(s) participate in the C-C bonding step is however unclear. From the observed pH-dependency of the hydrocarbon formation, it is clear that C-C bonding intermediate(s) of this mechanism share a common intermediate the pH-dependent formation of methane (CHO*). The articles above

all suggest that the formation of higher hydrocarbons proceeds through chain-coupling of the CH_2* intermediate following a Fisher-Tropsch mechanism, but no experimental proof of the intermediate on these catalysts exists in literature. Based on DFT calculations on a polarised nickel surface, Zhou and co-workers suggest a reaction between COOH* and CH_x* (x = 1,2) as the favoured C-C coupling step [27]. It is clear, however, that on non-copper metals the formation of C_{2+} products follows a different mechanism than the preferred CO-dimerisation on copper. This is a logical conclusion based on the nature of the metals; Only on Cu(100), the CO* intermediate has an intermediate binding strength that makes the dimerisation step possible [31], while on the other metals, the CO-binding strength is either too strong or weak to make its dimerisation reaction kinetically favourable. Therefore, C-C bonding is more likely through other intermediates than CO*, see Figure 3.6. Therefore, to enhance the formation of C_{2+} products on a non-copper alloy, it would be more advantageous to study these materials in a stronger buffer. The stronger buffer will enhance the production of C_{2+} products making it more likely to pass the limit of detection and easier to identify promising materials. However, this reaction mechanism is a hypothesis and further in-situ spectroscopic characterisation is needed to confirm it or give further insights.

3.4. Conclusion

In conclusion, a AuPd electrocatalyst has a higher activity towards hydrocarbons in a phosphate buffer compared to a bicarbonate buffer around the same pH. This observation also holds for a polycrystalline gold electrode and electrodeposited palladium on glassy carbon. Through the study of CO_2 reduction on AuPd in bicarbonate buffers of varying buffer strengths, we conclude that the observed differences in product activities are caused by the difference in buffer strength, not the presence of certain anions at the electrode interphase. The results presented here show a strong link between the buffer choice and product activity, further demonstrating the strong interaction between the catalyst activity and the local reaction conditions at the surface. Our data suggests that ethylene and higher hydrocarbons are formed via a pH-dependent reaction mechanism that is different from the pH-independent CO-dimerisation mechanism on a copper surface. These observations highlight the importance of the buffer choice on the catalytic activity. In conclusion, the study gives additional evidence that catalyst design cannot be a one-sided effort solely optimising the catalyst material. During the catalyst design process, the material should be evaluated under multiple reaction conditions to investigate their electrocatalytic response before conclusions are drawn on their selectivity.

BIBLIOGRAPHY

[1] Y. Hori, K. Kikuchi, and S. Suzuki, "Production of CO and CH_4 in electrochemical reduction of CO_2 at metal electrodes in aqueous hydrogencarbonate solution", *Chemistry Letters*, vol. 14, no. 11, pp. 1695–1698, 1985, ISSN: 1348-0715. DOI: https://doi.org/10.1246/cl.1985.1695.

[2] S. Asperti, R. Hendrikx, Y. Gonzalez-Garcia, and R. Kortlever, "Benchmarking the electrochemical reduction on polycrystalline copper foils: The importance of microstructure versus applied potential", *ChemCatChem*, e202200540, 2022, ISSN: 1867-3880. DOI: https://doi.org/10.1002/cctc.202200540.

[3] K. P. Kuhl, E. R. Cave, D. N. Abram, and T. F. Jaramillo, "New insights into the electrochemical reduction of carbon dioxide on metallic copper surfaces", *Energy & Environmental Science*, vol. 5, no. 5, pp. 7050–7059, 2012, ISSN: 1754-5692. DOI: https://doi.org/10.1039/C2EE21234J.

[4] S. Nitopi, E. Bertheussen, S. B. Scott, *et al.*, "Progress and perspectives of electrochemical CO_2 reduction on copper in aqueous electrolyte", *Chemical Reviews*, vol. 119, no. 12, pp. 7610–7672, 2019, ISSN: 0009-2665. DOI: https://doi.org/10.1021/acs.chemrev.8b00705.

[5] M. Moura de Salles Pupo and R. Kortlever, "Electrolyte effects on the electrochemical reduction of CO_2", *ChemPhysChem*, vol. 20, no. 22, pp. 2926–2935, 2019, ISSN: 1439-4235. DOI: https://doi.org/10.1002/cphc.201900680.

[6] Z. Han, R. Kortlever, H.-Y. Chen, J. C. Peters, and T. Agapie, "CO_2 reduction selective for $C_{\geq 2}$ products on polycrystalline copper with N-substituted pyridinium additives", *ACS central science*, vol. 3, no. 8, pp. 853–859, 2017, ISSN: 2374-7943. DOI: https://doi.org/10.1021/acscentsci.7b00180.

[7] J. He, N. J. J. Johnson, A. Huang, and C. P. Berlinguette, "Electrocatalytic alloys for CO_2 reduction", *ChemSusChem*, vol. 11, no. 1, pp. 48–57, 2018, ISSN: 1864-5631. DOI: https://doi.org/10.1002/cssc.201701825.

[8] S. Ma, M. Sadakiyo, M. Heima, *et al.*, "Electroreduction of carbon dioxide to hydrocarbons using bimetallic Cu catalysts with different mixing patterns", *Journal of the American Chemical Society*, vol. 139, no. 1, pp. 47–50, 2017, ISSN: 0002-7863. DOI: https://doi.org/10.1021/jacs.6b10740.

[9] S. Sarfraz, A. T. Garcia-Esparza, A. Jedidi, L. Cavallo, and K. Takanabe, "Cu bimetallic catalyst for selective aqueous electroreduction of CO_2 to CO", *ACS Catalysis*, vol. 6, no. 5, pp. 2842–2851, 2016, ISSN: 2155-5435. DOI: https://doi.org/10.1021/acscatal.6b00269.

[10] D. Kim, C. Xie, N. Becknell, *et al.*, "Electrochemical activation of CO_2 through atomic ordering transformations of AuCu nanoparticles", *Journal of the American Chemical Society*, vol. 139, no. 24, pp. 8329–8336, 2017, ISSN: 0002-7863. DOI: https://doi.org/10.1021/jacs.7b03516.

[11] E. L. Clark, C. Hahn, T. F. Jaramillo, and A. T. Bell, "Electrochemical reduction over compressively strained CuAg surface alloys with enhanced multi-carbon oxygenate selectivity", *Journal of the American Chemical Society*, vol. 139, no. 44, pp. 15 848–15 857, 2017, ISSN: 0002-7863. DOI: https://doi.org/10.1021/jacs.7b08607.

[12] D. A. Torelli, S. A. Francis, J. C. Crompton, *et al.*, "Nickel–gallium-catalyzed electrochemical reduction of CO_2 to highly reduced products at low overpotentials", *ACS Catalysis*, vol. 6, no. 3, pp. 2100–2104, 2016, ISSN: 2155-5435. DOI: https://doi.org/10.1021/acscatal.5b02888.

[13] A. R. Paris and A. B. Bocarsly, "Ni films on glassy carbon electrodes generate an array of oxygenated organics from CO_2", *ACS Catalysis*, vol. 7, no. 10, pp. 6815–6820, 2017, ISSN: 2155-5435. DOI: https://doi.org/10.1021/acscatal.7b02146.

[14] A. R. Paris and A. B. Bocarsly, "Mechanistic insights into C_2 and C_3 product generation using Ni_3Al and Ni_3Ga electrocatalysts for CO_2 reduction", *Faraday discussions*, vol. 215, pp. 192–204, 2019, ISSN: 1364-5498. DOI: https://doi.org/10.1039/C8FD00177D.

[15] R. Kortlever, I. Peters, C. Balemans, *et al.*, "Palladium–gold catalyst for the electrochemical reduction of CO_2 to C_1 hydrocarbons", *Chemical Communications*, vol. 52, no. 67, pp. 10 229–10 232, 2016, ISSN: 1359-7345. DOI: https://doi.org/10.1039/C6CC03717H.

[16] J. J. L. Humphrey, D. Plana, V. Celorrio, *et al.*, "Electrochemical reduction of carbon dioxide at gold-palladium core–shell nanoparticles: Product distribution versus shell thickness", *ChemCatChem*, vol. 8, no. 5, pp. 952–960, 2016, ISSN: 1867-3880. DOI: https://doi.org/10.1002/cctc.201501260.

[17] F. Studt, I. Sharafutdinov, F. Abild-Pedersen, *et al.*, "Discovery of a Ni – Ga catalyst for carbon dioxide reduction to methanol", *Nature chemistry*, vol. 6, no. 4, pp. 320–324, 2014, ISSN: 1755-4349. DOI: https://doi.org/10.1038/nchem.1873.

[18] Y. Hori, H. Wakebe, T. Tsukamoto, and O. Koga, "Electrocatalytic process of CO selectivity in electrochemical reduction of CO_2 at metal electrodes in aqueous media", *Electrochimica Acta*, vol. 39, no. 11-12, pp. 1833–1839, 1994, ISSN: 0013-4686. DOI: https://doi.org/10.1016/0013-4686(94)85172-7.

[19] F. Gao and D. W. Goodman, "Pd bimetallic catalysts: Understanding alloy effects from planar models and (supported) nanoparticles", *Chemical Society Reviews*, vol. 41, no. 24, pp. 8009–8020, 2012. DOI: https://doi.org/10.1039/C2CS35160A.

[20] Y. Wang, L. Cao, N. J. Libretto, *et al.*, "Ensemble effect in bimetallic electrocatalysts for CO_2 reduction", *Journal of the American Chemical Society*, 2019, ISSN: 0002-7863. DOI: https://doi.org/10.1021/jacs.9b05766.

[21] C. Hahn, D. N. Abram, H. A. Hansen, *et al.*, "Synthesis of thin film AuPd alloys and their investigation for electrocatalytic CO_2 reduction", *Journal of Materials Chemistry A*, vol. 3, no. 40, pp. 20 185–20 194, 2015, ISSN: 2050-7488. DOI: https://doi.org/10.1039/C5TA04863J.

[22] P. Lobaccaro, M. R. Singh, E. L. Clark, Y. Kwon, A. T. Bell, and J. W. Ager, "Effects of temperature and gas–liquid mass transfer on the operation of small electrochemical cells for the quantitative evaluation of CO_2 reduction electrocatalysts", *Physical Chemistry Chemical Physics*, vol. 18, no. 38, pp. 26 777–26 785, 2016. DOI: https://doi.org/10.1039/C6CP05287H.

[23] A. Bukhtiyarov, I. Prosvirin, A. Saraev, A. Y. Klyushin, A. Knop-Gericke, and V. Bukhtiyarov, "In situ formation of the active sites in Pd–Au bimetallic nanocatalysts for CO oxidation: NAP (near ambient pressure) XPS and MS study", *Faraday Discussions*, vol. 208, pp. 255–268, 2018. DOI: https://doi.org/10.1039/C7FD00219J.

[24] A. Venezia, V. La Parola, G. Deganello, B. Pawelec, and J. Fierro, "Synergetic effect of gold in Au/Pd catalysts during hydrodesulfurization reactions of model compounds", *Journal of Catalysis*, vol. 215, no. 2, pp. 317–325, 2003, ISSN: 0021-9517. DOI: https://doi.org/10.1016/S0021-9517(03)00005-8.

[25] H. Noda, S. Ikeda, A. Yamamoto, H. Einaga, and K. Ito, "Kinetics of electrochemical reduction of carbon dioxide on a gold electrode in phosphate buffer solutions", *Bulletin of the Chemical Society of Japan*, vol. 68, no. 7, pp. 1889–1895, 1995, ISSN: 1348-0634. DOI: https://doi.org/10.1246/bcsj.68.1889.

[26] M. Azuma, K. Hashimoto, M. Watanabe, and T. Sakata, "Electrochemical reduction of carbon dioxide to higher hydrocarbons in a $KHCO_3$ aqueous solution", *Journal of electroanalytical chemistry and interfacial electrochemistry*, vol. 294, no. 1-2, pp. 299–303, 1990, ISSN: 0022-0728. DOI: https://doi.org/10.1016/0022-0728(90)87154-C.

[27] Y. Zhou, A. J. Martín, F. Dattila, *et al.*, "Long-chain hydrocarbons by electroreduction using polarized nickel catalysts", *Nature Catalysis*, vol. 5, no. 6, pp. 545–554, 2022, ISSN: 2520-1158. DOI: http://dx.doi.org/10.1038/s41929-022-00803-5.

[28] K. J. P. Schouten, E. P. Gallent, and M. T. Koper, "The influence of pH on the reduction of CO and CO_2 to hydrocarbons on copper electrodes", *Journal of Electroanalytical Chemistry*, vol. 716, pp. 53–57, 2014, ISSN: 1572-6657. DOI: https://doi.org/10.1016/j.jelechem.2013.08.033.

[29] R. L. Cook and A. F. Sammels, "Electrocatalysis and novel electrodes for high rate CO_2 reduction under ambient conditions", in *Electrochemical and Electrocatalytic Reactions of Carbon Dioxide*, B. Sullivan, K. Krist, and H. Guard, Eds. Elsevier, 1992, ch. 7, pp. 217–262, ISBN: 9780444596611.

[30] A. Kudo, S. Nakagawa, A. Tsuneto, and T. Sakata, "Electrochemical reduction of high pressure CO_2 on Ni electrodes", *Journal of The Electrochemical Society*, vol. 140, no. 6, pp. 1541–1545, 1993, ISSN: 0013-4651. DOI: https://doi.org/10.1149/1.2221599.

[31] A. Bagger, W. Ju, A. S. Varela, P. Strasser, and J. Rossmeisl, “Electrochemical reduction: A classification problem”, *ChemPhysChem*, vol. 18, no. 22, pp. 3266–3273, 2017, ISSN: 1439-4235. DOI: https://doi.org/10.1002/cphc.201700736.

4

Direct Quantification of Electrochemical CO_2 Reduction Products with an Improved DEMS Setup

The analytical tools to quantify CO_2RR products are often slow and have high limits of detection. As a result, researchers are forced to extend the duration of their experiments to accumulate sufficient product and surpass these detection limits. This considerably slows down research, and the research scope often remains limited. To help speed up CO_2RR catalyst studies, we have developed a new Differential Electrochemical Mass Spectrometer (DEMS) setup and cell design that enables the quantification of the major gaseous and liquid products significantly faster than conventional analytical techniques. Special attention was given to the hydrodynamics of the cell to avoid mass transfer limitations and the calibration of the setup to accurately quantify the major CO_2 reduction products. As proof of concept of the methodology, the products formed during CO_2RR on a polycrystalline silver and copper electrode in a 0.1 M $KHCO_3$ electrolyte at different potentials were measured and quantified.

This chapter has been published in https://doi.org/10.1016/j.checat.2024.101065

4.1. INTRODUCTION

The electrochemical CO_2 reduction reaction (CO_2RR) towards valuable products using renewable electricity can offer an efficient route to reduce CO_2 emissions and the dependency on fossil resources [1]–[3]. However, a stable and selective catalyst for the direct conversion of CO_2 towards these valuable products has yet to be found. Depending on the catalyst, different gaseous and liquid products are produced on the cathode. During initial catalyst development studies, researchers generally use in-line gas chromatography (GC) and offline high-performance liquid chromatography (HPLC) or nuclear magnetic resonance (NMR) spectroscopy to quantify the gaseous and liquid products, respectively [4]. However, these analytic techniques have long analysis times and relatively high limits of detection, forcing researchers to extend the duration of experiments to accumulate a detectable concentration of products. Furthermore, HPLC and NMR measurements are offline and indirect, making it difficult to keep track of time-dependent processes such as reaction kinetics or catalyst stability. Therefore, considerable effort has been taken to develop techniques that are able to quantify the production rates of major CO_2RR products directly and in real-time. Differential electrochemical mass spectrometry (DEMS) uses a pervaporation membrane to separate (dissolved) gases and volatile organic compounds from the electrolyte. The production rates of both gaseous and liquid products are quantified by monitoring the responses of the products' mass peaks in the mass spectrum. Since mass spectrometry has a lower limit of detection and both liquid and gaseous products are measured directly in the same setup, the development of new CO_2RR catalysts can potentially be sped up significantly.

One of the earliest DEMS setups that was applied for the reduction of CO_2, was used to monitor the adsorption of CO on platinum [5]. Wolter and co-workers placed a thin, porous Teflon membrane close to the working electrode inside the cell [6]. The setup allows for the detection and quantification of gaseous and dissolved molecules in the electrolyte. However, by placing the membrane close to the electrode surface, reactants are removed from the electrolyte alongside the products, affecting the reaction conditions near the surface. Kita et al. developed another configuration that uses a small tip close to the electrode surface to remove formed products [7] thereby inspiring later similar setups by Hillier et al. [8] and by Wonders et al. [9]. These setups are able to detect a wide range of gaseous and volatile products including hydrocarbons from electrochemical CO_2 reduction, CO_2 from CO adlayer oxidation, reduction and oxidation of acetylene, or methanol oxidation, and NO and N_2O from hydroxylamine electrochemistry [9]. However, it is difficult to quantify these measurements as the placement of the tip relative to the electrode surface is poorly controlled and leads to reproducibility issues. Recently, Clark et al. developed two setups that were able to semi-quantitatively monitor the production of formed alcohols during electrochemical CO_2 reduction. By deconvoluting the contribution of different species to the mass peaks, they were able to quantitatively determine the production rate of ethanol and 1-propanol on copper [10], [11]. However, the setup has several downsides. First, the cell requires a restrictive working electrode design, where the catalyst is either coated on the PTFE membrane itself or has a specific ring-like geometry. Second, once the solubility limit of gaseous products in the electrolyte is reached and bubbles start to form, large standard deviations are encountered in both the current and mass signal response. Lastly, full deconvolution of the mass spectrum is not possible without separate measurements from a separate flow cell setup and additional HPLC measurements.

While for ethanol oxidation DEMS setups for product quantification already exists [12], [13], all of the examples above are not able to rapidly quantify the product spectrum of previously untested catalyst material for CO_2RR products. Therefore, we here set out to develop a DEMS setup capable of directly quantifying major CO_2RR products in both the gaseous and liquid phases in real-time without any prior knowledge of the catalyst's product distribution. We discuss the design choices of a newly developed electrochemical cell and MS setup, specifically regarding the mass transfer rate of CO_2 to the electrode and the quantification of the CO_2RR products. Finally, we devise a numerical model to deconvolute the obtained mass peaks and quantify the production rates of the major CO_2RR products without the need of additional measurements. We show that with the help of this setup, we can determine the product spectrum as a function of applied potential in a much shorter time scale than is currently possible. This setup can thus enable rapid screening of different catalyst materials thereby speeding up catalyst development and facilitate testing catalyst under different process conditions.

4.2. Experimental

4.2.1. Materials

All solutions were prepared using ultrapure water (Millipore Milli-Q gradient A10 system, 18 MΩ cm) and reagents of high purity. Electrolytes were prepared using $KHCO_3$ (≥ 99.95%, Sigma-Aldrich), $K_3Fe(CN)_6 \cdot H_2O$ (99.9%, Sigma Aldrich) and $K_4Fe(CN)_6$ (99.9%, Sigma Aldrich). Polycrystalline silver foils (25 x 25 x 1 mm, 99.995%) were purchased from MaTecK GmbH, Polycrystalline copper foils (25 x 25 x 1 mm, 99.99%) were obtained from Sigma-Aldrich, while glassy carbon electrodes (25 x 25 x 1 mm) were purchased from HTW (Sigradur®, polished). As a counter electrode either a platinum foil (MaTeck Gmbh, 25 x 25 x 0.1 mm, 99.995%) or glassy carbon electrode (HTW, Sigradur®, polished) was used. For the calibration of the liquid products, methanol (≥ 99.9 % Sigma-Aldrich), ethanol (≥ 99.8 %, Sigma-Aldrich), 1-propanol (≥ 99.9 % Sigma-Aldrich) and allyl-alcohol (≥ 99 % Sigma-Aldrich) were used to make dilution series.

4.2.2. Electrochemical Measurements

All electrochemical experiments were performed using a Biologic SP-200 potentiostat, using a RE-6 Ag/AgCl reference electrode (BASi).

4.2.3. Electrode preparation

Prior to every measurement, the polycrystalline silver and copper foils were polished by hand using 3 µm and 1 µm diamond paste (DP-floc, Struers, USA) and a microfiber cloth (DP-floc, Struers, USA) for a couple of minutes to ensure that contaminants were removed from the surface. After each polishing step, the electrode was washed using ultrapure water and subsequently dried using compressed nitrogen or argon. After mechanical polishing, the copper foil was electropolished twice in 85 v/v % H_3PO_4 (aq) solution (Sigma–Aldrich, USA). In short, a two-electrode setup was used with the copper foil as the working electrode and a carbon rod as the counter electrode. Copper tape (AT528, Advance Tapes) was used to hold up the copper foil while both electrodes were immersed in a 100 mL beaker containing the electrolyte. A potential difference of 2.1 V was applied between the two electrodes for 3

minutes. After electropolishing, the copper foil was washed with ultrapure water and dried using compressed argon. Glassy carbon electrodes were first cleaned using acetone to remove any left-over glue on the surface from the tape used in the previous experiments. Next, the electrode was ultrasonicated using ultrapure water for at least 15 minutes and manually polished for a couple of minutes using undiluted alumina paste (DP-floc, Struers, USA) and a microfiber cloth (DP-floc, Struers, USA). After another washing step with ultrapure water, the electrode was ultrasonicated in ultrapure water for 15 minutes to remove any residual alumina particles from the surface. Subsequently, the electrodes were ultrasonicated for 15 min in a 20 v% HNO_3 (aq) solution (prepared with 70 v% HNO_3 from Sigma-Aldrich) to make sure all leftover alumina dissolved from the electrode surface. Then, the electrode was washed and ultrasonicated for at least 15 minutes using ultrapure water to ensure all acid was removed from the electrode. Finally, the electrodes were dried using compressed nitrogen or argon. Prior to each experiment, the platinum counter electrode was polished by hand using 3 µm diamond paste and a microfiber cloth (DP-floc, Struers, USA) for about 1 to 2 minutes to make sure any contaminants were removed from the surface. Next, it was washed with ultrapure water and flame annealed until the surface glowed red-hot.

4.2.4. FERRO/FERRICYANIDE EXPERIMENTS

The ferro-/ferricyanide redox couple was used to determine the hydrodynamics of the cell. A buffer of 0.1 M $KHCO_3$ (99.95%, Sigma Aldrich) + 5 mM $K_3Fe(CN)_6 \cdot H_2O$ (99.9%, Sigma Aldrich) + 5 mM $K_4Fe(CN)_6$ (99.9%, Sigma Aldrich) was flown through the cell, using glassy carbon as both the working and counter electrode [14]. Furthermore, argon was bubbled through the electrolyte to remove any dissolved oxygen, to prevent ferrocyanide oxidation [15]. Lastly, all experiments were performed in the dark to prevent photolysis of the cyanide complexes through photodissociation under UV light leading to cyanide formation [16]. Linear sweep voltammetry was performed from open circuit potential to +0.6 V vs. at a sweep rate of 1 mV s^{-1} and maintaining different flowrates. The sweep rate was kept low to limit the contribution of double layer charging. Cell resistances could not be determined using PEIS since faradaic reactions occur at any potential. Therefore, these results are shown without ohmic drop compensation.

4.2.5. FORMATE QUANTIFICATION

Because ions cannot pass the DEMS membrane, it was not possible to quantify the formate production at each potential. Instead, formate production was quantified using HPLC. Following the obtained residence time distribution, the electrolyte exiting the liquid DEMS inlet was collected 7 minutes after the chronoamperometry measurement started. The concentration of formate was measured by injection 100 µL of sample into the high-performance liquid chromatograph (HPLC, Agilent Technologies 1260 Infinity, USA) to quantify the formed liquid products. The HPLC was calibrated with a dilution series in the range of 0.01 mM to 5 mM of formic acid (95%, Sigma–Aldrich). The flowrate of the eluent (1 mM H_2SO_4 (aq)) was set to 0.6 mL min^{-1} and the measurement ran for one hour. The HPLC used two Aminex HPX-87H columns (Biorad) in series heated to 60 °C. A refractive index detector (RID) was used for the detection of products.

4.2.6. MASS SPECTROMETER SETTINGS

Mass spectrometry was performed on a Hiden HPR40 dissolved-species mass spectrometer. All incoming species were first ionised and subsequently accelerated with a voltage of 3 V and an electron current of 500 µA. Finally, all cations were detected by a Secondary Electron Multiplier (SEM) which was set at a voltage of 870 V. The electron current and SEM voltage were optimised to maximise the signal-to-noise ratio of liquid products (see section B.4 in appendix B).

4.2.7. PRODUCT CALIBRATION

For the gaseous products, five standard concentration bottles were used from Linde. The concentration of analytes in these bottles ranged from 50, 100, 1000, 3000 and 8000 ppm. The bottles were balanced with CO_2 and the flowrate used for calibration was 2 mL_n/min. Additionally, the background values of each mass peak were measured by flowing pure CO_2 through the setup. At startup or after changing the bottle, the signal was first stabilized for at least three hours. Each liquid product was calibrated by flowing a series of increasingly diluted standards from 5 mM, 1 mM, 500 µM, 100 µM to 50 µM. Each standard was prepared using ultrapure water and was pumped through the liquid inlet with a flowrate of 1 mL min^{-1} for 30 minutes before measurements were taken. After each dilution series had ended, ultrapure water was pumped through the system to obtain the background noise of each signal.

4.3. RESULTS & DISCUSSION

4.3.1. CELL DESIGN

An exploded view of the cell is shown in Figure 4.1. The catholyte enters the cell through the side of the catholyte endplate (f), where it encounters the tip of the reference electrode (BASI RE-6) (g). From here, the electrolyte takes a sharp 90-degree turn and enters the flow plate (c). Here, the electrolyte flows through ten parallel channels over the working electrode. Here, parallel channels are chosen to increase the flow velocity of the electrolyte through the channel, enhancing the mass transfer inside the cell. One side of the channel is exposed to the working electrode, while the other is in contact with the membrane (e, Nafion 117) to prevent product cross-over to the counter electrode. At the end of the channel, the electrolyte flows back to the endplate and takes another sharp turn before exiting the cell. The same design is maintained on the anode side. The working and counter electrodes are placed parallel to each other to ensure a uniform potential distribution. The exposed surface areas of the working and counter electrodes are 2.75 cm^2 each. The flow- and endplates are all manufactured from PEEK and are separated by Silicon (0.015" High-Temperature Silicone Rubber Sheets, McMaster-Carr) gaskets to ensure leak tightness.

4.3.2. CELL MASS TRANSFER

When the conversion rate of CO_2 at the electrode becomes higher than the supply rate, the concentration of CO_2 at the electrode surface drops. A lower CO_2 concentration at the electrode surface affects the local reaction conditions and gives skewed results for the catalyst activity and selectivity. Therefore, CO_2 depletion at the surface due to mass transfer limitations should be prevented. Additionally, improved mass transfer conditions aid in

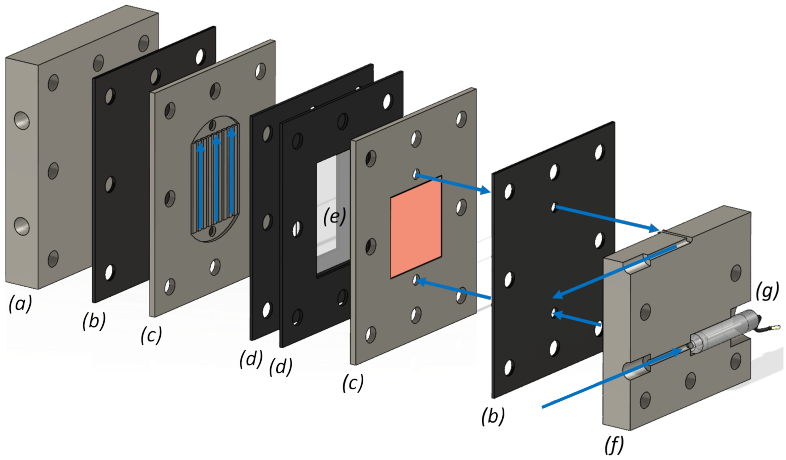

Figure 4.1: Exploded view of the DEMS cell. Each of the components is labelled accordingly: Counter electrode endplate (a), silicon gasket (b), flow plate (c), membrane gasket (d), cationic membrane (NAFION 117) (e), catholyte endplate (f) and BASi RE-6 reference electrode (g).

product removal and hinder bubble formation. The mass transfer of CO_2 can be improved by increasing the flowrate of electrolyte through the cell, thereby decreasing the thickness of the diffusion boundary layer. However, the liquid product concentration also decreases at higher flowrates and could drop below the limit of detection of the MS. Therefore, the flowrate was varied to determine the optimal trade-off for product detection and the hydrodynamics of the cell.

The hydrodynamics of the new cell were determined using the ferri-/ferrocyanide redox system [17]. Since both redox systems use an aqueous electrolyte under the same temperature and flowrates, the governing hydrodynamics in both systems were considered to be the same. Therefore, any derived equations to describe the hydrodynamics in one system, could be applied to the other by plugging in the corresponding values. The ferri-/ferrocyanide system is less complex than the CO_2RR system since it only has a single electron transfer and one reaction product. Linear sweep voltammograms were recorded at increasing electrolyte flow rates ranging between 0.2 mL min^{-1} – 5 mL min^{-1}. Figure 4.2A shows that the limiting current goes up with electrolyte flowrate through the channels, as expected. An expression for the mass transfer of CO_2 to the electrode surface was derived using the film model (see section B.1 of Appendix B). A Sherwood expression was obtained from van Male et al. for flow in a microchannel [18]. Using this expression, limiting currents from the model were calculated and compared with the experimentally obtained values in Figure 4.2B and 4.2C. As shown in Figure 4.2B, the experimental data fits well with the obtained expression for the Sherwood number. Therefore, the Sherwood expression can be used to calculate the concentration of CO_2 at the interface for a given flow rate and partial current densities during an experiment. Alternatively, the dependence upon the flowrate can be estimated using the Koutecky-Levich equation for limiting currents in channel electrodes that was derived by Scherson et al. [19]:

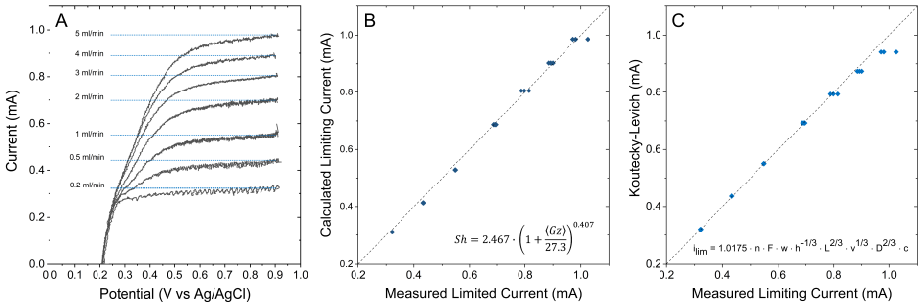

Figure 4.2: **A.**Linear sweep voltammograms with a sweep rate of 1 mV s^{-1} on glassy carbon in the DEMS setup using a 0.1 molar $KHCO_3$ + 5 mM $K_3Fe(CN)_6 \cdot H_2O$ + 5 mM $K_4Fe(CN)_6$. Anodic limiting currents are obtained for each flow rate (dashed lines show the flowrates maintained through the cell). **B+C:** The experimentally measured limiting currents are set out against the calculated limiting currents from the Sherwood model and Koutecky-Levich equation, respectively. <Gz> is defined as the averaged Graetz number and calculated by averaging the function $\frac{v}{D}\frac{d^2}{z}$ over the distance z, where v is the average velocity through the channel, d the height of the channel, and D the diffusion coefficient.

$$i_{lim} = 1.0175 \cdot n \cdot F \cdot w \cdot h^{-1/3} \cdot L^{2/3} \cdot v^{1/3} \cdot D^{2/3} \cdot c \tag{4.1}$$

Here, n is the number of electrons that is transferred, F the Faraday constant, w stands for the width of the channel, h is the half-height of the channel, L represents the length of the channel, v the fluid flow velocity in the centre of channel, D is the diffusion coefficient and c is the bulk concentration of the reacting species. Figure 4.2C shows that the experimentally obtained values also fit well with the Koutecky-Levich equation. Section B.2 of the appendices provides more details on how the limiting currents were calculated using these two models. According to equation 4.1, the limiting current scales with the flowrate to the power of 1/3. This means that even though there is some initial gain from increasing the flowrate, the gain in mass transport to the surface is limited at higher flowrates. Therefore, the flowrate was set at 1 mL min^{-1} for all quantification measurements. The liquid-phase product detection limit is 5 µM at this flowrate according to Clark et al. [10]. The limiting current density at this flowrate is 5.3 mA cm^{-2} for 2 e^-/mol_{CO_2} such as carbon monoxide and formate and 16 mA cm^{-2} for 6 e^-/mol_{CO_2} products, such as ethylene and ethanol, as calculated by equation 4.1. These limiting currents are on par with limiting current densities of other electrochemical cells in literature [20] and this thesis (see section A.3 in appendix A).

4.3.3. REPRODUCIBLE COLLECTION EFFICIENCY

A schematic overview of the setup is given in Figure 3. During an experiment, electrolyte is stored in a reservoir and pumped through the cell by a peristaltic pump (Masterflex L/S®Digital Miniflex®Pump, Dual-Channel) lined with Precision Pump Tubing, Versilon™ 2001 Tubing, L/S 13. The electrolyte is pumped through the cell using positive pressure, as otherwise, the liquid flowrate would become irregular when bubbles start to form. This is due to the fixed volume per minute that the peristaltic pump transports. Therefore, if the

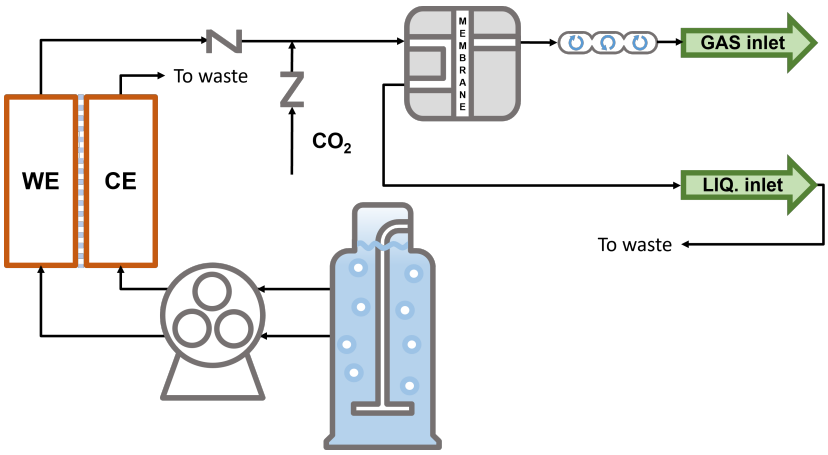

Figure 4.3: Schematic overview of the DEMS setup. CO_2 saturated electrolyte is pumped through both compartments of the cell. The catholyte flows via a check valve through a tee-junction where it mixes with dry CO_2 gas. Afterwards, the two phases are separated using a bubble trap. The separated gas flows through a static mixer into the gas inlet of the DEMS, while the liquid directed goes to the liquid inlet of the setup. CE, Counter Electrode, LIQ., liquid; WE, Working Electrode.

electrolyte is pumped using a negative pressure, the pump has to transport both gas and liquid and the volume amount of electrolyte will not be the same for every experiment. 1/16" OD PTFE tubing (Darwin Microfluidics, 1/32" ID) was used to connect all parts of the setup.

For reproducible and steady CO_2RR product detection it is vital that the products are collected by the mass spectrometer in a manner corresponding with their rate of production inside the cell. However, if the cell outlet is directly connected to the DEMS inlet, the mass spectrum signal becomes unstable when bubbles start to form on the electrode and pass over the DEMS membrane after their release. This is in correspondence with Clark et al., who reported that as soon as bubbles were formed, the standard deviation of the mass signal increased instantaneously by a factor hundred [10]. This observation can be explained by the vast difference in the density of gaseous products in the gas phase and dissolved in the electrolyte, as the product density in a bubble is much higher than in the saturated electrolyte. Therefore, when a released bubble passes over the DEMS inlet membrane, much more product passes through in a short period of time compared to when saturated electrolyte flows over the inlet of the DEMS. As a result, the amount of product passing the membrane will fluctuate greatly when the membrane is presented with an immiscible flow of bubbles and saturated electrolyte.

To stabilise the signal of the mass spectrometer, the electrolyte and bubbles exiting the flow cell need to be separated and enter the mass spectrometer simultaneously via two different inlets. However, simply separating bubbles from the saturated electrolyte is not enough. If both phases are immediately separated from each other after they exit the flow cell, part of the formed gaseous products will enter the mass spectrometer from the gas phase while the dissolved gaseous products in the electrolyte will enter from the liquid phase. Each of these phases has a different collection efficiency. As a result, the mass signal will no longer be linearly dependent on the product formation rate [21]. Therefore, all dissolved gaseous prod-

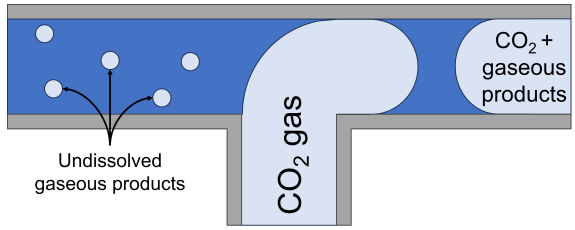

Figure 4.4: Schematic drawing of the tee-junction where the catholyte is mixed with a dry flow of CO_2 gas. Both phases travel down together a stainless-steel tube during which dissolved gaseous products are drawn from the electrolyte into the gas slugs.

ucts need to be extracted from the liquid electrolyte. In that case, all the gaseous products will enter the mass spectrometer in the gas phase while all the liquid products will enter the mass spectrometer dissolved in the electrolyte. Each does so simultaneously through their respective inlets, which will be referred to as the gas and liquid inlet, respectively. Drawings and pictures of the gas and liquid inlet can be found in section B.3 of appendix B.

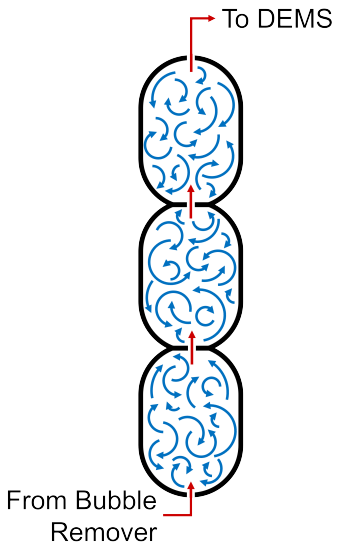

Figure 4.5: Schematic drawing of the static mixer. The incoming gas flow is mixed over the direction of the flow through the 3 metal bulbs that are stacked on top of one another. The static mixer is added to the setup to improve the homogeneity in product concentration in the gas flow before it enters the DEMS.

To adhere to these design criteria, the catholyte is pumped through a PEEK tee-union where it mixes with dry CO_2 gas that is delivered by a CO_2 mass flow controller (EL-FLOW Select). A schematic drawing of this can be found in Figure 4.4. Due to the absence of products in the CO_2 gas, dissolved gaseous products are withdrawn from the liquid phase into the gas slugs while travelling down the tube. Before both the gas and electrolyte inlet, a microfluidic check-valve prevents the fluid from flowing the wrong way (Masterflex ®One-Way, Avantor ®and IDEX, inline check valve). A microfluidic check valve was chosen for the liquid stream to minimize bubble hold-up. A 4.5 cm long 100 µm ID PEEK tube (VWR) was used to insert the gas into the tee-junction, while a 4.5 cm long 0.010" ID PEEK (VWR) tube was used for the catholyte to create a stable Taylor flow regime to enhance the mass transfer of gaseous products from the electrolyte to the gas phase. After the tee-union, both electrolyte and gas flow together through a 15 cm long stainless-steel tube (1/8" OD, 1/16" ID, Swagelok) in a Taylor flow regime. A rigid material is used here to stabilise the flowrate of the Taylor flow. The gas and liquid are subsequently separated from each other using a commercial bubble trap (Large PEEK bubble remover, Elveflow)

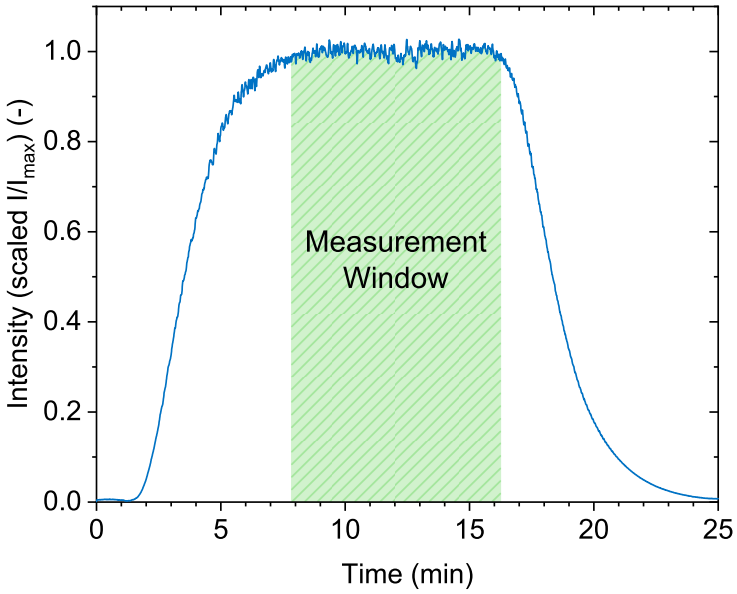

Figure 4.6: Step response function of the DEMS setup. The intensity was rescaled to the maximal measured intensity to show that all formed hydrogen was collected by the DEMS setup. The measurement window is shaded in green.

with a hydrophobic membrane.

From here, the separated phases are sent to their respective DEMS inlet. However, the product concentration that flows into the gas inlet still remains intermittent even when the product formation is constant, as bubbles containing gaseous products will still leave the flow cell at irregular time intervals. To smoothen the concentration gradient at the gas inlet over time, a static mixer was placed between the bubble trap and gas inlet to mix the gas stream before it enters the mass spectrometer. The design of the mixer was based on a series of three small spherical mixing chambers of about 3 cm in diameter with small 3 mm holes to separate them. At the end of the mixer, two PEEK frits (2 µm, IDEX) were placed to increase the pressure inside the mixer. Figure 4.5 shows a schematic drawing of the static mixer. In the liquid inlet, a PTFE membrane (20 nm pore size, Hangzhou Cobetter Filtration Equipment Co.) is used to separate the dissolved liquid products from the electrolyte.

Including the static mixer will result in a more spread-out residence time distribution that has to be taken into account to correctly link the production rate in the cell to the corresponding mass peak signal. To determine the residence time distribution of the setup, a step input experiment was performed by carrying out chronopotentiometry experiments at -20 mA for 15 minutes in a CO_2 sparged 0.1 M $KHCO_3$ electrolyte using a platinum working electrode [22]. Since platinum is relatively inactive for CO_2 reduction, the only obtained product is hydrogen, and the mass peak 2 m/e can be used to follow the retention time of hydrogen in the setup. The results can be found in Figure 4.6. Here, the influence of the static mixer can be clearly seen. Even though hydrogen is being produced in the cell at t

= 0, there is a clear delay until the produced hydrogen is detected by the MS. In the first minute, there is no hydrogen detection due to the tubing between the cell and the MS. Once the gas reaches the static mixer, the concentration starts to increase steadily. After roughly seven minutes, the concentration stabilises and the production in the cell matches the collection of the MS. When the chronopotentiometry is stopped at t = 15 min, the process proceeds in reverse order: First there seems to be no change for about a minute, then the concentration at the inlet begins to drop until it reaches the background value. Concluding, the rate of production matches what the mass spectrometer measures only seven minutes after an experiment has started. Then, about a minute after the experiment ends, the measured products start to decline. Therefore, to make sure that the production rate accurately quantifies products, only measurements within such a measurement window were taken into account. In practice, this means that instead of sweeping between two potentials, a series of chronoamperometry measurements is performed for fifteen minutes each. For each measured potential measurement data acquired between 7.8 minutes to 16.3 minutes after the start of the chronoamperometry were taken into account to quantify products.

4.3.4. PRODUCT DETECTION AND QUANTIFICATION

The setup must be able to quantify the most common CO_2 reduction products, being hydrogen, carbon monoxide, formic acid, methane, ethylene, methanol, ethanol, allyl-alcohol, and 1-propanol [23], [24]. Carboxylic acids, such as formic or acetic acid, are present as ions in the neutral electrolyte and are therefore unable to pass the PTFE membrane at the inlet of the mass spectrometer. Therefore, they cannot be detected by the DEMS and are omitted from the calibration. Instead, these products were quantified using HPLC. Carbon monoxide suffers from a lot of background signal as its mass spectrum overlaps with CO_2 (12 m/e, 16 m/e, and 28 m/e) and N_2 (28 m/e). To minimize the background noise from carbon dioxide, mass 28 m/e is measured at a lower electron energy (19.5 eV), which is the dissociative ionisation barrier for CO^+ from CO_2 [25]. As a result, the electron current for this mass peak signal had to be lowered to 50 µA to avoid filament failure. To remove the background signal coming from air-derived nitrogen as much as possible, the back pressure of the scroll pump is supplied with argon at 1.15 bar_g and a flow rate of 0.4 L min^{-1}.

Moreover, since PTFE tubing is not leak-tight under vacuum conditions, air will leak into the setup and create background noise from air that leaks into the setup as a result of the vacuum. To circumvent this, all tubing between the gas outlet of the bubble trap and the gas inlet of the DEMS is made from stainless steel and has Swagelok fittings. Due to the similar structure and small mass of the main products, there is much overlap between the mass peaks of the different products. Moreover, mass peaks cannot be used for the quantification of products if they are obstructed by too much background signal from other species, such as CO_2, water, air, or argon. Therefore, there is a limited number of mass peaks that can be used to detect and quantify the formed products. To optimise the settings of the mass spectrometer (electron current and SEM voltage), ethanol is calibrated by flowing a series of increasingly diluted standards from 5 mM to 50 µM through the mass spectrometer using different settings (see section B.4 of appendices). The limit of detection for each mass peak is estimated by dividing the standard deviation by the slope of the obtained calibration coefficient for each mass peak signal. The lowest overall limit of detection was obtained at an electron current of 500 µA, an electron energy at 70 eV, and Secondary Electron

Multiplier (SEM) voltage of 870 V. At these settings, 11 mass peaks could be used to quantify products with a limit of detection of 5 µM. These are: 2 m/e, 15 m/e, 26 m/e, 27 m/e, 28 m/e, 30 m/e, 31 m/e, 41 m/e, 57 m/e, 58 m/e, 59 m/e. Other mass peaks that should give a mass peak signal, such as 29 m/e, have too much background noise to be used for product quantification. As mentioned earlier, mass 28 m/e is measured at an electron energy of 19.5 eV and an electron current of 50 µA. 2 m/e is also measured at these settings to prevent overload at high production rates. Most of these mass peaks have overlapping contributions from multiple reduction products and must be deconvoluted.

4.3.5. MASS PEAK DECONVOLUTION AND PRODUCT QUANTIFICATION

For the mass peak deconvolution, the measured mass peak signals Y and the relative product concentrations X are assumed to satisfy the following linear model:

$$Y = \mu + BX + E \tag{4.2}$$

where Y is an 11-dimensional vector containing the eleven measured mass peak signals, B is an 11x8 dimensional matrix that contains the coefficients, X is an 8-dimensional vector that contains the concentrations of the eight products to be calibrated, μ is an 11-dimensional vector that contains the background signals of each of the 11 mass peak signals, and finally E is an 11-dimensional random vector representing the measurement error. The quantification of products is done in two major parts. The first part is a calibration step in which the matrix B is estimated on the basis of observed combinations of mass peak signals and relative gas concentrations. The second part is the quantification step in which the vector X of gas concentrations is determined from newly measured mass peak signals and background signals.

Each liquid product is calibrated separately with aqueous solutions of each analyte in concentrations between 5 mM and 50 mM, while the gas products are simultaneously calibrated using calibration mixtures with concentrations between 8000 ppm and 50 ppm of analytes balanced in CO_2. Since the units of concentration of the gaseous and liquid products are not the same, they are converted to their corresponding molar production rate in mol s^{-1}. The values of the coefficients are first estimated through calibration. If there was no linear correlation between the product and mass peak according to NIST reference spectra [26], the coefficient was set to zero. On the basis of $n = 26$ observed pairs $((\bar{Y}_i, X_i)$ of (averaged) mass peak signals and relative gas concentrations, the remaining non-zero elements in the coefficient matrix are estimated by means of constrained least squares minimisation, conditional on having non-negative coefficients. Each $(\bar{Y}_i)$ is the average of multiple observed mass peak signals with the same gas concentration X_i. More details about the minimisation and the resulting coefficient matrix $\hat{B}$ can be found in the Appendix (B.5).

To quantify the products during a chronoamperometry measurement, new mass peak signals $Y_1^*, ..., Y_m^*$ are obtained during the measurement window (see Figure 4.6) and are averaged, such that a vector $\bar{Y}^* = (\bar{y}_1^*, ..., \bar{y}_{11}^*)$ with eleven averaged mass peak signals is obtained:

$$\bar{y}_j^* = \frac{1}{m} \sum_{k=1}^{m} y_{k,j}^*, j = 1, ..., 11 \tag{4.3}$$

Finally, the background varies from day to day and must therefore be measured separately at the beginning of each experiment or calibration series. To get an estimate of the background value, the cell is run at open circuit potential for 30 minutes before the chronoamperometry measurements. The mass peaks $Y_1^{BG}, \cdots, Y_p^{BG}$ measured during these 30 minutes are averaged to obtain a new estimate for the vector of background signals $\hat{\mu}^* = (\hat{\mu}_1^*, \cdots, \hat{\mu}_{11}^*)$ in the same way mass peak signals obtained during the measurement window were averaged before:

$$\hat{\mu}_j^* = \frac{1}{p} \sum_{k=1}^{p} \mu_{k,j}^{BG}, j = 1, ..., 11 \tag{4.4}$$

Here, p denotes the number of mass peak signal measurements that were obtained during the 30 minutes of open circuit potential. To extract the concentrations from the new mass peak signals $Y_1^*, ..., Y_m^*$ we assume that they satisfy the linear model in equation 4.3. Before the quantification step, a qualitative identification step is taken to determine which products could be present. Each compound of interest has one or several major mass peak signals that must be significantly higher than the baseline ($\hat{\mu}^*$) when the compound is present. To identify which peaks were significantly higher than their baseline value, for each mass peak signal ($j = 1, ..., 11$) a two-sample t-test is performed for the groups of background signals $y_{1,j}^{BG}, ..., y_{p,j}^{BG}$ and mass peak signals $y_{1,j}^*, ..., y_{m,j}^*$. To this end, the value of the test statistic is computed as:

$$t_j = \frac{\bar{y}_j^* - \hat{\mu}_j^*}{\sqrt{\frac{s_{1,j}^2}{m} + \frac{s_{2,j}^2}{p}}} \tag{4.5}$$

where $s_{(1,j)}^2$ and $s_{(2,j)}^2$ are the sample variances of the mass peak signals $y_{1,j}^*, ..., y_{m,j}^*$ and background signals $y_{1,j}^{BG}, ..., y_{p,j}^{BG}$, respectively. They are calculated using the following formulas:

$$s_{1,j}^2 = \frac{1}{m-1} \sum_{k=1}^{m} (y_{k,j}^* - \bar{y}_j^*)^2 \tag{4.6}$$

$$s_{1,j}^2 = \frac{1}{p-1} \sum_{k=1}^{p} (y_{k,j}^{BG} - \hat{\mu}_j^*)^2 \tag{4.7}$$

If all identifying mass peaks of a compound pass the t-test with a one-tailed alpha of 0.05, the compound is produced and can be quantified. Otherwise, it is not likely that the compound was produced, and its concentration is set to zero during the quantification. The selected identifying mass peaks for each of the compounds can be found in Appendix B.5. After the identification step, the concentrations are computed by means of constrained least squares minimisation:

$$\min_{0<x_s<UB; s=1,...,8} \|\bar{Y}^* - \hat{\mu} - \hat{B}X\|^2 \tag{4.8}$$

During the least squares minimisation, each coordinate x_s of X is constrained to be between zero and an upper bound UB_s. The upper boundary is determined by first calculating a 95% confidence upper bound for $\sum_{s=1}^{8} \beta_{j,s} x_s$, for each mass peak ($j = 1, ..., 11$) separately, by means of the formula:

$$CB_j = \bar{Y}_j^* - \hat{\mu}_j^* + z_{0.95} \sqrt{\frac{s_{1,j}^2}{m} + \frac{s_{2,j}^2}{p}} \tag{4.9}$$

where $z_0.95$ denotes the 95 percentile of the standard normal distribution. An upper bound for x_s can then be determined by setting all other elements of X to zero and plugin the estimate for $\beta_{j,s}$. If a compound has multiple identifying mass peaks, the smallest upper bound is taken. This leads to the formula:

$$UB = \min_{j=1,...,11} \frac{CB_j}{\hat{\beta}_{j,s}}, s = 1, ..., 8 \tag{4.10}$$

4.3.6. RAPID ELECTROCATALYST SCREENING

To demonstrate the ability of the setup to quantify all major CO_2RR reaction products, a series of fifteen-minute chronoamperometry measurements are performed with decreasing potential from -0.6 V vs RHE to -1.3 V vs RHE on both a polycrystalline silver and copper electrode in triplicates. Polycrystalline silver and copper are chosen as benchmark in accordance with the benchmark set by Bell and co-workers [27]. The results can be found in Figure 4.7. The trends of products over the potential range fit well with other literature sources for both polycrystalline silver [28] and copper [24]. For silver, the current partial densities (Figure B.2 in appendix B.6) are comparable to reported values in literature ($\sim$ 3 mA cm^{-2} for CO at higher potentials, see figure B.2 of appendix B.6) and follow similar trendlines over the measured potential range [28]: At low potentials, hydrogen production is dominant, but CO production slowly picks up and around -0.9 V vs RHE, the catalyst is more selective towards CO. However, at higher potentials the production of CO stagnates, and hydrogen production picks up. Meanwhile, formate production slowly rises from lower to higher potentials and at higher potentials further reduced products such as ethanol and methane are detected. On copper, the product current densities follow the same trendlines as in literature [23], [24]; the selectivity of formic acid and carbon monoxide decreases from low to high potentials. At intermediate potentials, ethylene selectivity increases but at higher potentials this decreases as well, similar to the alcohol selectivity. Finally, methane production becomes more prevalent towards higher potentials. Overall, this measurement confirms that the designed setup and analysis procedure is able to rapidly and accurately quantify the product distribution of CO_2RR electrocatalysts.

At low overpotentials, and therefore low production rates, the faradaic efficiency balance could not be closed to 100%. This is due to a relatively bigger influence of the value of the predetermined background signal (μ) at concentrations close to the lower limit of detection. Additionally, if there are remaining sources contributing to the background in the setup (residual nitrogen), this will result in a higher estimate of the background signal. These background noises will diminish over time and at the start of the first chronoamperometry the actual background signal will be less, leading to an underestimation of the

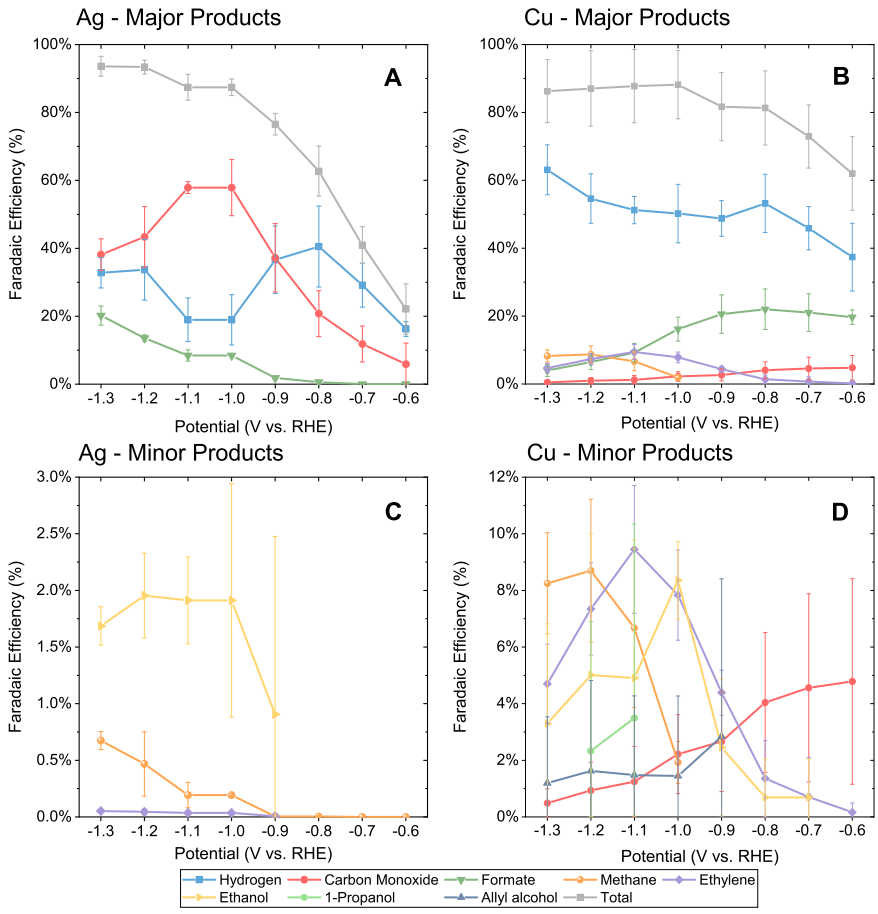

Figure 4.7: Faradaic efficiencies of detected CO_2 reduction products as a function of potential for both silver (A & C) and copper (B & D) electrodes divided into major and minor products, respectively.

production rate. Especially at low activities, these slight underestimations have a relatively bigger influence. Additionally, some data points have larger standard deviations, especially the alcohols and carbon monoxide. This is a result of the identifying step taken during the product deconvolution procedure. These products have a mass peak with a relatively large background noise (28 m/e and 31 m/e for CO and alcohols, respectively) and small coefficients compared to the other products such as hydrogen, methane, and ethylene. As a result, the resulting mass peak signal of 28 m/e and 31 m/e when CO or alcohols are produced will not always be significantly higher than the background signal and the production rate will be set at 0. This results in much larger standard deviation between the different product runs.

The quantification could be sped up even further by shortening the governing residence time distribution of the setup. The residence time distribution itself is limited by the gas-holdup in the cell and the intermittent, discrete manner gas products leave the cell in the

form of bubbles. Therefore, some mixing is required to obtain some level of continuous product effluent. To shorten the residence time, the PEEK cell could be pretreated by ozone making the cell more hydrophilic and thereby reducing the gas holdup. Also, the setup could be slightly redesigned to work under high pressure conditions [10]. Under high pressure, the solubility of gasses in the electrolyte is enhanced, limiting the number of bubbles that get formed and increasing the mass transfer rate to the electrode surface.

4.4. CONCLUSION

An improved differential electrochemical mass spectrometer (DEMS) setup was designed that enables the simultaneous quantification of gaseous and liquid products during the electrochemical reduction of CO_2 significantly faster than conventional analytical techniques and without the need for additional ex-situ measurements. Alternatively, the setup could be used for probing the long-term stability of catalysts by extending the time of the chronoamperometry measurement. The DEMS setup was validated by comparing the catalytic activity of a polycrystalline copper and silver electrode against benchmarks from the literature. Currently, the setup is able to quantify the production rate of most of the major CO_2 reduction products; carbon monoxide, methane, ethylene, methanol, ethanol, 1-propanol, and allyl alcohol. Thereby, to the best of our knowledge, it is the first DEMS setup that is able to simultaneously quantify carbon monoxide and liquid products without the need for additional measurements.

To further improve the current setup, the residence time distribution could be shortened, or the detection limit could be lowered. To shorten the residence time distribution of the setup, the bubble hold-up over the cell needs to decrease. One could treat the PEEK cell with ozone, similar to Clark et al. [10], but this needs specialised setups like an ozone generator. Alternatively, the cell could be redesigned to work under high pressure. At elevated pressure, the solubility of the gas products increases, and bubble formation is prevented. To reduce the product detection limit, the background noise of the mass spectrometer signal can be reduced by optimising the vacuum setup and regularly baking out the setup or by increasing the area of the PTFE membrane to the liquid inlet. A larger area would increase the flow of products into the mass spectrometer and thereby increase the detectability of the MS to liquid products.

Compared to conventional research in H-cells, where the researcher needs to accumulate liquid products for about an hour, the designed setup is about four times faster in determining the catalytic response of a new electrocatalyst over a wide potential range. Therefore, the DEMS setup can significantly speed up electrocatalyst development by enabling the testing of different catalyst materials in a short period of time. Additionally, it enables researchers to widen the number of reaction conditions they can test, for instance using wider potential ranges or different electrolytes. As the hydrodynamics of the cell were quantified and successfully modelled, different hydrodynamic conditions can be used to probe reaction kinetics. Finally, unlike previously reported DEMS setups, the researcher is not limited to a single cell design and the setup can be easily adapted to different cell designs.

BIBLIOGRAPHY

[1] P. De Luna, C. Hahn, D. Higgins, S. A. Jaffer, T. F. Jaramillo, and E. H. Sargent, "What would it take for renewably powered electrosynthesis to displace petrochemical processes?", *Science*, vol. 364, no. 6438, pp. 1–9, 2019, ISSN: 0036-8075. DOI: https://doi.org/10.1126/science.aav3506.

[2] H. Shin, K. U. Hansen, and F. Jiao, "Techno-economic assessment of low-temperature carbon dioxide electrolysis", *Nature Sustainability*, vol. 4, no. 10, pp. 911–919, 2021, ISSN: 2398-9629. DOI: https://doi.org/10.1038/s41893-021-00739-x.

[3] G. A. Olah, G. S. Prakash, and A. Goeppert, "Anthropogenic chemical carbon cycle for a sustainable future", *Journal of the American Chemical Society*, vol. 133, no. 33, pp. 12 881–12 898, 2011, ISSN: 0002-7863. DOI: https://doi.org/10.1021/ja202642y.

[4] D. Trivedi, "Electrochemical reduction of carbon dioxide: Product analysis and cell design", PhD Thesis, 2021. DOI: https://doi.org/10.17635/lancaster/thesis/1611.

[5] O. Wolter and J. Heitbaum, "Adsorption of CO on a porous Pt-electrode in sulfuric acid studied by DEMS", *Berichte der Bunsengesellschaft für physikalische Chemie*, vol. 88, no. 1, pp. 6–10, 1984. DOI: https://doi.org/10.1002/bbpc.19840880104.

[6] O. Wolter and J. Heitbaum, "Differential electrochemical mass spectroscopy (DEMS) — a new method for the study of electrode processes", *Berichte der Bunsengesellschaft für physikalische Chemie*, vol. 88, no. 1, pp. 2–6, 1984, ISSN: 0005-9021. DOI: https://doi.org/10.1002/bbpc.19840880103.

[7] Y. Gao, H. Tsuji, H. Hattori, and H. Kita, "New on-line mass spectrometer system designed for platinum-single crystal electrode and electroreduction of acetylene", *Journal of Electroanalytical Chemistry*, vol. 372, no. 1-2, pp. 195–200, 1994, ISSN: 1572-6657. DOI: https://doi.org/10.1016/0022-0728(93)03291-V.

[8] K. Jambunathan and A. Hillier, "Measuring electrocatalytic activity on a local scale with scanning differential electrochemical mass spectrometry", *Journal of the Electrochemical Society*, vol. 150, no. 6, pp. 312–320, 2003, ISSN: 1945-7111. DOI: https://doi.org/10.1149/1.1570823.

[9] A. H. Wonders, T. H. Housmans, V. Rosca, and M. T. Koper, "On-line mass spectrometry system for measurements at single-crystal electrodes in hanging meniscus configuration", *Journal of applied electrochemistry*, vol. 36, no. 11, pp. 1215–1221, 2006, ISSN: 0021-891X. DOI: http://dx.doi.org/10.1007/s10800-006-9173-4.

[10] E. L. Clark, M. R. Singh, Y. Kwon, and A. T. Bell, "Differential electrochemical mass spectrometer cell design for online quantification of products produced during electrochemical reduction of CO_2", *Analytical chemistry*, vol. 87, no. 15, pp. 8013–8020, 2015, ISSN: 0003-2700. DOI: https://doi.org/10.1021/acs.analchem.5b02080.

[11] E. L. Clark and A. T. Bell, "Direct observation of the local reaction environment during the electrochemical reduction of CO_2", *Journal of the American Chemical Society*, vol. 140, no. 22, pp. 7012–7020, 2018, ISSN: 0002-7863. DOI: https://doi.org/10.1021/jacs.8b04058.

[12] V. Rao, C. Cremers, U. Stimming, *et al.*, "Electro-oxidation of ethanol at gas diffusion electrodes a DEMS study", *Journal of the Electrochemical Society*, vol. 154, no. 11, B1138, 2007, ISSN: 1945-7111. DOI: https://doi.org/10.1149/1.2777108.

[13] W. Silva, A. Queiroz, V. A. Paganin, and F. H. B. d. Lima, "Faradaic efficiency of ethanol oxidation to CO_2 at metallic nanoparticle/short-side-chain PFSA solid-state electrolyte interfaces investigated by on-line DEMS", *Journal of Electroanalytical Chemistry*, vol. 824, pp. 99–107, 2018, ISSN: 1572-6657. DOI: https://doi.org/10.1016/j.jelechem.2018.07.035.

[14] W. Blaedel and G. Schieffer, "A hydrodynamic voltammetric study of the ferricyanide/ferrocyanide system with convective electrodes of platinum, gold, glassy carbon, carbon film, and boron carbide", *Journal of Electroanalytical Chemistry and Interfacial Electrochemistry*, vol. 80, no. 2, pp. 259–271, 1977, ISSN: 0022-0728. DOI: https://doi.org/10.1016/S0022-0728(77)80048-X.

[15] A. Sutey and J. Knudsen, "Effect of dissolved oxygen on redox method for measurement of mass transfer coefficients", *Industrial & Engineering Chemistry Fundamentals*, vol. 6, no. 1, pp. 132–139, 1967, ISSN: 0196-4313. DOI: https://doi.org/10.1021/i160021a023.

[16] C. A. P. Arellano and S. S. Martínez, "Effects of pH on the degradation of aqueous ferricyanide by photolysis and photocatalysis under solar radiation", *Solar Energy Materials and Solar Cells*, vol. 94, no. 2, pp. 327–332, 2010, ISSN: 0927-0248. DOI: https://doi.org/10.1016/j.solmat.2009.10.008.

[17] J. C. Bazán and A. J. Arvia, "The diffusion of ferro- and ferricyanide ions in aqueous solutions of sodium hydroxide", *Electrochimica Acta*, vol. 10, no. 10, pp. 1025–1032, 1965, ISSN: 0013-4686. DOI: https://doi.org/10.1016/0013-4686(65)80014-7.

[18] P. Van Male, M. De Croon, R. M. Tiggelaar, A. van den Berg, and J. Schouten, "Heat and mass transfer in a square microchannel with asymmetric heating", *International Journal of Heat and Mass Transfer*, vol. 47, no. 1, pp. 87–99, 2004, ISSN: 0017-9310. DOI: https://doi.org/10.1016/S0017-9310(03)00401-0.

[19] D. A. Scherson, Y. V. Tolmachev, Z. Wang, J. Wang, and A. Palencsar, "Extensions of the Koutecky–Levich equation to channel electrodes", *Electrochemical and Solid-State Letters*, vol. 11, no. 2, F1, 2007, ISSN: 1944-8775. DOI: http://dx.doi.org/10.1149/1.2818649.

[20] P. Lobaccaro, M. R. Singh, E. L. Clark, Y. Kwon, A. T. Bell, and J. W. Ager, "Effects of temperature and gas–liquid mass transfer on the operation of small electrochemical cells for the quantitative evaluation of CO_2 reduction electrocatalysts", *Physical Chemistry Chemical Physics*, vol. 18, no. 38, pp. 26 777–26 785, 2016. DOI: https://doi.org/10.1039/C6CP05287H.

[21] C. J. Bondue and M. T. M. Koper, "A DEMS approach for the direct detection of CO formed during electrochemical reduction", *Journal of Electroanalytical Chemistry*, 2020, ISSN: 1572-6657. DOI: https://doi.org/10.1016/j.jelechem.2020.113842.

[22] H. S. Fogler and L. Brown, "Distributions of residence times for chemical reactors", in *Elements of chemical reaction engineering*, 5th. Pearson, 2006, ch. 16.

[23] S. Asperti, R. Hendrikx, Y. Gonzalez-Garcia, and R. Kortlever, "Benchmarking the electrochemical reduction on polycrystalline copper foils: The importance of microstructure versus applied potential", *ChemCatChem*, e202200540, 2022, ISSN: 1867-3880. DOI: https://doi.org/10.1002/cctc.202200540.

[24] K. P. Kuhl, E. R. Cave, D. N. Abram, and T. F. Jaramillo, "New insights into the electrochemical reduction of carbon dioxide on metallic copper surfaces", *Energy & Environmental Science*, vol. 5, no. 5, pp. 7050–7059, 2012, ISSN: 1754-5692. DOI: https://doi.org/10.1039/C2EE21234J.

[25] P. L. Kronebusch and J. Berkowitz, "Photodissociative ionization in the 21–41 eV region: O_2, N_2, CO, NO, CO_2, H_2O, NH_3 and CH_4", *International Journal of Mass Spectrometry & Ion Physics*, vol. 22, no. 3-4, pp. 283–306, 1976, ISSN: 0020-7381. DOI: https://doi.org/10.1016/0020-7381(76)80088-5.

[26] NIST, *NIST Standard Reference Database 69: NIST Chemistry WebBook*. 2023. DOI: https://doi.org/10.18434/T4D303.

[27] E. L. Clark, J. Resasco, A. Landers, *et al.*, "Standards and protocols for data acquisition and reporting for studies of the electrochemical reduction of carbon dioxide", *ACS Catalysis*, vol. 8, no. 7, pp. 6560–6570, 2018, ISSN: 2155-5435. DOI: https://doi.org/10.1021/acscatal.8b01340.

[28] T. Hatsukade, K. P. Kuhl, E. R. Cave, D. N. Abram, and T. F. Jaramillo, "Insights into the electrocatalytic reduction of CO_2 on metallic silver surfaces", *Physical Chemistry Chemical Physics*, vol. 16, no. 27, pp. 13 814–13 819, 2014. DOI: https://doi.org/10.1039/C4CP00692E.

5

EXPERIMENTAL SCREENING OF INTERMETALLIC ALLOYS FOR ELECTROCHEMICAL CO_2 REDUCTION

In this chapter, we experimentally screen a promising class of intermetallic alloys for the electrochemical reduction of CO_2 toward hydrocarbon products. Based on previous DFT-based screening papers combinations of strongly CO-binding metals such as iron, cobalt, and nickel with weakly CO-binding metals such as gallium, aluminium or zinc were selected as potentially promising catalytic materials. Despite the challenging production of these alloys, we report a general two-step synthesis method for intermetallic alloys and discuss the specific synthesis conditions that must be taken into account when synthesising these materials. After their synthesis, we use a recently developed DEMS setup to rapidly quantify the CO_2 reduction products over a range of potentials. Almost all newly developed intermetallic catalysts are shown to produce methane and ethylene, while the CoSn catalyst was more selective towards formate. However, all tested catalysts mostly produce hydrogen and only reduce CO_2 to a small extent, despite the favourable computational screening results. We discuss possible reasons for this discrepancy and outline a more holistic approach for future DFT calculation studies.

This chapter has been published in https://doi.org/10.1016/j.cattod.2024.114805

5.1. INTRODUCTION

We currently find ourselves in an energy transition from a society based on fossil fuels to one based on renewable energy. This transition requires many technological changes and innovations. One of the main challenges is developing new processes to produce bulk chemicals using renewable energy and circular raw materials rather than extracting and producing them from fossil feedstocks. If successful, these processes can provide sustainable commodity chemicals in the chemical industry and transportation fuels. Additionally, these processes can serve as a storage medium for renewably generated electricity and as such level off fluctuations between renewable energy generation to match global demand. Currently, synthetic fuels can only be made at an industrial scale via an indirect route, where CO_2 and electrochemically produced hydrogen react to form (higher) hydrocarbons or alcohols. However, it would be more efficient to produce these synthetic fuels directly from CO_2 and water via an electrochemical reaction. This process can be performed at milder conditions and can potentially provide a more direct, efficient route compared to the thermochemical production route.

Unfortunately, it has proven difficult to find an electrocatalyst that selectively reduces CO_2 to a (higher) hydrocarbon or alcohol. Most transition metals generally reduce CO_2 to 2-electron reduction products such as CO and formate. Only copper is able to produce highly desired hydrocarbons and alcohols [1]–[4]. Copper is able to reduce CO_2 beyond CO due to its optimal binding strength of the key surface intermediate CO* [5]. This intermediate is crucial for the reduction of CO_2 towards synthetic fuels. If the binding strength is too strong, for instance with nickel, iron and palladium, the catalyst surface is poisoned by CO* and only hydrogen is produced [6]. On the other hand, if the CO* binding strength is too weak, which, for instance, is the case with gold, silver and zinc, CO* desorbs before it gets the chance to be reduced further [7]. However, the CO* binding strength is not the only parameter that enables copper to reduce CO_2 towards further reduced products. Additionally, copper has a no under potential deposited hydrogen (H_{upd}) [5], displays a favourable binding strength of C* [8] and an ideal atomic spacing that enables it to perform C-C bond forming reactions via CO dimerisation [9]. The major disadvantages of copper are that it produces (oxygenated) hydrocarbons unselectively at relatively high overpotentials and experiences stability issues making it less attractive for industrial applications [3], [10], [11].

Alloying different metals provides an alternative approach to design new catalyst materials that could have superior catalytic performances and superior stability. By alloying, the binding strength of multiple key intermediates can be finetuned by varying the alloy ratio or their geometric structure. However, the combination of more than two metals massively expands the number of possible combinations and materials to be tested compared to the limited selection of only pure metals. Synthesising and testing each of these materials individually would be an enormous and unpractical task. Fortunately, the activity of a material toward CO_2 reduction to further reduced products can be predicted to some extent using density functional theory (DFT) calculations, allowing the relatively fast screening of many different materials. In the literature, many studies have reported simulations on a range of different materials and predictions on potentially interesting materials [12]–[16]. Two of these DFT studies, Li et al. and Tran et al., concluded that the combination of strong CO-binding metals (iron, nickel, cobalt, and palladium) together with weak CO-binding p-block metals (aluminium, gallium, tin, and zinc) can provide good candidates for CO_2 reduction

towards further reduced products [12], [13]. Moreover, combinations of these metals can form a subclass of alloys referred to as intermetallic alloys. The two metal constituents of these materials are arranged in a well-defined crystal structure with fixed atom positions and site occupancies leading to long-range ordering [17]. This well-defined structure can give intermetallic alloys an edge over ordinary bimetallic alloys as it provides a more homogeneous catalyst surface and better control over the catalyst design. Moreover, intermetallic compounds are known for their excellent long-term stability.

However, only a few of these non-copper intermetallic compounds of this combination have been studied for their CO_2 reduction activity. So far only alloy combinations of nickel-group 13 have been tested in the literature [18]–[20]. This could be because of their difficult synthesis process or because of slow analysis techniques to quantify the formed products. Therefore, the goal of this study is twofold: first to design a generalised method for the synthesis of different intermetallic alloys and second to rapidly screen the activity of these alloys for their CO_2RR activity using the DEMS setup developed in chapter 4 to show the effectiveness of this technique. Overall, six different intermetallic alloys, namely AlFe, AlNi, CoSn, NiGa, $FeGa_3$, and $FeZn_4$, were synthesised, characterised, and tested in for their catalytic activity towards CO_2 reduction. Each of these alloys was predicted to be selective binary alloys for the further reduction of CO_2 beyond CO by either one of the two previously mentioned DFT screening papers [12], [13]. We find that although most of these alloys produce hydrocarbon products during CO_2 electroreduction, they mostly produce hydrogen and only reduce CO_2 to a limited extent. Therefore, we outline several causes for the observed mismatch between the computational and experimental results. Moreover, we advocate for a more holistic approach to computational material screening for CO_2RR to improve its accuracy.

5.2. EXPERIMENTAL

5.2.1. MATERIALS

All solutions were prepared using ultrapure water (Millipore Milli-Q gradient A10 system, 18 MΩ cm) and reagents of high purity. Electrolytes were prepared using $KHCO_3$ (≥ 99.95%, trace metal basis, Sigma-Aldrich). As counter electrode, glassy carbon counter electrodes (25x25x1 mm) were purchased from HTW (Sigradur ®, polished). For the calibration of the liquid products, formic acid (≥ 95 % Sigma-Aldrich), methanol (≥ 99.9 % Sigma-Aldrich), ethanol (≥99.8 %, Sigma-Aldrich), 1-propanol (≥ 99.9 % Sigma-Aldrich) and allyl-alcohol (≥ 99 % Sigma-Aldrich) were used to make dilution series. The gaseous products (hydrogen, carbon monoxide, methane, and ethylene) were calibrated using calibration mixtures with concentrations between 8000 ppm and 50 ppm of analytes balanced in CO_2 (Linde). To equilibrate the incoming electrolyte into the cell with CO_2 and in the DEMS setup highly pure CO_2 gas was used (4.5N, Linde). To synthesise the alloys, pure metals were used: Iron powder (99.9%, 100-325 mesh, ChemPur), Nickel powder (99.99%, 100 mesh, MaTeck), Cobalt powder (99.9%, 200 mesh, MaTeck), Aluminium powder (99.95%, 100-325 mesh, MaTeck), Gallium pellets (99.999%, < 3 mm, MaTeck), Tin granules (99.9%, ~3 mm, MaTeck), Zinc granules (99.999%, 1-5 mm, MaTeck).

Table 5.1: Synthesis conditions of the six prepared alloys. In the second and third columns, the temperature and duration of the thermal diffusion step are shown. In the final two columns, the temperature and duration of the subsequent SPS step are shown. *: The CoSn, $FeZn_4$, and NiGa samples were synthesised in a tube oven. Furthermore, the NiGa sample was obtained as one piece and therefore did not need to be spark plasma sintered.

Alloy	Thermal diffusion temperature (°C)	Thermal diffusion duration (h)	Temperature SPS (°C)	Duration SPS (h)
AlFe	1250	2.5	1050	2
AlNi	1250	2.5	1050	1.5
CoSn*	1200	24	900	1.5
$FeGa_3$	900	1.5	700	1.5
NiGa*	1200	24	-	-
$FeZn_4$*	670-550	12-24	500	2.5

5.2.2. ELECTROCHEMICAL MEASUREMENTS

All electrochemical experiments were performed using a Biologic SP-200 potentiostat, using a RE-6 Ag/AgCl reference electrode (BASi). The measurements were performed in a PEEK electrochemical flow cell where the electrolyte flowed over the electrodes in ten parallel channels with 1 mL min^{-1} to improve mass transfer to the electrode surface. All electrochemical measurements were measured in triplicate. A cationic membrane (Nafion 117) was used to prevent any crossover of formed products. Further details about the electrochemical cell can be found in section 4.3.1 of chapter 4. As a counter, a polished glassy carbon (HTW, Sigradur ®) was used. Prior to every measurement run, the glassy carbon electrode was polished using a 3 µm diamond paste (DP-floc, Struers, USA) and a microfiber cloth (DP-floc, Struers, USA) to remove any contaminants. After polishing the glassy carbon electrode was washed with Milli-Q water. The PEEK cell was stored every night in an aqueous 20 vol.% HNO_3 solution to prevent any build-up of contaminants. Further details about the DEMS setup are given in section 4.3.3 of chapter 4.

5.2.3. INTERMETALLIC ALLOY SYNTHESIS

Thermal diffusion was used in this study to obtain the desired alloys. For this method, the pure metals were mixed in their desired atomic ratios and placed inside a crucible with a lid. Typically, around 20 g of each metal was used. The crucible and contents were subsequently heated up to a temperature based on the phase diagram of the alloy in question. The $FeZn_4$ alloy suffered from the high vapour pressure of zinc. Therefore, instead of placing the metals in an open crucible, they were placed in a quartz ampule which was purged with argon and sealed off under vacuum. This ampule was placed in a tube furnace and heated up. To prevent the formation of different intermetallic phases, the ampule was first heated up to 670 °C with a heating rate of 5 °C min^{-1} to form the Γ-phase. Then, the ampule was cooled down with a cooling rate of 5 °C min^{-1} to 550 °C to obtain the desired Γ_1-phase [21]. The CoSn and NiGa samples were synthesised in a tube oven in an alumina crucible under a constant argon flow of 250 mL_n/min. Their heating rate was 5 °C min^{-1}. The other three samples were synthesised in a pressureless SPS setup and were heated and cooled at a rate of 15 °C min^{-1}. During the pressureless SPS synthesis, the die was kept at an overpressure of 20 mbar with argon.

However, after their synthesis, most alloys were often irregular in size, porous, or fragile and could therefore not be used directly in an electrochemical flow cell. Therefore, the metals were crushed into a fine powder and sintered in carbon moulds using spark plasma sintering (SPS) at a pressure of 50 MPa. Only the NiGa sample was obtained as a single piece after melting and therefore did not need a spark plasma sintering treatment. Finally, the obtained disks were sanded to remove the carbon outer layer and polished to obtain a flat surface. The precise synthesis conditions used for each alloy combination can be found in Table 5.1.

5.2.4. XRD MEASUREMENTS

For the XRD measurements, several settings and apparatus were used. For the CoSn and NiGa a Bruker D8 Advance diffractometer Bragg-Brentano geometry and Lynxeye-XE-T position sensitive detector was used. The source was Cu Kα radiation at 45 kV and 40 mA. The variable divergence slit was set to 12 mm irradiated length, and the air scatter screen height to 5 mm. The detector settings were set to "high resolution". For the $FeGa_3$ sample a graphite monochromator and Vantec position-sensitive detector with graphite monochromator was used with Co Kα radiation at 40 kV and 40 mA. Also, the air scatter screen height was set to 8 mm. The AlNi, AlFe, and $FeZn_4$ were measured with a Bruker AXS D2 Phaser using radiation Cu Kα radiation at 30 kV and 10 mA current. For the iron samples that were measured with this setup, the lower discriminator value was set at 0.190 V and the upper value was set at 0.25 V.

5.2.5. ELECTRODE PREPARATION

After sintering, the residual carbon was removed from the metal surface using P180-grid sandpaper and sanded into the desired dimensions for the electrochemical DEMS cell, see 4.3.1. Subsequently, the electrodes were sanded stepwise with sandpaper of finer grid sizes (P320, P800, P1200. P2000). Finally, the alloyed electrodes were polished using 3 µm and 1 µm diamond paste (DP-floc, Struers, USA) and a microfiber cloth (DP-floc, Struers, USA). Prior to each measurement, the polishing steps were repeated to remove any roughened surface and contaminants from the electrodes. Finally, the electrodes were washed using ultrapure water and subsequently dried using compressed nitrogen or argon before cell assembly.

5.2.6. PRODUCT ANALYSIS

MASS SPECTROMETRY SETTINGS

Mass spectrometry was performed on a Hiden HPR40 dissolved-species mass spectrometer. All incoming species were first ionised and subsequently accelerated with a voltage of 3 V and an electron current of 500 µA at an electron energy of 70 eV, except for mass 28 and mass 2. These two masses were accelerated using an electron beam with a current of 50 µA at an electron energy of 19.5 eV. Finally, all masses were detected by a Secondary Electron Multiplier (SEM) which was set at a voltage of 935 V. The calibration method for each of the major reduction products (gasses and alcohols) is discussed in section 4.2.7 of chapter 4.

CARBOXYLIC ACID DETECTION AND QUANTIFICATION

Since carboxylic acids are in the deprotonated form in the 0.1 M $KHCO_3$ electrolyte (pH = 6.8), they cannot pass the DEMS membrane and hence cannot be quantified with the mass spectrometer. Instead, carboxylic acid production was detected and quantified using high-performance liquid chromatography (HPLC). Following the obtained residence time distribution of the DEMS, see figure 4.6 in chapter 4, the electrolyte exiting the liquid DEMS inlet was collected 7 minutes after the chronoamperometry measurement started. The concentration of carboxylic acids was measured by injecting 100 µL into the HPLC (Agilent Technologies 1260 Infinity, USA) to quantify the formed carboxylic acid products. For the catalysts tested in this study only formic acid was detected. The HPLC was calibrated with a dilution series in the range of 0.01 mM to 5 mM of formic acid (95%, Sigma–Aldrich). The flowrate of the eluent (1 mM H_2SO_4 (aq)) was set to 0.6 mL min^{-1} and the measurement ran for one hour. The HPLC used two Aminex HPX-87H columns (Biorad) in series heated to 60 °C. A refractive index detector (RID) was used for the detection of products.

5.3. RESULTS & DISCUSSION

5.3.1. SYNTHESIS AND CHARACTERISATION OF INTERMETALLIC ALLOYS

The main challenge in testing different intermetallic alloys for their electrochemical CO_2 reduction activities was their synthesis. While there are several methods in literature to produce specific intermetallic combinations, these methods are often not transferable to other combinations. Furthermore, wet synthesis methods are often unreliable since there is often not an a-priori known relationship between the starting ratio between the elements and the resulting desired composition [17]. Instead, the alloys of interest were synthesised using thermal diffusion by mixing the pure metal constituents in a crucible and heating the mixture. Here, the different metals diffuse into one another and form the desired alloy phase. Although this method is rather straightforward, several considerations had to be made. For instance, the choice of crucible material was limited due to the nature of all the metals involved; carbon or silicon carbide crucibles will leach carbon into the resulting alloy, while boron nitride will react with both cobalt and nickel at higher temperatures. Therefore, high-purity alumina crucibles were used, except in the case of cobalt-containing alloys, since cobalt oxide and alumina from the crucible react at 1200 °C to form the pigment cobalt blue [22]. Moreover, the temperature could not be increased too much as the crucibles often cracked at higher temperatures. Therefore, the higher melting metals could not be liquefied and had to dissolve into the liquid to form the desired alloy below their melting point. To enhance the mixing of the constituents and shorten the diffusion time of the metals into one another, the high-melting-point metals were added as a fine powder. Finally, due to the low boiling point and high vapour pressure of zinc, this metal was difficult to work with. To prevent the zinc from boiling off, the temperature of these alloys was kept below 900 °C and the metals were sealed in a quartz ampule under vacuum. All alloys were prone to oxidation and were therefore synthesised under an inert argon atmosphere. An oxygen filter was used to keep the oxygen level at ppb levels. However, gallium is much more prone to oxidation and even trace amounts of oxygen below 1 ppb for prolonged periods of time caused the formation of a layer of gallium oxide (Ga_2O_3). Therefore, the gallium alloys were synthe-

sised in a pressureless SPS setup where the presence of graphite foils at high temperatures removes any trace of oxygen from the atmosphere and by using a much shorter synthesis time of 1.5 hours.

Figure 5.1 shows the XRD analysis to indicate the presence of the desired intermetallic compounds. In some cases, relatively small amounts of other phases are detected, which could be due to the incomplete thermal diffusion of both metals into one another. However, in all cases, the relative amount of these other compounds is negligible compared to the desired material following Rietveld refinement. In the case of AlFe, 9% of Al_2O_3 was detected, while in the CoSn sample, 5% Co_2Sn_3 was observed.

5.3.2. ELECTROCHEMICAL MEASUREMENTS

The CO_2 reduction activity of the intermetallic compounds was evaluated using a recently designed DEMS setup. The mathematical model to deconvolute the mass peak signal is described in section 4.3.5 of chapter 4. Consecutive fifteen-minute chronoamperometry measurements were conducted with decreasing potential steps of 0.2 V from -0.3 V vs. RHE to -1.3 V vs. RHE, using 0.1 M $KHCO_3$ as electrolyte. The potential range is chosen based on the conditions outlined in the screening paper that formed the basis of the selection of alloys for this study [12]. All catalysts were stable when emerged in the electrolyte at open circuit potential, with the exception of $FeZn_4$. Due to the ignobility of zinc, the material corrodes and dissolves to form Zn^{2+} and hydrogen. Therefore, the catalyst activity of this catalyst was tested at a more negative potential range between -0.7 V vs. RHE and -1.5 V vs. RHE. Moreover, the potential was always kept at -0.7 V vs. RHE prior to the chronoamperometry measurements to keep corrosion to a minimum.

Figure 5.2 presents the results of the chronoamperometry measurements. At lower potentials, the catalysts do not reach a hundred percent faradaic efficiency balance (see section C.1 of appendix C), most likely due to side reactions where metal oxides on the surface are reduced. These oxide layers can be formed during exposure to air prior to or during the assembly of the cell. It is also possible that at lower potentials, hydrogen is adsorbed on the surface. These reactions cannot be quantified by the DEMS and will therefore not account for the faradaic balance. Eventually, most of the surface oxides are reduced and at higher potentials, the faradaic efficiency balances are closed.

Most catalysts produce methane and ethylene with AlNi being the most active towards hydrocarbon formation, displaying an onset potential for methane production of -0.5 V vs. RHE. Ethylene formation is further observed on $FeGa_3$, $FeZn_4$, and NiGa. AlFe produces only methane and seems to be unable to form a C-C bond necessary to produce ethylene. Among all the tested catalysts only CoSn does not produce any hydrocarbons, but instead only reduces CO_2 to CO and formate. It is, however, quite active towards formate production with an onset potential of -0.3 V. Its inability to form any further reduced products is in stark contrast to the prediction from Li et al. that CoSn should be selective towards C_{2+} products [12].

Since the catalysts in this study have mostly not been tested in literature for their CO_2RR performance before, it is difficult to compare the results with literature sources. Nevertheless, their results are in reasonable accordance with other literature sources that tested comparable materials. Paris and colleagues tested Ni_3Al around -0.8 V vs. RHE and found that the catalyst produced mostly hydrogen and some carbon monoxide when a buffered solution

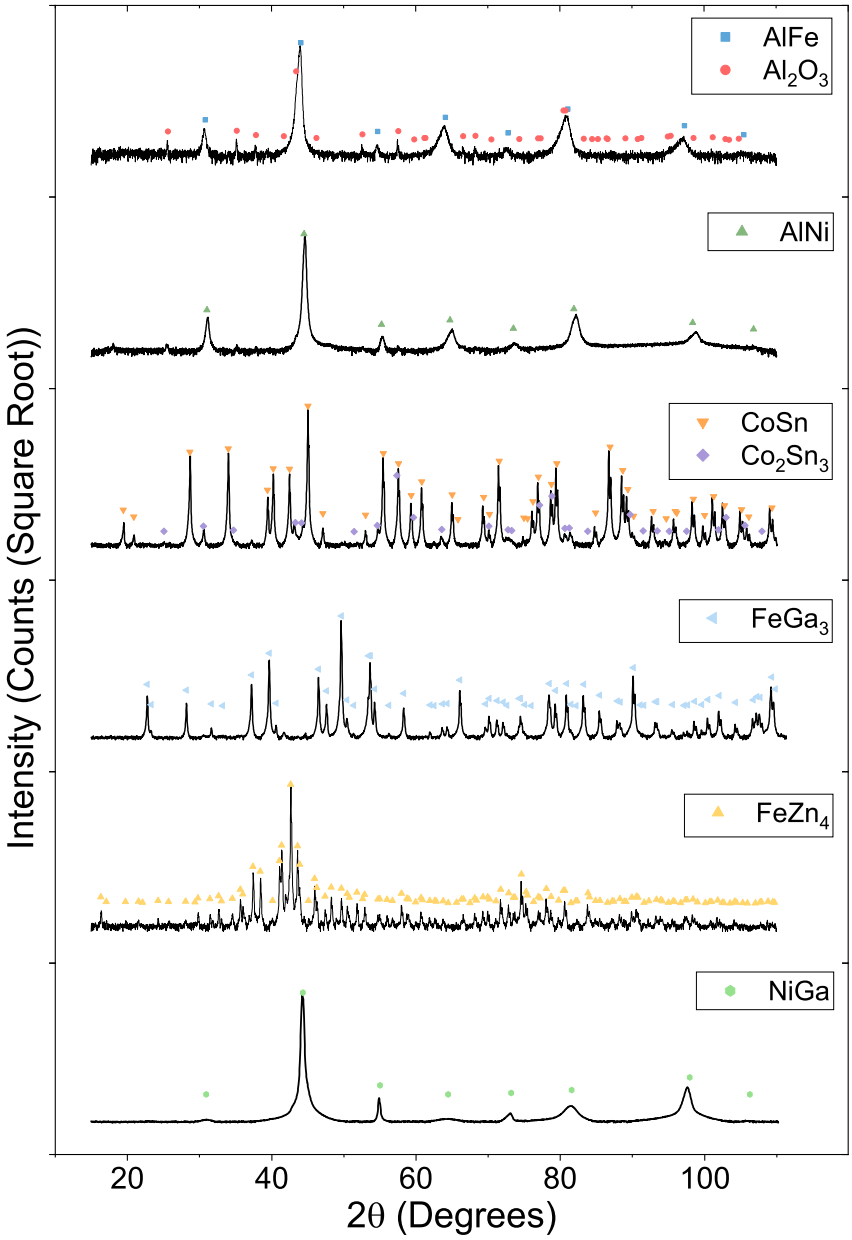

Figure 5.1: XRD diffractograms of the six investigated alloys. The symbols mark the location of the standard diffraction patterns of each respective material. The square root of the intensity is taken to be able to better distinguish the smaller peaks in the diffractogram.

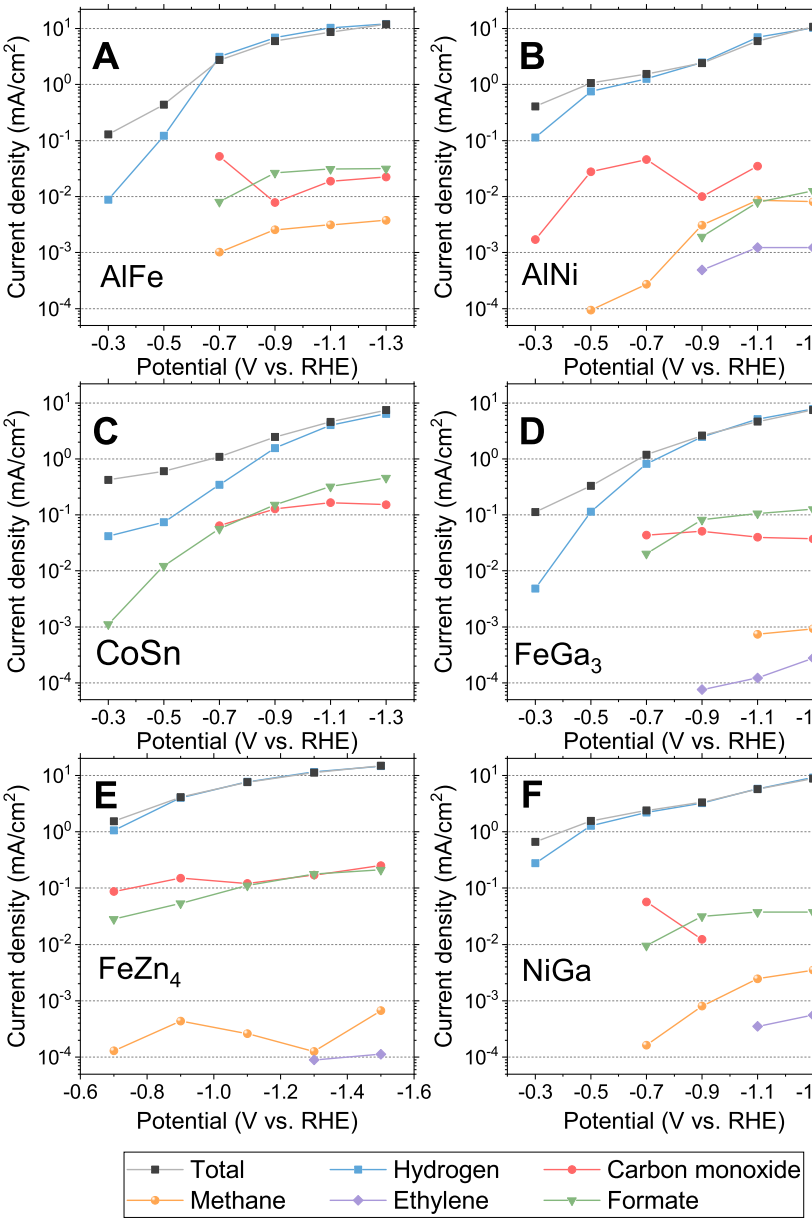

Figure 5.2: Partial current densities for CO_2 reduction in a 0.1 M $KHCO_3$ buffer for AlFe, AlNi, CoSn, $FeGa_3$, $FeZn_4$, and NiGa. The major products observed on the electrodes are hydrogen (■), carbon monoxide (●), formate (▼), methane (●), and ethene (◆). To indicate the activity of the catalyst and the complete quantification of all products, the total measured current is shown as well (■).

was used of 0.1 M K_2SO_4 with $KHCO_3/CO_2$ at a pH of 6.5 [18]. Additionally, Torelli et al. found that NiGa mostly produced hydrogen with some hydrocarbons and trace amounts of CO in 0.1 M Na_2CO_3 acidified to pH 6.8 with 1 atm CO_2 [20]. They found that the catalyst is more active towards ethane rather than ethylene. However, it is difficult to distinguish these two products using the DEMS setup at these production levels, since both products have a similar mass spectrum. Therefore, the activities towards both products could not be quantified in our system.

Finally, the results clearly show that, although most catalysts produce hydrocarbon products, all tested catalysts mostly produced hydrogen and were far from selective towards further CO_2RR products under the tested conditions. This observation is in contrast to the predictions made by screening papers that these materials would selectively produce C_{2+} or further reduced products. Possibly, due to the testing conditions in ambient, aqueous electrolytes, hydrogen evolution is quickly the dominant product due to the overwhelming presence of water and the low solubility of CO_2. Studies have shown that under elevated pressure where there is a higher amount of CO_2 present at the surface, the selectivity of different catalysts can shift significantly [23]–[25], for example, nickel and iron catalysts that produce mostly hydrogen at atmospheric pressures.

Alternatively, the surface composition or structure of the catalyst material during electrochemical testing could differ from the as-synthesised materials. Jovanov and coworkers found a similar discrepancy between prediction and experimental results on Au – Cd alloys [26]. They attributed this discrepancy to the dissolution of cadmium from the alloy. The $FeZn_4$ sample was observed to have some hydrogen formation at open circuit potential inferring some zinc dissolution. This could possibly explain why the $FeZn_4$ sample was not selective towards CO_2 reduction, while this was suggested by Li et al. [12]. Significant leaching of metals from the other alloys is unlikely. If there would have been substantial leaching, there would have been an accompanying reduction reaction to the oxidation of the alloy components. However, no reduction products at open circuit potential for any of the other catalysts or a substantial unbalance in our faradaic efficiency balance during catalyst testing was observed. Alternatively, the in-situ crystal structure could be reformed due to the electrolyte or the applied potential as was observed on a PdAu electrode [27]. Further in-operando spectro analysis of the alloys could indicate if this is the case. Finally, the catalyst surfaces are unavoidably most likely to be slightly oxidised either ex-situ or in-situ prior to the measurements. These oxides are reduced before or during the catalytic measurements. However, the reduction of these oxides will have an effect on the structure and surface roughness of the alloys in-operando. To correctly identify the role of these processes, specialised equipment such as Synchrotron X-ray absorption spectroscopy or XANES in combination with specially designed cells are needed.

Nevertheless, our results stress the impact that the hydrogen evolution reaction has on the selectivity towards CO_2 reduction for a catalyst material. The effect of its hydrogen affinity on a catalyst's CO_2RR selectivity was already highlighted by multiple researchers [28]–[30]. However, in computational CO_2RR screening studies, the hydrogen evolution reaction is often not considered. Therefore, we advocate for a more holistic approach to CO_2RR catalyst screening where both the CO_2RR and the HER are taken into account. This practice is already more common for electrochemical nitrogen reduction screening papers [31], [32]. Furthermore, computational screening studies should also take into account a

material's selectivity towards formate or CO. Many studies focus on the binding strengths of CO_2RR intermediates after the reduction to CO to screen catalyst materials towards further reduced products. However, this step could be premature as CO_2 first has to reduce to CO. However, if this step is not favourable, formic acid is produced instead. However, finding a single descriptor to determine whether a catalyst is selective towards CO or formate has been proven difficult; no clear reason has been found why monometallic catalysts such as silver or gold are selective towards CO under experimental conditions but should be selective towards formate according to DFT simulations. Morrison and coworkers have shown that the surface coverage plays an important role in predicting whether a surface is selective towards CO or formate [33] while Christensen and coworkers show that the materials lattice constant could be used to classify materials [34]. Finding such a descriptor for alloys can greatly enhance the accuracy of computational screening methods.

Finally, screening papers often limit themselves to specific crystal structures or bimetallic compositions (A_3B or AB), due to the large computational efforts that are involved in DFT calculations. However, these structures or compositions might not exist in reality or separate into two stable phase compositions. Examples of this can be found in literature where a catalyst material was synthesised with a specific initial composition, but in-situ segregated into two phases [35], [36]. Also, several predicted alloys from Li et al. could not be synthesised in this study due to this reason (FeGa, FeZn). Therefore, instead of specific bimetallic compositions for all alloys, researchers should use databases of electronic structures of stable compositions to obtain usable predictions from computational screenings. For instance, Tran and coworkers already obtained their intermetallic combinations from the Materials project [37]. Alternatively, researchers could use phase diagrams to check if an alloy is (likely) to be stable at room temperature [38]. Without the use of these databases, computational time and effort are wasted on materials that are impossible to synthesise in practice.

5.4. CONCLUSION

We have synthesised and tested several intermetallic alloys for their CO_2 reduction reaction activity. Moreover, we have outlined a general method to produce these materials and several lessons that were learned. The alloy compositions were selected based on predictions highlighting their CO_2RR selectivity towards further reduced products from previous computational screening papers. The selected compositions were AlFe, AlNi, CoSn, $FeGa_3$, $FeZn_4$, and NiGa. Almost all catalysts were shown to produce hydrocarbons (methane and ethylene), while CoSn was active towards formate. Most materials that were characterised in this chapter have not been tested before in the literature. Nevertheless, their results matched well with similar tested alloy materials in the literature. However, the materials were mostly active towards hydrogen formation and only had limited CO_2 reduction activity. We have postulated several reasons for this discrepancy and outlined several ways to improve CO_2RR screening methods. These results highlight the importance of experimental validation of DFT results and how modelling and experimental work should work together to iteratively find selective CO_2 reduction materials.

BIBLIOGRAPHY

[1] Y. Hori, K. Kikuchi, and S. Suzuki, "Production of CO and CH_4 in electrochemical reduction of CO_2 at metal electrodes in aqueous hydrogencarbonate solution", *Chemistry Letters*, vol. 14, no. 11, pp. 1695–1698, 1985, ISSN: 1348-0715. DOI: https://doi.org/10.1246/cl.1985.1695.

[2] S. Nitopi, E. Bertheussen, S. B. Scott, *et al.*, "Progress and perspectives of electrochemical CO_2 reduction on copper in aqueous electrolyte", *Chemical Reviews*, vol. 119, no. 12, pp. 7610–7672, 2019, ISSN: 0009-2665. DOI: https://doi.org/10.1021/acs.chemrev.8b00705.

[3] K. P. Kuhl, E. R. Cave, D. N. Abram, and T. F. Jaramillo, "New insights into the electrochemical reduction of carbon dioxide on metallic copper surfaces", *Energy & Environmental Science*, vol. 5, no. 5, pp. 7050–7059, 2012, ISSN: 1754-5692. DOI: https://doi.org/10.1039/C2EE21234J.

[4] S. Asperti, R. Hendrikx, Y. Gonzalez-Garcia, and R. Kortlever, "Benchmarking the electrochemical reduction on polycrystalline copper foils: The importance of microstructure versus applied potential", *ChemCatChem*, e202200540, 2022, ISSN: 1867-3880. DOI: https://doi.org/10.1002/cctc.202200540.

[5] A. Bagger, W. Ju, A. S. Varela, P. Strasser, and J. Rossmeisl, "Electrochemical reduction: A classification problem", *ChemPhysChem*, vol. 18, no. 22, pp. 3266–3273, 2017, ISSN: 1439-4235. DOI: https://doi.org/10.1002/cphc.201700736.

[6] M. Azuma, K. Hashimoto, M. Hiramoto, M. Watanabe, and T. Sakata, "Electrochemical reduction of carbon dioxide on various metal electrodes in low-temperature aqueous $KHCO_3$ media", *Journal of the Electrochemical Society*, vol. 137, no. 6, pp. 1772–1778, 1990, ISSN: 0013-4651. DOI: https://doi.org/10.1149/1.2086796.

[7] M. Azuma, K. Hashimoto, M. Watanabe, and T. Sakata, "Electrochemical reduction of carbon dioxide to higher hydrocarbons in a $KHCO_3$ aqueous solution", *Journal of electroanalytical chemistry and interfacial electrochemistry*, vol. 294, no. 1-2, pp. 299–303, 1990, ISSN: 0022-0728. DOI: https://doi.org/10.1016/0022-0728(90)87154-C.

[8] Y. Peng, M. Cui, Z. Zhang, *et al.*, "Bimetallic composition-promoted electrocatalytic hydrodechlorination reaction on silver–palladium alloy nanoparticles", *ACS Catalysis*, vol. 9, no. 12, pp. 10 803–10 811, 2019, ISSN: 2155-5435. DOI: https://doi.org/10.1021/acscatal.9b02282.

[9] F. Calle-Vallejo, J. Martínez, J. M. García-Lastra, J. Rossmeisl, and M. Koper, "Physical and chemical nature of the scaling relations between adsorption energies of atoms on metal surfaces", *Physical review letters*, vol. 108, no. 11, p. 116 103, 2012. DOI: https://doi.org/10.1103/PhysRevLett.108.116103.

[10] S. Popović, M. Smiljanić, P. Jovanovič, J. Vavra, R. Buonsanti, and N. Hodnik, "Stability and degradation mechanisms of copper-based catalysts for electrochemical CO_2 reduction", *Angewandte Chemie*, vol. 132, no. 35, pp. 14 844–14 854, 2020, ISSN: 0044-8249. DOI: https://doi.org/10.1002/anie.202000617.

[11] J. Vavra, G. P. Ramona, F. Dattila, *et al.*, "Solution-based Cu^+ transient species mediate the reconstruction of copper electrocatalysts for CO_2 reduction", *Nature Catalysis*, pp. 1–9, 2024, ISSN: 2520-1158. DOI: https://doi.org/10.1038/s41929-023-01070-8.

[12] J. Li, J. H. Stenlid, M. T. Tang, H.-J. Peng, and F. Abild-Pedersen, "Screening binary alloys for electrochemical CO_2 reduction towards multi-carbon products", *Journal of Materials Chemistry A*, vol. 10, no. 30, pp. 16 171–16 181, 2022. DOI: https://doi.org/10.1039/D2TA02749F.

[13] K. Tran and Z. W. Ulissi, "Active learning across intermetallics to guide discovery of electrocatalysts for CO_2 reduction and H_2 evolution", *Nature Catalysis*, vol. 1, no. 9, pp. 696–703, 2018, ISSN: 2520-1158. DOI: https://doi.org/10.1038/s41929-018-0142-1.

[14] X. Ma, Z. Li, L. E. K. Achenie, and H. Xin, "Machine-learning-augmented chemisorption model for CO_2 electroreduction catalyst screening", *The Journal of Physical Chemistry Letters*, vol. 6, no. 18, pp. 3528–3533, 2015. DOI: https://doi.org/10.1021/acs.jpclett.5b01660.

[15] H. Hansen, C. Shi, A. Lausche, A. Peterson, and J. Nørskov, "Bifunctional alloys for the electroreduction of CO_2 and CO", *Physical Chemistry Chemical Physics*, vol. 18, no. 13, pp. 9194–9201, 2016. DOI: https://doi.org/10.1039/C5CP07717F.

[16] M.-J. Cheng, E. L. Clark, H. H. Pham, A. T. Bell, and M. Head-Gordon, "Quantum mechanical screening of single-atom bimetallic alloys for the selective reduction of CO_2 to C_1 hydrocarbons", *ACS Catalysis*, vol. 6, no. 11, pp. 7769–7777, 2016, ISSN: 2155-5435. DOI: https://doi.org/10.1021/acscatal.6b01393.

[17] A. Dasgupta and R. M. Rioux, "Intermetallics in catalysis: An exciting subset of multimetallic catalysts", *Catalysis Today*, vol. 330, pp. 2–15, 2019, ISSN: 0920-5861. DOI: https://doi.org/10.1016/j.cattod.2018.05.048.

[18] A. R. Paris and A. B. Bocarsly, "Mechanistic insights into C_2 and C_3 product generation using Ni_3Al and Ni_3Ga electrocatalysts for CO_2 reduction", *Faraday discussions*, vol. 215, pp. 192–204, 2019, ISSN: 1364-5498. DOI: https://doi.org/10.1039/C8FD00177D.

[19] A. R. Paris and A. B. Bocarsly, "Ni films on glassy carbon electrodes generate an array of oxygenated organics from CO_2", *ACS Catalysis*, vol. 7, no. 10, pp. 6815–6820, 2017, ISSN: 2155-5435. DOI: https://doi.org/10.1021/acscatal.7b02146.

[20] D. A. Torelli, S. A. Francis, J. C. Crompton, *et al.*, "Nickel–gallium-catalyzed electrochemical reduction of CO_2 to highly reduced products at low overpotentials", *ACS Catalysis*, vol. 6, no. 3, pp. 2100–2104, 2016, ISSN: 2155-5435. DOI: https://doi.org/10.1021/acscatal.5b02888.

[21] O. K. von Goldbeck, "Fe-Zn iron—zinc", *IRON—Binary Phase Diagrams*, pp. 172–175, 1982, ISSN: 3662080265. DOI: https://doi.org/10.1007/978-3-662-08024-5_79.

[22] A. Zhang, B. Mu, H. Li, X. An, and A. Wang, "Cobalt blue hybrid pigment doped with magnesium derived from sepiolite", *Applied Clay Science*, vol. 157, pp. 111–120, 2018, ISSN: 0169-1317. DOI: https://doi.org/10.1016/j.clay.2018.02.032.

[23] K. Hara, A. Kudo, and T. Sakata, "Electrochemical reduction of carbon dioxide under high pressure on various electrodes in an aqueous electrolyte", *Journal of Electroanalytical Chemistry*, vol. 391, no. 1-2, pp. 141–147, 1995, ISSN: 1572-6657. DOI: https://doi.org/10.1016/0022-0728(95)03935-A.

[24] K. Hara, A. Kudo, and T. Sakata, "Electrochemical reduction of high pressure carbon dioxide on Fe electrodes at large current density", *Journal of Electroanalytical Chemistry*, vol. 386, no. 1-2, pp. 257–260, 1995, ISSN: 1572-6657. DOI: https://doi.org/10.1016/0022-0728(95)03917-6.

[25] A. Kudo, S. Nakagawa, A. Tsuneto, and T. Sakata, "Electrochemical reduction of high pressure CO_2 on Ni electrodes", *Journal of The Electrochemical Society*, vol. 140, no. 6, pp. 1541–1545, 1993, ISSN: 0013-4651. DOI: https://doi.org/10.1149/1.2221599.

[26] Z. P. Jovanov, H. A. Hansen, A. S. Varela, *et al.*, "Opportunities and challenges in the electrocatalysis of CO_2 and CO reduction using bifunctional surfaces: A theoretical and experimental study of Au alloys", *Journal of Catalysis*, vol. 343, pp. 215–231, 2016, ISSN: 0021-9517. DOI: https://doi.org/10.1016/j.jcat.2016.04.008.

[27] J. S. Jirkovský, I. Panas, S. Romani, E. Ahlberg, and D. J. Schiffrin, "Potential-dependent structural memory effects in Au nanoalloys", *The Journal of Physical Chemistry Letters*, vol. 3, no. 3, pp. 315–321, 2012, ISSN: 1948-7185. DOI: https://doi.org/10.1021/jz201660t.

[28] R. Chaplin and A. Wragg, "Effects of process conditions and electrode material on reaction pathways for carbon dioxide electroreduction with particular reference to formate formation", *Journal of Applied Electrochemistry*, vol. 33, no. 12, pp. 1107–1123, 2003, ISSN: 0021-891X. DOI: https://doi.org/10.1023/B%3AJACH.0000004018.57792.B8.

[29] M. Jitaru, D. Lowy, M. Toma, B. Toma, and L. Oniciu, "Electrochemical reduction of carbon dioxide on flat metallic cathodes", *Journal of Applied Electrochemistry*, vol. 27, pp. 875–889, 1997, ISSN: 0021-891X. DOI: https://doi.org/10.1023/A:1018441316386.

[30] A. Bagger, "Reduction reactions versus hydrogen", *Current Opinion in Electrochemistry*, vol. 40, p. 101 339, 2023, ISSN: 2451-9103. DOI: https://doi.org/10.1016/j.coelec.2023.101339.

[31] A. Bagger, H. Wan, I. E. Stephens, and J. Rossmeisl, "Role of catalyst in controlling N_2 reduction selectivity: A unified view of nitrogenase and solid electrodes", *ACS Catalysis*, vol. 11, no. 11, pp. 6596–6601, 2021, ISSN: 2155-5435. DOI: https://doi.org/10.1021/acscatal.1c01128.

[32] E. Skulason, T. Bligaard, S. Gudmundsdóttir, *et al.*, "A theoretical evaluation of possible transition metal electro-catalysts for N_2 reduction", *Physical Chemistry Chemical Physics*, vol. 14, no. 3, pp. 1235–1245, 2012. DOI: https://doi.org/10.1039/C1CP22271F.

[33] A. R. Morrison, M. Ramdin, L. J. Van Der Broeke, W. De Jong, T. J. Vlugt, and R. Kortlever, "Surface coverage as an important parameter for predicting selectivity trends in electrochemical CO_2 reduction", *The Journal of Physical Chemistry C*, vol. 126, no. 29, pp. 11 927–11 936, 2022, ISSN: 1932-7447. DOI: https://doi.org/10.1021/acs.jpcc.2c00520.

[34] O. Christensen, A. Bagger, and J. Rossmeisl, "The missing link for electrochemical CO_2 reduction: Classification of CO vs HCOOH selectivity via PCA, reaction pathways, and coverage analysis", *ACS Catalysis*, vol. 14, pp. 2151–2161, 2023, ISSN: 2155-5435. DOI: https://doi.org/10.1021/acscatal.3c04851.

[35] E. L. Clark, C. Hahn, T. F. Jaramillo, and A. T. Bell, "Electrochemical reduction over compressively strained CuAg surface alloys with enhanced multi-carbon oxygenate selectivity", *Journal of the American Chemical Society*, vol. 139, no. 44, pp. 15 848–15 857, 2017, ISSN: 0002-7863. DOI: https://doi.org/10.1021/jacs.7b08607.

[36] S. Chandrashekar, N. T. Nesbitt, and W. A. Smith, "Electrochemical reduction over bimetallic Au thin films: Comparing activity and selectivity against morphological, compositional, and electronic differences", *The Journal of Physical Chemistry C*, vol. 124, no. 27, pp. 14 573–14 580, 2020, ISSN: 1932-7447. DOI: https://doi.org/10.1021/acs.jpcc.0c01894.

[37] A. Jain, S. P. Ong, G. Hautier, *et al.*, "Commentary: The materials project: A materials genome approach to accelerating materials innovation", *APL materials*, vol. 1, no. 1, pp. 1–11, 2013. DOI: https://doi.org/10.1063/1.4812323.

[38] H. Okamoto, *Desk handbook: phase diagrams for binary alloys*, 1st ed. Materials Park: ASM International, 2000, ISBN: 0871706822 9780871706829.

6

Conclusions & Recommendations

6.1. CONCLUSION

Following the global energy transition from a fossil fuel-based to a renewable energy-based society, new processes must be developed to produce many different bulk chemicals from electricity and CO_2. This dissertation investigated the role bimetallic electrocatalysts could play within this transition. This thesis aimed to develop a new bimetallic catalytic material that could produce renewable fuels directly from CO_2, water, and electricity. The focus was on non-copper alloys, as copper alloys have already been widely tested in literature.

The field of bimetallic electrode materials has so far mainly focused on copper alloys, yet has made no significant improvement in the performance of monometallic copper. Therefore, we first studied the currently available literature to identify possible causes for this lack of improvement. In chapter 2, several of the main shortcomings in the current literature were highlighted and several ways were indicated to circumvent them. As of now, progress in research is mostly hindered in three ways: firstly, catalyst material analysis is often only done on pristine catalysts in ex-situ conditions without consideration whether these structures are maintained during in-situ conditions. Therefore, the reported electrocatalytic material structure might deviate from the tested catalyst structure. Secondly, most research groups use different, custom-made cells for their research with different governing cell hydrodynamics. These hydrodynamics greatly influence the surface concentrations during CO_2 reduction or even lead to mass transfer limited conditions. By not standardising the hydrodynamics of the used cell, results could unknowingly be affected making comparisons between results difficult. Finally, analytical techniques used to quantify CO_2 reduction products are slow and have a high limit of detection. As a result, researchers have to extend the run time of experiments slowing down their research. Therefore, the research scope often remains limited to only a handful of catalysts and there is little to no variety in tested process conditions. So, there are still many more catalyst materials to be tested or materials that have been tested under sub-optimal conditions.

As was noted in the previous chapter most research is often done under the same reaction conditions and using the same electrolyte, the often overlooked role of the electrolyte (buffer) on the CO_2 reduction process was investigated in Chapter 3. The influence of two buffers, $KHCO_3$ and KH_2PO_4/K_2HPO_4, was studied on the selectivity of a bimetallic gold-palladium electrode to elucidate observed inconsistencies between different studies into this metal combination. Both the bimetallic AuPd electrocatalyst as well as monometallic gold and palladium catalysts were shown to have a higher activity towards hydrocarbons in a phosphate buffer compared to a bicarbonate buffer around the same pH. Through the study of CO_2 reduction on AuPd in bicarbonate buffers of varying buffer strengths, it was concluded that the observed differences in product activities were caused by the difference in buffer strength, not the presence of certain anions at the electrode interphase. The results showed a strong link between the buffer choice and product activity, further demonstrating the strong interaction between the catalyst activity and the local reaction conditions at the surface. Our data suggested that on the tested catalyst materials ethylene and higher hydrocarbons are formed via a pH-dependent reaction mechanism that differs from the pH-independent CO-dimerisation mechanism on a copper surface. In short, the study gave additional evidence that catalyst design cannot be a one-sided effort by solely optimising the catalyst material.

As stated in chapter 2, product quantification techniques are often slow, limiting the scope of researchers and the speed of catalyst development. To accelerate these quantitative techniques, a new differential electrochemical mass spectrometer (DEMS) setup was developed in Chapter 4 that enables the quantification of most major gaseous and liquid-products CO_2RR products four times faster than conventional analytical techniques and without the need for additional ex-situ measurements. The reproducibility of this new setup was demonstrated by comparing the catalytic activity of a polycrystalline copper and silver electrode against benchmarks from the literature. Moreover, the hydrodynamics of the cell were quantified and successfully modelled. This model enhanced the understanding of the mass transfer rate of CO_2 to the surface and helped to indicate when the conversion rate is suffering from mass transfer limitations. The methods used in this chapter provide a way to determine the mass transport of CO_2 in other cell configurations as well. As such, it provides a handle to keep process conditions consistent between measurements and research groups.

Finally, in chapter 5, several intermetallic compounds were synthesised and their electrochemical CO_2 reduction activity was quantified using the newly developed DEMS setup from the previous chapter. Although the synthesis of these materials has been proven difficult, a generalised method was devised for a wide range of different materials by applying a two-step process where the materials were first synthesised using thermal diffusion and subsequently pressed into the desired shape using spark plasma sintering. Several intermetallic compounds were selected that were predicted to be selective towards C_{2+} products based on two DFT-based screening papers. While most materials did reduce CO_2 to further (higher) hydrocarbons, all materials mostly produced hydrogen and only produced CO_2RR products to a minor extent. These results suggest that there is a mismatch between the computational screening of catalyst materials and their in-situ selectivity. Several possible reasons for this discrepancy were discussed. Also, the mismatch shows that instead of a detailed screening of materials based on their CO reduction capacity, computational screening of CO_2RR catalyst materials should take a more holistic approach where the catalyst activity towards hydrogen, formate, and carbon monoxide should be taken into account.

6.2. RECOMMENDATIONS

The vast number of different materials that are still left to be tested, their ability to break scaling relations, and their large freedom of design, make bimetallic CO_2 reduction catalysts interesting for the development of new active and selective catalysts. However, the field currently lacks a systematic approach which leads to inefficiency and a lack of a significant breakthrough. The recommendations to improve each step of the catalyst development cycle are listed below:

- Currently, new catalyst designs are often based on DFT calculations that assume ideal conditions. These conditions rarely hold in practice. Instead, new materials should be developed based on experimental results. Given enough data points from different catalyst materials under various conditions, machine learning could offer a great tool to help catalyst development further. With the current analytical techniques and cell designs, this task would be impossible, but with the newly developed DEMS setup, these two tools could work together, where the DEMS would provide the quantitative experimental results as input for the machine learning model. Meanwhile, the ma-

chine learning model would use this input to predict possible new catalyst material designs that will be tested by the DEMS setup. The feedback loop created this way would be able to get more accurate predictions with every iterative step and spur on high throughput catalyst development.

- Successful catalyst synthesis remains one of the most challenging aspects of catalyst development. Thermal diffusion is a more consistent method to acquire the desired alloy composition compared to other synthesis methods like wet synthesis methods and results in more stable catalyst configuration under in-situ conditions. However, the method often requires a second sintering step to produce a solid electrode that can be used in cell configurations. These sintering setups are not always available and are expensive. Therefore, research into (new) reliable catalyst synthesis methods is crucial for rapid catalyst development. Alternatively, one could explore different sintering, casting or spray-coating methods to manufacture stable electrodes.

- While the new DEMS setup is able to successfully quantify products at a potential about four times as fast as with conventional setups, it would be beneficial to speed this up even further. The main bottleneck towards rapid measurements is the governing residence time distribution of the setup. The residence time distribution itself is limited by the gas holdup in the cell and the intermittent, discrete manner gas products leave the cell in the form of bubbles. Therefore, mixing is required to obtain a stable measurement signal. To shorten the residence time, the PEEK cell could be treated with ozone making the cell more hydrophilic and thereby the gas holdup.

- Currently, the DEMS setup and most conventional setups work under ambient pressure, it would be beneficial to redesign the cell to work under high-pressure conditions for two reasons: under high pressure, the solubility of gasses in the electrolyte is greatly enhanced, limiting the number of bubbles that get formed, removing the need for mixing and shortening the residence time distribution. Additionally, under high-pressure conditions, the reaction conditions resemble industrial conditions more closely, making further scale-up easier.

- In electrochemical CO_2 reduction, deriving kinetic rate equations for CO_2RR catalyst development is not widely applied. However, knowing the effect of surface conditions on catalyst activity and selectivity can provide important insights into the reaction mechanism and rate-determining steps. These kinetic insights could help focus catalyst development and lead to interesting new materials. To measure the catalyst kinetics, a setup needs to be developed that is able to vary the surface concentration of CO_2 and H^+ under well-defined hydrodynamics. Here, the newly developed DEMS setup developed in this thesis could be used. If the setup would be redesigned to work under high-pressure conditions, such a system would be ideal for probing the kinetic behaviour of new catalyst materials.

ACKNOWLEDGEMENTS

When you are doing your PhD and climbing this unforgiving mountain without knowing if you will ever reach the top, it is the people around you that keep you going or guide you in the right direction. Over these four-odd years, I have met many people to whom I am extremely grateful for their help, guidance, and support. These two pages are not enough to thank everyone sufficiently, but I will give it a go.

First of all, I want to thank **Dr. Ruud Kortlever**. You were the one who started it all by giving me this project on bimetallic electrodes, free of any consortium or backers to follow. You gave me the absolute freedom to build further on your PhD and postdoc work and follow my own path. I have always been very grateful for this freedom and trust you gave me. Besides, during my PhD, you guided my perfectionism in the right direction. Without that, I might still be in the lab right now, trying to improve my DEMS setup.

Secondly, I want to thank **Prof. dr. ir. Wiebren de Jong**. Although you might have been a bit further away from the day-to-day supervision, you were always ready to jump into action and help out wherever possible. I also very much appreciated the open-door policy and the way you always treat everyone equally. That creates a relaxed and open feeling in the group which makes it a great place to work.

Furthermore, I would like to thank the members of my thesis committee, **Dr. A. B. Bansode**, **Prof. dr. M. Escudero Escribano**, **Prof. dr. M. K. M. Koper**, **Prof. dr. ir. J. R. van Ommen**, and **Prof. dr. M. Tromp** for their timely feedback and their presence during the defence.

Then, without the knowledge of many technicians at the university and outside, I would still be at the foot of the mountain, not knowing where to start. Their invaluable guidance, knowledge and ideas helped me make big jumps in my research. **Michel van den Brink**, as the sole technician in the lab, you are the go-to person for any question in the lab, big or small, and you are always ready to help. With your experience, nothing phases you anymore, saving us all many times. **Jim Melling**; although we have never met face-to-face, I have sent you more emails than any other person in my quest to troubleshoot the DEMS setup. You were always quick to respond, ready with new solutions and answered all my (sometimes silly) questions. Maybe we will finally meet one day! Then, the guys at DEMO, **Bas, Daniël, Gerard, and Martijn**, were always ready to help, think along, or make any weird design I had come up with that day. **Hans Brouwer**, when I was running out of options to make my intermetallic alloys, you gave me access to all the amazing setups in your lab. Your creativity, knowledge, and fearlessness to try any idea, motivated me to bring my final project to a good end. Finally, **Ruud Hendrikx**, my fellow train-taker, thank you for all the swift help with the XRD measurements. You always were ready to help out and your speed and efficiency were greatly appreciated.

Many other people also helped me along the way: **Rik Lopuaä**, thank you for guiding me through the forest of statistics. I would never have been able to find my way out of it. Our discussions mostly consisted of trying to understand each other's field, but somehow

we got there. **Isabell Bagemihl**: Thank you for your help with all my questions on getting the Taylor flow stable. **Albert Santoso**: Thank you for your help on the microfluidic mixer, it was interesting to dive into that topic. **Em. prof. dr. Rob van Veen** and **Ruud de Regt**, thank you both for thinking along with me and for supplying me with those beautifully sputtered AlPd samples.

In the time that I was with the Large Scale Energy Storage group, we have rapidly grown. COVID gave us a difficult start, but over the course of all the lunches, group outings, and conferences, we finally had the chance to come together. I am going to miss you all: **Ahmed**, thank you for your in-depth discussions and help in the lab with your deep knowledge of electrochemistry. **Aleksandra**, thank you for all the sweets you brought from all over the world. **Andrea**, thank you for helping out during the beginning of my PhD and showing me the ropes. You showed us we should not be afraid to stand up for ourselves during our PhD. **Asvin**, thank you for your steady help in the lab as an unofficial lab manager. I could always count on you. **Boaz**, my conference roommate, thank you for all your help during sparring sessions in the lab and for introducing me to half the people I met during my PhD. Your stoic, yet positive outlook on our PhD, helped me take the load of the PhD a lot less heavy. **Henga**, thank you for your kind and happy presence in the lab and the office. **Iris**, thank you for the talks and the help in organising. You work very hard and get stuff done. I always liked taking a detour for coffee-star coffee, even though I never got coffee there myself. **Katherine**, we only got to meet in the last few months, but your positivity brightened up the lab. Take good care of my baby in the lab: the DEMS. **Katie**, thank you for always being a listening ear. You are always happy to help even if you're way too busy yourself. I am going to miss the coffee talks and the lunches. **Liangyuan**, thank you for being my supervisor during my master's thesis and my deskmate during my PhD. **Marilia**, thank you for teaching me the beginnings of most techniques in the lab. Your tenacity in building the lab really helped us get on our way. **Nandalal**, it was great fun to play football with you, I wish we could have gone more often. **Shahid**, it was great getting to know you. Good luck with your grant, if you work as hard at it as you follow cricket, I am sure you will crush it. **Shilong**, thank you for all your non-wavering help in the lab and for the great talks about food, culture and everything in between. I really learned a lot from you and am happy you found your post-doc position here. **Sohan**, thank you for the talks, your great presentations in the group meetings and keeping my chemical engineering skills sharp.

And of course to all my friends outside the university: thank you for supporting me by providing the best distraction I could wish for from the hectic life of a PhD. **Amantrita, Ben, Clarissa, Esmee, Georg, Giulia, Hongyu, Jordi, Joseph, Lena, Marco, Mark, Mayur, Mehul, Nienke, Pavithra, Ruben, Sara, Shridhar, Soraya, Thorben, Vidhi, Yesaswini, Zoey**: Thank you all for the laughs, discussions, company, and food. Even though we seem to be spreading out all over the globe, the moment we get together again, everything is back to normal. I hope there will be many more dinners, picnics, holidays, trips, bars, weddings, movies, paintball and laser tag games, Sinterklaas, Christmases, Diwali, and New Year's celebrations to come. Also, I won't forget my high school friends: **Ben, Casper, Evert, Luc, Lucien, Sander, and Shin**. We have hung out now for about fifteen years from where it all began at the surfboard. Yes, Lucien, that means we are getting old. Thank you for letting me forget all other worries and just be our idiotic selves the moment we get together. I hope we can work out a tekentafel soon again.

Many thanks to my family for their support over the last few years. **Age, Emma, Hella, Iris, Lena, Marcel, Martijn, Odette, Rosa**, thank you for being there when I grew up and for everything you have done for me. En natuurlijk ook **Opa** en **Oma**: dit is dan eindelijk mijn boekje. Jullie waren altijd ontzettend geïnteresseerd in mijn onderzoek en dat maakte het uitleggen extra leuk! **Sarah** and **Lukas**, my big little sister and brother, thank you for letting me be your big brother. Thank you for the talks and the laughs. I hope my companion piece helps to explain what I work on. Of course, I cannot forget the big family that I gained during my PhD in Kerala: **Amma, Acha, Appuchettan, Gayathri, and the whole extended families** (I have to keep it short or write a whole page of names), thank you for the warm welcome into your family and the amazing care you always give me. I am truly grateful for that. Thank you also for showing me how to worry less in life, I still have much to learn.

Above all, I would like to thank my parents. You have put me where I am today. Your unwavering support for everything I did, helped me more than you can imagine. I have said it before, but through both of your different personalities, I was able to find my own balance. **Papa**, if I had let you, you would have jumped in and solved every problem I encountered on the way during my PhD, even if that would have come at your own expense. You helped me in any way you could and in case I have not said it yet: thank you. **Mama**, thank you for the mental support, the talks over the weekly dog walks in het Leidse Hout, just letting me vent about anything, or bringing over Charlie (whom I thank for all the laughs and pets!). Thank you for fostering my imagination and love for cooking. It helped me more in my PhD than you can imagine.

Finally, **Meera**, what do I write to thank you? This part of my thesis was the hardest to write. I am sure that if I would ask you, you would probably know exactly what to say because you always do. But this is the only part of my thesis you do not get to read beforehand. Thank you for being my calm and for calling me out on my perfectly rationalised, irrational thinking. Your calm and stoic view of life has taught me how to overthink less, but I still have much to learn. I could not have survived this PhD without you. I do not know what else life will bring us, but I cannot wait.

Daniël van den Berg
Leiden, September 2024

A

APPENDIX CHAPTER 3

A.1. SEM-EDX RESULTS

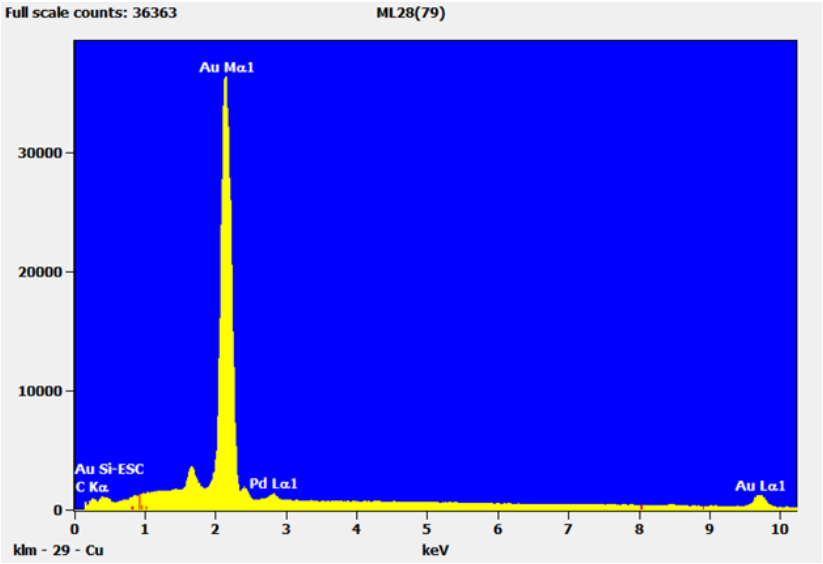

Figure A.1: EDX spectrum of the gold-palladium electrode surface.

A

A.2. XPS RESULTS

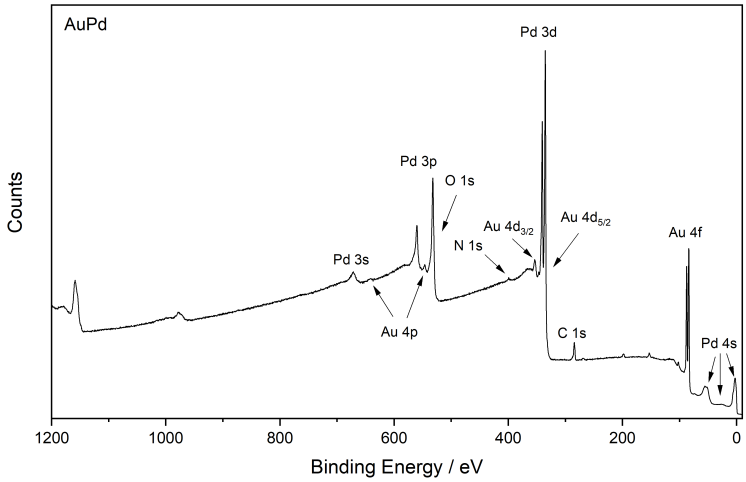

Figure A.2: XPS survey spectrum from -10 eV to 1200 eV of a Pd-Au electrode. Pass energy is 200 eV with step size 0.1 eV.

Table A.1: AuPd and Pd foil XPS fitting parameters.

	AuPd		Pd Foil	
Name	**Position**	**FWHM**	**Position**	**FWHM**
PdO 5/2	335	1.05	335.17	1.1
PdO 3/2	340.3	1.05	340.47	1.1
PdO 5/2	336.1	1.33	336.1	1.5
PdO 3/2	341.4	1.33	341.4	1.5
PdO_2 5/2	337.5	2	337.3	3
PdO_2 3/2	342.8	2	342.6	3
Au 4d 5/2	334.5	4		
Au 4f 7/2	83.91	0.94		
Au 4f 5/2	87.59	0.96		

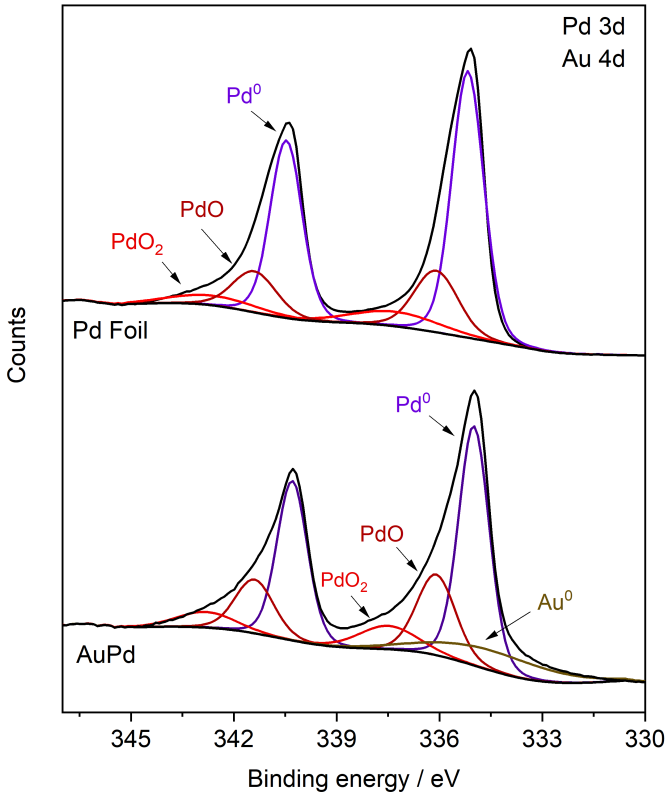

Figure A.3: XPS high-resolution Pd 3d and Au 4d spectral region for a Pd foil and AuPd electrode.

A.3. FERRO/FERRICYANIDE EXPERIMENTS

Ferro-/ferricyanide redox couple was used to determine the hydrodynamics of the flow within the cell. A buffer of 0.1 M $KHCO_3$ (99.95%, Sigma Aldrich) + 5 mM $K_3Fe(CN)_6 \cdot H_2O$ (99.9%, Sigma Aldrich) + 5 mM $K_4Fe(CN)_6$ (99.9%, Sigma Aldrich) was made and inserted through the cell, using polished glassy carbon (HTW) as both the working and counter electrode, since unpolished glassy carbon or metal surfaces could lead to unwanted side reactions [1]. Furthermore, Argon was bubbled through the electrolyte to simulate the CO_2 bubbles during the experiment and to remove any dissolved oxygen to prevent ferrocyanide oxidation [2]. Lastly, all experiments were performed in the dark to prevent photolysis of the cyanide complexes through photo dissociation under UV light leading to cyanide formation [3]. Linear sweep voltammetry was performed between open circuit potential to + 0.7 V vs. E_{oc} at a sweep rate of 1 mV s^{-1} and maintaining an Argon flowrate of 8 mL_n/min. The sweep rate was kept low to limit the contribution of double-layer charging. Cell resistance could not be determined using PEIS since at any potential faradaic reactions occur. Therefore, these results are shown without ohmic drop compensation.

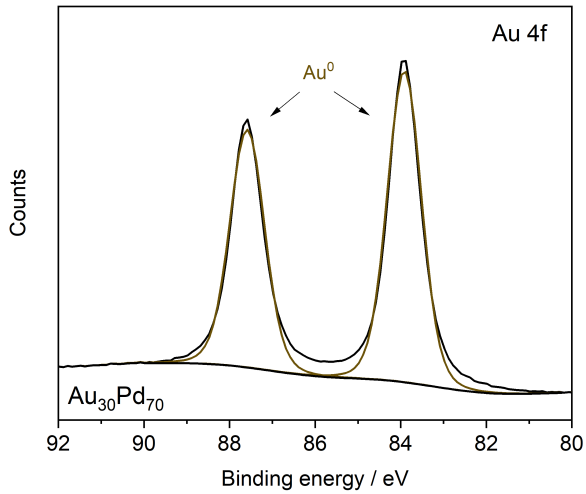

Figure A.4: XPS high-resolution Au 4f spectrum for a AuPd electrode.

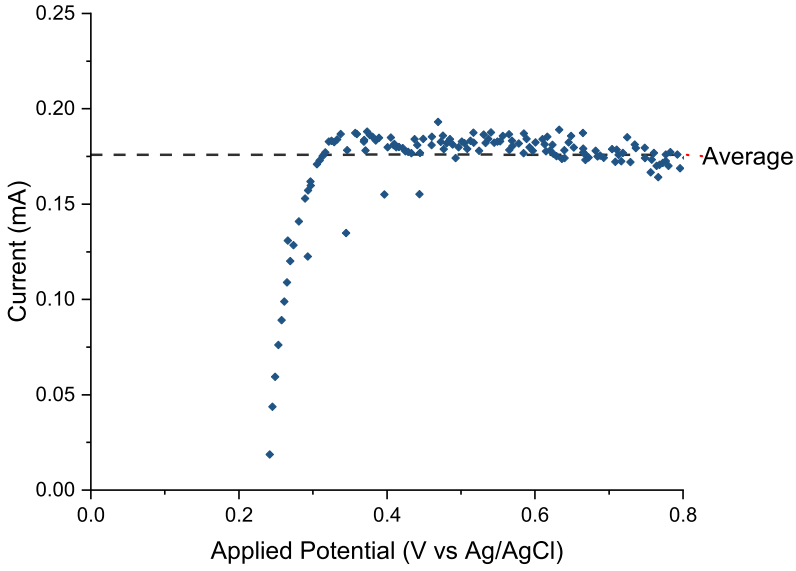

Figure A.5: Reversible ferrocyanide oxidation during a LSV of 0.1 mV s^{-1} from open circuit potential to E_{oc} + 0.7 V. Results shown are the average of eight consecutive LSVs. The potential is shown up until 0.8 V. The average oxidation current is shown as a dashed line in the figure and the average of the current between 0.6 V vs. Ag/AgCl and 0.8 V vs. Ag/AgCl.

Table A.2: CO_2 consumption rates on a polycrystalline gold electrode in both a phosphate and bicarbonate buffer at a potential range between -0.8 V vs. RHE and -1.2 V vs. RHE. The consumption rates are calculated from the sum of average partial current densities of all CO_2 reduction products at each respective potential.

	CO_2 consumption (nmol s^{-1})	
Applied potential vs. RHE	**Phosphate buffer (0.1 M KH_2PO_4 +0.1 M K_2HPO_4)**	**Bicarbonate buffer (0.1 M $KHCO_3$)**
-0.8	4.6	10.5
-0.9	12.8	11.1
-1.0	22.7	19.5
-1.1	25.1	24.5
-1.2	22.9	23.6

B

Appendix Chapter 4

B.1. Film Theory

CO_2 availability near the electrode surface has a major influence on the catalyst activity and selectivity. Therefore, it is important to ensure that enough CO_2 can reach the surface to prevent depletion and keep the CO_2 concentration the same during and between experiments. Therefore, the mass transfer of species towards the electrode surface was analysed using the so-called film model. Here, the molar flux from the bulk of the solution is defined as follows:

$$\phi = k \cdot A_{surf} \cdot (c_{bulk} - c_{surf}) \tag{B.1}$$

Here, k, the mass transfer coefficient, can be expressed as follows: $textitk = (Sh \cdot D)/d$. Here, Sh (Sherwood number) is a dimensionless number representing the ratio between convective and diffusion mass transfer rate to the surface. d is the height of the flow channels and D is the diffusion coefficient. A_{surf} is the area of the electrode that is exposed to the electrolyte, while c_{bulk} and c_{surf} represent the bulk and surface concentration of the reactant concerned. Now, the expression becomes:

$$\phi = \frac{Sh \cdot D \cdot A_{surf} \cdot (c_{bulk} - c_{surf})}{d} \tag{B.2}$$

Since it is not possible to measure the concentration of a species at the surface directly, the current is measured using linear sweep voltammograms (LSV, sweep rate 1 $mV\,s^{-1}$) until the mass transport becomes limiting instead. When mass transport becomes limiting, the concentration near the surface approaches zero. To link the mass transport towards the surface to the measured current, Faraday's laws of electrolysis were used. Since CO_2 reduction can have multiple parallel reactions, the ferro-/ferricyanide redox couple was used as it is a single electron reaction without side reactions.

$$\phi = \frac{Sh \cdot D \cdot A_{surf} \cdot (c_{bulk})}{d} \tag{B.3}$$

B.2. CALCULATING LIMITING CURRENTS

In this paper, the limiting currents for the new cell design were calculated in two ways: following the Koutecky-Levich expression, as derived by Scherson et al. for the limiting current over a channel electrode [1]:

$$i_{lim} = 1.0175 \cdot n \cdot F \cdot w \cdot h^{-1/3} \cdot L^{2/3} \cdot v^{1/3} \cdot D^{2/3} \cdot c \tag{B.4}$$

Where, n is the number of electrons that is transferred, F the Faraday constant (96485 C/mol_{e^-}), w stands for the width of the channel, h is the half-height of the channel, L represents the length of the channel, v the fluid flow velocity in the centre of channel, D is the diffusion coefficient and c is the bulk concentration of the reacting species. The width, height, and length of the channel were taken from the design and were 1 mm, 1 mm, and 25 mm respectively. The fluid velocity was calculated by dividing the fluid flowrate by the cross-sectional area of a channel ($w \cdot h$) and 10 to account for the fact that the fluid divides itself over 10 different channels. The diffusion coefficient, D, was taken from the literature as $6.67 \cdot 10^{-10}$ $m^2\,s^{-1}$ for ferrocyanide and $19.7 \cdot 10^{-10}$ $m^2\,s^{-1}$ for CO_2 [2], [3]. The concentration of CO_2 in the bulk, c_{bulk}, was calculated using Henry's law where the value for the Henry law coefficient was taken from the literature and equal to 0.034 $mol\,L^{-1}\,bar^{-1}$ [4].To obtain the total limiting current over all the channels, this value was multiplied by the number of channels N.

Secondly, the limiting current was calculated following equation S.3 in combination with an expression for the Sherwood number for flow through a microchannel from van Male et al. [5]:

$$Sh = 2.467 \cdot \left(1 + \frac{Gz}{27.3}\right)^{0.407} \tag{B.5}$$

Where Gz is the Graetz number, which is calculated as follows:

$$Gz = Re \cdot Sc \cdot \frac{h}{z} = \frac{v \cdot h^2}{D} \frac{1}{z} \tag{B.6}$$

Where Re is the Reynolds number, Sc is the Schmidt number, h is the height of the channel. v is the fluid velocity, D is the diffusion coefficient, and z is the coordinate along the length of the channel. Since the Graetz number changes over time, to obtain the average of the Sherwood number, the Gz number is averaged over the length of the electrode by integrating over z between the position where the electrode begins and ends (2.5 mm and 27.5 mm)

$$\langle Gz \rangle = \frac{1}{L} \int \frac{v \cdot h^2}{D} \frac{1}{z} \, dz \tag{B.7}$$

Since the fluid velocity, height of the channel, and diffusion coefficient is constant over the length of the channel, these can be taken out of the integration:

$$\langle Gz \rangle = \frac{1}{L} \frac{v \cdot h^2}{D} \int \frac{1}{z} \, dz = \frac{v \cdot h^2}{D \cdot L} \Big[\ln z \Big]_{z=2.5}^{z=27.5} = \ln 11 \cdot \frac{v \cdot h^2}{D \cdot L} \tag{B.8}$$

Subsequently, the average Graetz number was calculated for the different flowrates and used to calculate the corresponding Sherwood number with formula B.5. This value was

used in formula B.2, where D was the diffusion coefficient for ferrocyanide or CO_2 ($6.67 \cdot 10^{-10}$ $m^2\,s^{-1}$ and $19.7 \cdot 10^{-10}$ $m^2\,s^{-1}$ respectively [2], [3]). A_{surf} is the area of the electrode that is exposed to the electrodes ($A_{surf} = w \cdot L \cdot N$), where w is the width of the channel, L is the length of the channel, and N is the number of channels. Finally, n is the number of electrons that is transferred, F the Faraday constant (96485 C/mol_{e^-}), the concentration of CO_2 in the bulk, c_{bulk}, was calculated using Henry's law where the value for the Henry law coefficient was taken from literature and equal to 0.034 $mol\,L^{-1}\,bar^{-1}$ [4], and h is the height of the channel.

B.3. GAS AND LIQUID INLET DESIGNS

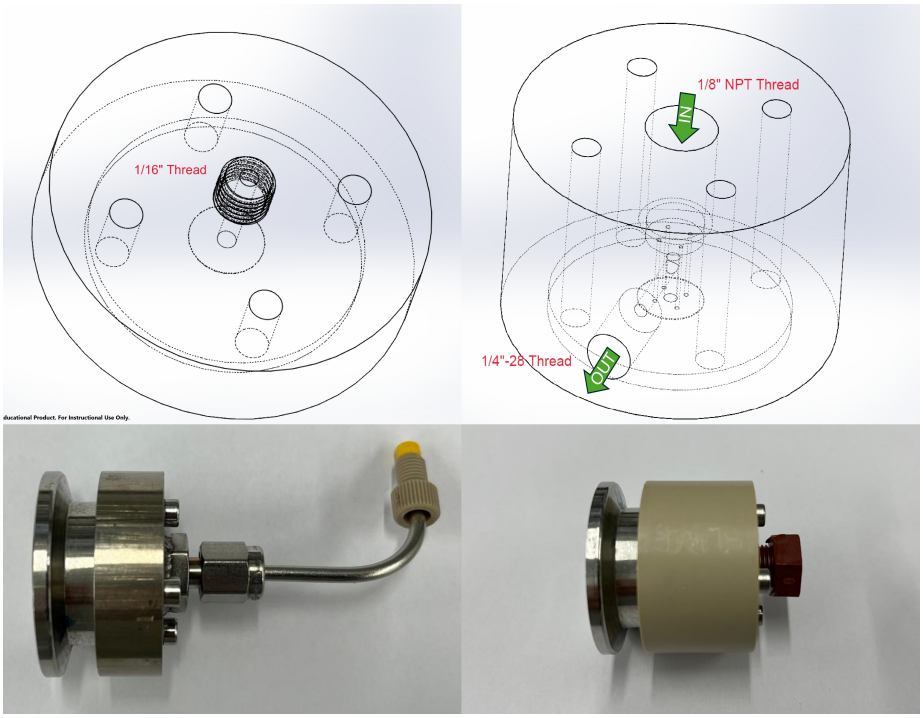

Figure B.1: Drawings and pictures of the gas (left) and liquid inlet respectively. The top two figures show the SolidWorks designs and the ones below show the manufactured inlets mounted on the KF25 support from HIDEN.

B.4. MASS SPECTROMETER SETTINGS

Table B.1: Estimated lower limits of detection for ethanol for four different mass peaks at different mass spectrometer settings.

	Estimated Coefficient	Baseline error	LOD (mM)	R^2
	19.5 eV - 50 µA - 1400 V			
Mass 15	7.74×10^{-13}	1.67×10^{-13}	0.216	0.969
Mass 26	1.93×10^{-13}	5.06×10^{-14}	0.261	0.924
Mass 27	1.24×10^{-12}	8.76×10^{-14}	0.071	0.982
Mass 28	2.25×10^{-11}	1.29×10^{-13}	0.006	0.999
	70 eV - 50 µA - 1200 V			
Mass 15	6.29×10^{-12}	4.19×10^{-13}	0.067	0.998
Mass 26	2.54×10^{-12}	9.00×10^{-14}	0.036	0.996
Mass 27	5.94×10^{-12}	6.08×10^{-13}	0.102	0.996
Mass 28	2.70×10^{-11}	1.10×10^{-13}	0.004	0.997
	70 eV - 500 µA - 1200 V			
Mass 15	3.24×10^{-10}	6.59×10^{-12}	0.020	0.999
Mass 26	9.63×10^{-11}	7.46×10^{-13}	0.008	0.999
Mass 27	2.70×10^{-10}	6.92×10^{-12}	0.026	0.999
Mass 28	1.47×10^{-9}	1.20×10^{-12}	0.001	0.999
	70 eV - 500 µA - 870 V			
Mass 15	1.31×10^{-11}	1.73×10^{-13}	0.013	0.999
Mass 26	3.80×10^{-12}	5.80×10^{-14}	0.015	0.999
Mass 27	1.03×10^{-11}	1.07×10^{-13}	0.010	0.999
Mass 28	5.54×10^{-11}	9.68×10^{-14}	0.002	0.999

B.5. COEFFICIENT MATRIX

Table B.2: Coefficient matrix between the calibrated products and mass peak signals. Coefficients in bold indicate the identifying mass peaks for the respective product.

	Mass 2	**Mass 15**	**Mass 26**	**Mass 27**	**Mass 28**	**Mass 30**	**Mass 31**	**Mass 41**	**Mass 57**	**Mass 58**	**Mass 59**
Hydrogen	**61.38**	0	0	0	0	0	0	0	0	0	0
Carbon monoxide	0	0	0	0	**5.09**	**4.09**	0	0	0	0	0
Methane	0	**1743.8**	0	0	0	0	0	0	0	0	0
Ethylene	**6.60**	**221.18**	**951.28**	**889.53**	**17.23**	**9.45**	0	0	0	0	0
Methanol	0	**4.30**	0	0	0	**1.06**	**7.18**	0	0	0	0
Ethanol	0	**3.61**	**1.09**	**2.62**	0	**0.85**	**12.02**	**0.13**	0	0	0
1-Propanol	0	**1.42**	**1.30**	**3.80**	0	**0.68**	**18.91**	**0.88**	**0.19**	**0.36**	**0.76**
Allyl Alcohol	0	**0.60**	**1.46**	**2.60**	0	**0.99**	**1.91**	**0.40**	**1.87**	**0.44**	0

B.6. PARTIAL CURRENT DENSITIES

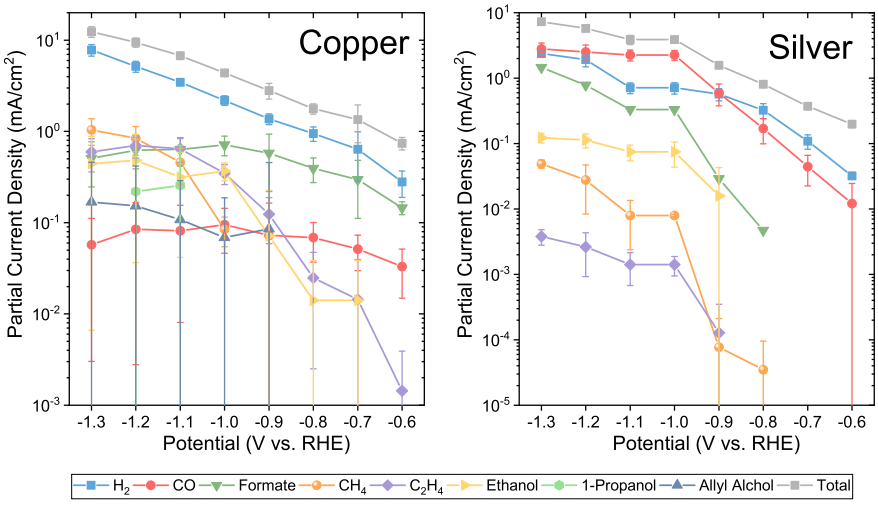

Figure B.2: Partial current densities of detected CO_2 reduction products as a function of potential for both silver and copper electrodes.

B.7. NYQUIST PLOT

Potentiostatic electrochemical impedance spectroscopy (PEIS) was performed to determine the total uncompensated resistance (R_u) of the system while running a CO_2-equilibrated buffer solution of 0.1 mol $KHCO_3$. Potential waveforms with a sinus amplitude of 20 mV between frequencies of 300 kHz and 100 mHz. Per decade 100 different frequencies were applied at the open circuit potential. For every data point, three measurements were averaged for every applied frequency. The results are shown in the Nyquist plot shown in Figure B.3.

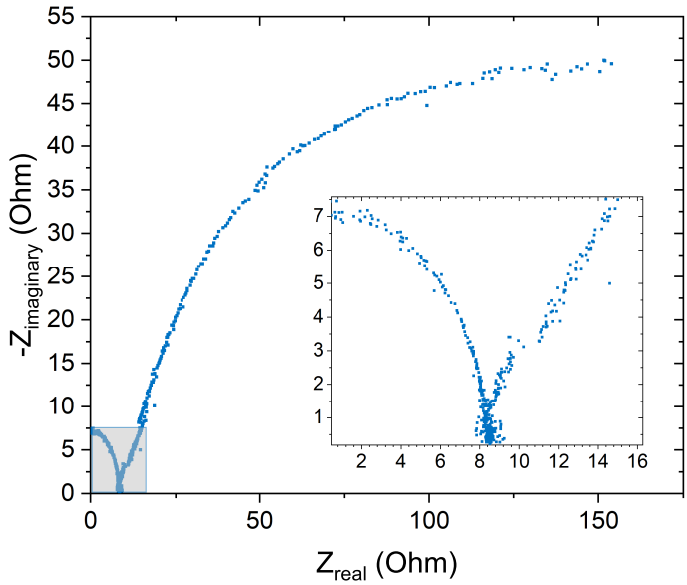

Figure B.3: Nyquist impedance plot of the DEMS cell obtained at an electrolyte flow rate of 1 mL min^{-1} at the open circuit potential.

B.8. CHRONOAMPEROMETRY MEASUREMENTS

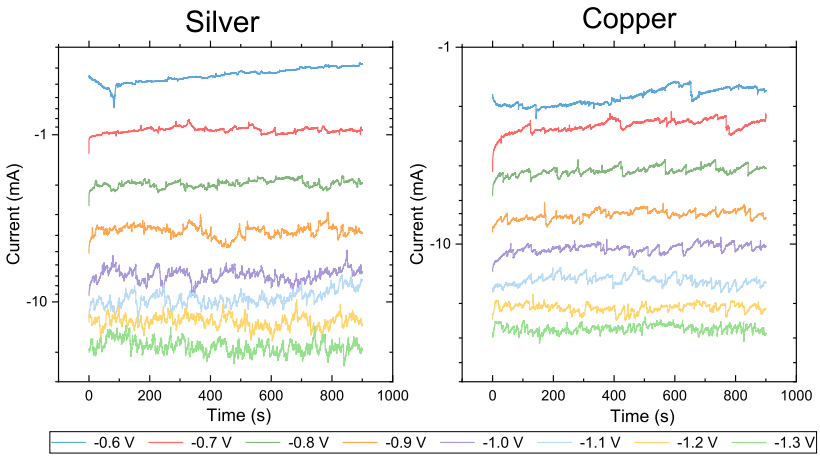

Figure B.4: Currents measured during a set of chronoamperometry measurements between -0.6 V and -1.3 V on silver and copper respectively, using a CO_2-equilibrated buffer solution of 0.1 mol $KHCO_3$ in water.

BIBLIOGRAPHY

[1] D. A. Scherson, Y. V. Tolmachev, Z. Wang, J. Wang, and A. Palencsar, "Extensions of the Koutecky–Levich equation to channel electrodes", *Electrochemical and Solid-State Letters*, vol. 11, no. 2, F1, 2007, ISSN: 1944-8775. DOI: http://dx.doi.org/10.1149/1.2818649.

[2] S. Konopka and B. McDuffie, "Diffusion coefficients of ferri-and ferrocyanide ions in aqueous media, using twin-electrode thin-layer electrochemistry", *Analytical Chemistry*, vol. 42, no. 14, pp. 1741–1746, 1970, ISSN: 0003-2700. DOI: https://doi.org/10.1021/ac50160a042.

[3] M. J. Frank, J. A. Kuipers, and W. P. van Swaaij, "Diffusion coefficients and viscosities of CO_2+H_2O, CO_2+ CH_3OH, NH_3+H_2O, and NH_3+CH_3OH liquid mixtures", *Journal of chemical engineering data*, vol. 41, no. 2, pp. 297–302, 1996, ISSN: 0021-9568. DOI: https://doi.org/10.1021/je950157k.

[4] R. Sander, "Compilation of Henry's law constants (version 5.0.0) for water as solvent", *Atmospheric Chemistry and Physics*, vol. 23, no. 19, pp. 10 901–12 440, 2023, ISSN: 1680-7324. DOI: https://doi.org/10.5194/acp-23-10901-2023.

[5] P. Van Male, M. De Croon, R. M. Tiggelaar, A. van den Berg, and J. Schouten, "Heat and mass transfer in a square microchannel with asymmetric heating", *International Journal of Heat and Mass Transfer*, vol. 47, no. 1, pp. 87–99, 2004, ISSN: 0017-9310. DOI: https://doi.org/10.1016/S0017-9310(03)00401-0.

C

Appendix Chapter 5

C.1. Faradaic Efficiencies

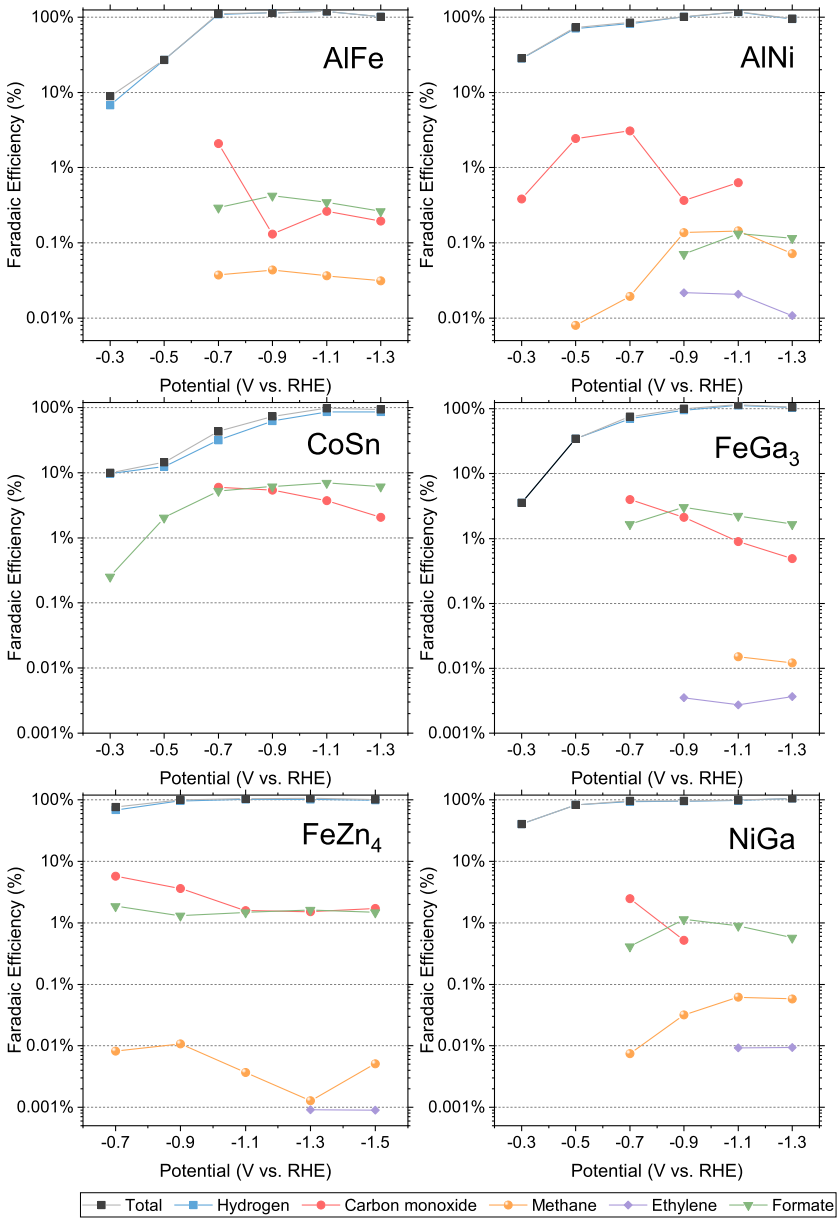

Figure C.1: Faradaic efficiencies of all detected CO_2 reduction in a 0.1 M $KHCO_3$ buffer for AlFe, AlNi, CoSn, $FeGa_3$, $FeZn_4$, and NiGa. The major products observed on the electrodes are hydrogen (■), carbon monoxide (●), formate (▼), methane (●), and ethene (◆). To indicate the faradaic efficiency balance of each catalyst the sum of all faradaic efficiencies per potential is shown as well (■).

Curriculum Vitæ

Daniël van den Berg

19-09-1995 Born in Leiden, The Netherlands.

Education

2007–2013 Highschool
Stedelijk Gymnasium Leiden

2013–2016 Bachelor Molecular Science & Technology
University of Leiden & Delft University of Technology
Thesis: Influence of noble metals on the selectivity of a ceria based NO_x reduction catalyst
Promotor: Dr. ir. M. Makee

2016–2018 Master Chemical Engineering
Delft University of Technology
Thesis: Breaking the Balance - The preparation and kinetics of CO_2 methanation zeolite catalysts.
Promotor: Prof. dr. ir. W. de Jong

2019-2024 PhD Chemistry
Delft University of Technology
Thesis: Scaling the Mountain - The search for bimetallic CO_2 reduction electrocatalysts.
Promotor: Prof. dr. ir. W. de Jong & Dr. R. Kortlever

Experience

Feb - Aug 2019 Research Intern
Sekisui Chemical

2024-… Hydrogen Researcher & Scientist
Magneto Special Anodes

List of Publications

Publications within the scope of this thesis

1. **D. van den Berg**, B. Izelaar, S. Fu, R. Kortlever, "The effect of surface conditions on the electrochemical CO_2 reduction performance of bimetallic AuPd electrocatalysts", *Catalysis Science & Technology*, vol. 14, no. 3, 555-561, 2024, DOI: https://doi.org/10.1039/D3CY01411H.

2. **D. van den Berg**, H. P. Lopuhaä, R. Kortlever, "Direct Quantification of Electrochemical CO_2 Reduction Products with an Improved DEMS Setup", *Chem Catalysis*, DOI: https://doi.org/10.1016/j.checat.2024.101065.

3. **D. van den Berg**, J. C. Brouwer, R. W. A. Hendrikx, R. Kortlever, "Experimental screening of intermetallic alloys for electrochemical CO_2 reduction", *Catalysis Today*, vol. 439, 2024, 114805, DOI: https://doi.org/10.1016/j.cattod.2024.114805.

4. **D. van den Berg**, R. Kortlever, "Can we go beyond copper in CO_2 electrolysis?", *Current Opinion in Electrochemistry*, **In preparation**

Publications outside the scope of this thesis

1. Y. Wang, R. Oord, **D. van den Berg**, B. M Weckhuysen, M. Makkee, "Oxygen Vacancies in Reduced Rh/ and Pt/Ceria for Highly Selective and Reactive Reduction of NO into N_2 in excess of O_2", *ChemCatChem*, vol. 9, no. 15, p. 2935-2938, 2017, DOI: https://doi.org/10.1002/cctc.201700578.

2. K. R. Lawrence, A. Sajeev Kumar, S. Asperti, **D. van den Berg**, N. Girichandran, R. Kortlever, in *Chemical Valorisation of Carbon Dioxide*, ed. G. Stefanidis and A. Stankiewicz, The Royal Society of Chemistry, ch. 17, pp. 388-412, 2022, DOI: https://doi.org/10.1039/9781839167645-00388.

Oral Presentations

1. **D. van den Berg**, R. Kortlever, Rapid Quantitative Screening of Bimetallic CO_2 electrocatalysts, 74th Annual Meeting of the International Society of Electrochemistry, September 3 to 8, 2023, Lyon, France.

2. **D. van den Berg**, R. Kortlever, Direct Quantification of Electrochemical CO2 Reduction Products with an Improved DEMS Setup, Regional Meeting of the International Society of Electrochemistry, 1st 15 to 19 August 2022, Prague, Czech Republic.

POSTER PRESENTATIONS

1. **D. van den Berg**, R. Kortlever, The Effect of Surface Conditions on the Performance of a Bimetallic AuPd Electrocatalyst for CO_2 Reduction, 1st Regional Meeting of the International Society of Electrochemistry, 15 to 19 August 2022, Prague, Czech Republic.

2. **D. van den Berg**, R. Kortlever, The Effect of Surface Conditions on the Performance of a Bimetallic AuPd Electrocatalyst for CO_2 Reduction, 23rd Netherlands Catalysis and Chemistry Conference (NCCC), 9 to 11 May 2022, Noordwijkerhout, The Netherlands.

3. **D. van den Berg**, R. Kortlever, Bimetallic electrode design for direct CO_2 reduction to renewable fuels, 20th Netherlands Catalysis and Chemistry Conference (NCCC), 2 to 4 March 2019, Noordwijkerhout, The Netherlands.